Studies on generalizations and complex behaviors of quantum modular values

LE BIN HO

MARCH 2018

Studies on generalizations and complex behaviors of quantum modular values

A dissertation submitted to

THE GRADUATE SCHOOL OF ENGINEERING SCIENCE
OSAKA UNIVERSITY

in partial fulfillment of the requirements for the degree of
DOCTOR OF PHILOSOPHY IN SCIENCE

BY

LE BIN HO

MARCH 2018

Abstract

In quantum mechanics, measurements of an observable of a quantum system allow for the prediction of the attentive characteristics of that system. The average value of the observable is described by its operator and the quantum wave function that represents the system state, and is well known as "expectation value." If the system, however, described by a two-state vector, i.e., an initial state and a final state, such that the system's initial state is preselected and its final state is postselected, then the corresponding average value is known as "weak value," which was first named by Aharonov, Albert, and Vaidman in their groundbreaking study in 1988. Weak values, however, mainly go along with weak measurements, which usually require an infinitely small interaction strength.

In order to allow a finite strength in the measurement interaction, the concept of modular value was proposed by Kedem and Vaidman in 2010. Although the concept of modular values is similar to that of weak values, there also are many different exciting points. However, the research on modular values is not so well developed as research on weak values. A generalized relationship between modular values and weak values is still not explicitly stated. Furthermore, fully generalized characterizations, as well as the complex-behavior understanding of modular values, are still missing.

This dissertation, therefore, introduces and develops a general approach for strong measuring quantum modular values in the two-state vector formalism, along with several applications in quantum physics. Our work here provides more detailed generalized characterization and fundamental understanding the complex behaviors of the quantum modular values. Particularly, we indicate generalized relationships between modular values and weak values for finite-dimensional systems by using the Lagrange interpolation and then apply to analyze and interpret some quantum paradoxes in quantum physics. We then theoretically characterize the generalized modular values by studying generalized modular-value-based schemes which are extended from conventional two-dimensional pointers to finite-dimensional discrete pointers and continuous pointers. We particularly illustrate our proposal in the three cases of a spin-s particle pointer, a semiclassical pointer, and a continuous Gaussian pointer. We also further describe the

time-dependent weak values and modular values in enlarged forms and show how to implement an enlarged Hilbert space in various physical platforms. Finally, we investigate the statistical property and the physical meaning of modular values in the polar form for both cases of the discrete and continuous pointers. As a consequence, a relationship between the modulus and phase is also fully investigated and simply illustrated on a Bloch sphere.

Contents

Abstract i

List of Figures iv

1 Introduction 1

1.1 Introduction . . . 1
1.2 Measurements in quantum mechanics . . . 4
1.2.1 The total Hamiltonian . . . 4
1.2.2 The evolution operator . . . 5
1.2.3 The pointer shift as a measurement result . . . 5
1.2.4 POVM measurements . . . 6
1.3 A brief to weak measurements and weak values . . . 8
1.3.1 Weak interactions . . . 8
1.3.2 Weak values . . . 8
1.3.3 Properties of weak values . . . 9
1.4 Dissertation overview and key results . . . 10
1.4.1 Dissertation overview . . . 10
1.4.2 Key results . . . 11

2 Quantum modular values 13

2.1 A brief review to quantum modular values . . . 13
2.1.1 A von Neumann measurement approach . . . 13
2.1.2 A postselection measurement with a qubit pointer . . . 14
2.1.3 Modular values and weak values . . . 16

2.2 A quantum circuit for modular-value measurements 16
2.2.1 Controlled-R_Z gate 16
2.2.2 Example 18

3 Quantum modular values and weak values: full relations and applications to quantum paradoxes 19
3.1 Full relations of modular values to weak values 20
3.1.1 The Lagrange interpolation 20
3.1.2 Two-dimensional Hilbert space 21
3.1.3 Three-dimensional Hilbert space 22
3.2 Nonlocal joint measurements induced by modular values 24
3.2.1 Nonlocal observables 24
3.2.2 Lagrange interpolation for nonlocal observables 24
3.3 Applications to quantum paradoxes 26
3.3.1 The EPR paradox 26
3.3.2 The Hardy paradox 28
3.3.3 The Cheshire-cat paradox 31
3.3.4 Measurements on the two-qubit pointer 34

4 Generalized modular-value-based schemes and generalized modular values 35
4.1 Finite-dimensional pointer states 36
4.1.1 A POVM approach to postselection measurements 36
4.1.2 Adjoint-form modular values 38
4.1.3 Generalized modular values 39
4.1.4 Generalized modular values and generalized weak values 41
4.2 Continuous pointer states 43
4.2.1 Momentum-dependent modular values 43
4.2.2 A POVM approach to postselection measurements 44
4.2.3 Adjoint-form modular values 44
4.3 Applications 45
4.3.1 Spin-s particle pointer 45
4.3.2 Semiclassical pointer state 49

4.3.3 Continuous Gaussian pointer state 51

5 Weak and modular values in enlarged Hilbert spaces 55

5.1 Uncausal weak/modular measurements problem 55

5.2 Enlarged Hilbert space method 56

5.2.1 The enlarged state 57

5.2.2 The enlarged Schrödinger equation 57

5.3 Time-dependent quantum weak and modular values 59

5.3.1 Time-dependent weak values in a normal Hilbert space 59

5.3.2 Time-dependent weak values in an enlarged Hilbert space: expectation-value forms 60

5.3.3 Example 61

5.3.4 Time-dependent modular values in an enlarged Hilbert space . . 64

5.4 Implementation of enlarged Hilbert spaces 64

5.4.1 Trotter technique 65

5.4.2 Trotter technique for the enlarged spaces 65

5.4.3 Example 66

6 Probabilistic representation of complex modular values 68

6.1 Complex conditional probability 68

6.2 Complex modular values 70

6.3 Chain rules 70

7 Polar representation of complex modular values 73

7.1 Polar representation 73

7.1.1 The modulus of modular values 74

7.1.2 The phase of modular values 75

7.2 The modulus-phase relation 78

7.2.1 The modulus-phase relation 78

7.2.2 An illustration for the modulus-phase relation on the Bloch sphere 79

8 Conclusions and Outlook 83

8.1 Conclusions 83

8.2 Outlook 84
8.2.1 Quantum state estimation 84
8.2.2 Continuous monitoring enlarged systems 84

References **85**

Appendix A. The Lagrange interpolation **93**
A.1 The Cayley-Hamilton theorem 93
A.2 Proof of the Lagrange interpolation 95

Appendix B. The generalized modular-value based scheme **97**
B.1 Joint probability and the expectation value 97
B.2 Kraus operator 98
B.3 The final state of the pointer 99

Appendix C. Enlarged weak values **101**
C.1 Weak values in the enlarged Hilbert space 101
C.2 An implementation the enlarged evolution 102

Acknowledgements **104**

Dedication **105**

List of Publications **106**

List of Figures

1.1 The shift of the pointer position before and after the measurement. The amount of shift corresponds to the eigenvalue of the measured observable. 6

1.2 "Ship-like" structure of the dissertation. 12

2.1 A postselection measurement scheme. The system (not necessary being a qubit but could be in a higher dimensional Hilbert space) is conditioned by a preselection state vector $|\psi\rangle$ and a postselection state vector $|\phi\rangle$. The system arbitrarily couples to an apparatus with its initial probe state $|\xi\rangle$. After the postselection in the system, the outcome M in the probe is measured, which gives the result of the measured observable $\hat{\boldsymbol{A}}$ in the system. 15

2.2 (a) Quantum circuit simulates the modular-value measurement. The system is prepared in state $|\psi\rangle$ and postselected to $|\phi\rangle$. The qubit pointer state is prepared as $|\xi\rangle = \gamma|0\rangle + \bar{\gamma}|1\rangle$, and measured on the $\hat{\boldsymbol{\sigma}}_z$ basis. The qubit pointer controls the system whenever its input is $|1\rangle$. The system is rotated θ angle around the z-axis. (b) The modular value as a function of coupling constant $g = \theta/2$. The highest position corresponds to weak value when $g = \pi/2$. 17

3.1 The schematic description of EPR-Bohm experiment. At time t_1, a pair of spin-$\frac{1}{2}$ particles, maximally entangled singlet state, is separated to Alice and Bod. They measure their particle with certain results at time t_2. Supporting that at time t ($t_1 < t < t_2$) only Alice measures her particle, or only Bob measures his particle, or they perform a joint measurement as shown in the figure. The paradox here is that the product of single measurements does not equal to the joint measurement. 27

3.2 The setup for the Hardy paradox, where a monochromatic electron (e^-) and a positron (e^+) are respectively put into each Mach-Zehnder interferometer. Here, state $|O\rangle_-$ (or $|O\rangle_+$) denotes the electron (or positron) that goes to the overlapping region, and the state $|NO\rangle_-$ (or $|NO\rangle_+$) denotes the electron (or positron) that goes to the non-overlapping region. BS means the beam splitter. 29

3.3 Setup for the Cheshire cat, where a horizontally polarized photon is put toward a Mach-Zehnder interferometer. The state $|H\rangle$ ($|V\rangle$) represents horizontally (vertically) polarized photon state, state $|L\rangle$ ($|R\rangle$) is the left (right) of photon path. These other notations are BS: beam splitter, PBS: polarized beam splitter, HWP: half waveplate, PS: phase splitter. 32

4.1 The probability displacements $\Delta P(\mu = s|f)$ and $\Delta P(\mu \neq s|f)$ in Eqs. (4.53) as functions of $(\hat{\boldsymbol{A}})^s_{\rm m}$ for $\gamma = 0.4$, 0.6 and 0.8, and $s = 1$, i.e., spin-1 pointer. Inset: the modular value of the system observable $\hat{\boldsymbol{\sigma}}_z/2$ varies as a function of ϵ, where the quantum system states are chosen as in Eqs. (4.50, 4.51), also we fix the value of $g = \pi$. 47

4.2 Contour plot of the average displacement in the measured value of the pointer observable $\hat{\boldsymbol{S}}^z_{\rm p}$ of spin-2 ($s = 2$) particle. The vertical line at $(\hat{\boldsymbol{A}})^s_{\rm m} = 1$ indicates the value zero, which means no "displacement". The quantum system is chosen the same as in Fig. 4.1. 48

4.3 The SNRs are shown as functions of $(\hat{\boldsymbol{A}})^s_{\rm m}$ and γ for $s = \frac{1}{2}, 2, \frac{7}{2}$ and 5 as can be seen in each panel. The quantum system is chosen the same as in Fig. 4.1. 50

4.4 The conditional probability-versus-n curves with different modular values $(\hat{\boldsymbol{A}})^n_{\rm m}$ and $|\alpha|^2$. All curves show the increasing with $(\hat{\boldsymbol{A}})^n_{\rm m}$ for each $|\alpha|^2$. This phenomenon can be regarded as the amplification effect of the modular value. The quantum system can be chosen the same as in Fig. 4.1, i.e., interactions between spin and photon. 51

4.5 The conditional probabilities and modular values as functions of momentum p for fixed $g = \pi/2$ and several values of θ as shown in the figure. 52

4.6 The contour plot of the momentum displacement $\Delta\langle\hat{\boldsymbol{p}}\rangle$. 53

4.7 The SNRs as functions of the measurement strength for several θ. . . . 54

5.1 A schematic setup of a single spin-$\frac{1}{2}$ particle under a magnetic field applied along the z-axis. The particle is initially prepared in spin up along the x-axis, and then postselected onto the three cases of spin up along the x-axis, spin up along the y-axis, and spin down along the x-axis. We calculate the weak value of Pauli matrix $\hat{\boldsymbol{\sigma}}_x(t)$ at time t between 0 and T. 62

5.2 Weak values of $\hat{\boldsymbol{\sigma}}_x$ for preselection state in (5.19) and various postselection states as in (5.20), which are the same in both cases of normal Hilbert space and enlarged Hilbert space. 63

5.3 A scheme of quantum gates acting on both the extra spin (e) and the system single-particle spin (s). 67

6.1 A vector graphic illustrates the chain rule. The chain rule describing the process of taking route $|\psi\rangle \to |a\rangle \to |\phi\rangle$ is the summation over all possible $|x\rangle$'s of the product of taking $|\psi\rangle \to |a\rangle \to |x\rangle$ and taking $|\psi\rangle \to |x\rangle \to |\phi\rangle$. 71

7.1 The phase of a modular value is the total phase shift of a system-state-evolution process that starting from an initial state, evolve onto an intermediate state, then project onto a final state and finally project back to the initial state. This total phase shift corresponds to the summation of the geometric phase and the intrinsic phase. 77

7.2 (a, b) The logarithm of the modulus and the minus of the phase of the complex modular value $(\hat{\boldsymbol{\sigma}}_z)_{\mathrm{m}}$, where their derivatives respect to g will give the corresponding imaginary and the real parts of the weak value in (c, d). The discrete values are obtained from an identical ensemble of 10^5 pre- and postselection states, while the curves are analytical results. 82

Chapter 1

Introduction

We are not one of the followers but belong to the founder of an exploding new area.

Nobuyuki Imoto

1.1 Introduction

During the past 30 years, the concept of weak value and weak measurement has been studied so far and gradually becomes a noncontroversial theory and attracts many studies both theoretical and experimental points of view. In 1988, a groundbreaking study by Aharonov, Albert, and Vaidman pointed out that the measurement value of a component of a spin-$\frac{1}{2}$ particle could turn out to be 100 [1]. This is the very first feature of weak values, such that their values can widely excess the eigenvalue boundaries, and unlike usual expectation values, they can be complex. These two strange features of weak values have been considered in the context of probabilistic interpretation [2] or contextuality [3], and become reliable sources to interpret many quantum phenomena, specifically in quantum paradoxes with the EPR paradox [4,5], the Hardy paradox [6–9], and the Cheshire-cat experiment [10,11]. Furthermore, the concept of weak values has been the most widely applied to amplification effects and small shifts [12–14], precision metrologies [15–18] and various exciting physical phenomena [19–21].

Beyond the standard weak value formalism, i.e., the most studies on weak values focus on a continuous-variable pointer of a measuring device, and constrain to a weak coupling, there were other attempts to increase the coupling strength (see Refs. therein [22]) or consider a qubit pointer apparatus [23–25]. Specifically, a proposal by Kedem and Vaidman, wherein a quantum system arbitrarily coupled a qubit pointer under the ideal von Neumann measurement for a quantum observable $\hat{\boldsymbol{A}}$, which led to the so-called "modular value" [25].

Indeed, modular values share some intriguing properties of weak values, such as complexity and anomalous values, i.e., lie outside the range of standard eigenvalues. Nonetheless, modular values are sometimes more beneficial than weak values, in the sense that measuring a modular value is more efficient than measuring a weak value because the measurement coupling constant can be made large. Moreover, from the experimental point of view, modular values are seemingly easier to measure. Supporting this point of view is because one can just perform the tomography using binary outcomes of the qubit pointer. It is also more practical to measure nonlocal observables by using modular values instead of using weak values. However, this concept has received slight attention since it was first introduced in 2010. A generalized relationship between modular values and weak values is still not explicitly stated. Furthermore, fully generalized characterizations, as well as the complex-behavior understanding of modular values, are still missing.

This dissertation firstly presents generalized relationships between modular values and weak values for finite-dimensional systems. More specifically, generalized modular values are also demonstrated by analyzing a generalized modular-value-based scheme. Also, time-dependent quantum weak and modular values in enlarged Hilbert spaces are investigated. Furthermore, a statistical and a physical significance of quantum modular values are also thoroughly characterized in this dissertation.

We first indicate generalized relationships between modular values and weak values for finite-dimensional systems by using the Lagrange interpolation. These relations enable us to evaluate weak values by experimentally obtainable modular values without requiring an infinitesimally small coupling. We also fully characterize the generalized relationships not only with the weak value of a single observable but also with a joint weak value of nonlocal observables. We then analyze and interpret some quantum

paradoxes by using modular values, such as the EPR paradox, the Hardy paradox, and the Cheshire-cat paradox.

These studies also lead to generalizations of modular values and clarifying the complex behaviors of modular values. As for the generalizations, we implement a generalized modular-value-based scheme based on a positive-operator-valued-measure (POVM) approach for postselection measurements, where we generalize from conventional two-level pointers to multi-level pointers and continuous pointers. These analyses lead to a so-called *generalized modular value*. We then apply our proposal to the case of a spin-s particle pointer, a semiclassical pointer state, a continuous pointer state, and also further discuss on nonclassical pointer states.

After that, the time-dependent weak values and modular values are also generalized onto an enlarged Hilbert space. Therein, we propose an enlarged state, which combines both pre- and postselection states at a given time t. Using this enlarged state, quantum weak and modular values can be completely interpreted as expectation values of a linear combination of given operators in the enlarged Hilbert space. We also apply this proposal to an example of a spin-$\frac{1}{2}$ particle evolves under an external magnetic field. Subsequently, a method for implementing the enlarged Hamiltonian is also discussed.

As for clarifying the complex behaviors of modular values, we firstly investigate the complex behaviors of modular values by using the spectral decomposition and connect the modular values to the complex conditional probabilities. Next, the chain rules of the conditional probabilities are also derived. Afterwards, we also investigate the physical significance of modular values. We derive the polar decomposition of a modular value into the modulus and phase components and connect these components onto some physical properties of the system and the pointer. Then, we also discuss a relationship between the modulus and phase, wherein the derivative of the phase is related to the derivative of the logarithm of the modulus via a Berry-Simon-like connection, which is in the form of a weak value. We also illustrate the modulus-phase relation on a Bloch sphere.

Before discussing on modular values in detail, I will first give a brief about the quantum measurement and the concept of weak values.

1.2 Measurements in quantum mechanics

In this section, we will briefly review an indirect measurement of an arbitrary observable of a given quantum system, following the standard treatment of von Neumann measurements and standard POVM measurements. Particularly, to measure an observable $\hat{\boldsymbol{A}}$ in the system, we couple it to a pointer observable of an apparatus. The coupling entangles the eigenstates of the observable and the states of the pointer so that we can measure an eigenstate of the system observable by *looking* at the final state of the pointer.

1.2.1 The total Hamiltonian

The total Hamiltonian including the coupling of the quantum system observable and the pointer observable has the form

$$\hat{\boldsymbol{H}} = \hat{\boldsymbol{H}}_0 + \hat{\boldsymbol{P}}_0 + g(t)\hat{\boldsymbol{A}} \otimes \hat{\boldsymbol{P}}, \tag{1.1}$$

where $\hat{\boldsymbol{H}}_0$ is the free Hamiltonian of the system to be measured, and $\hat{\boldsymbol{P}}_0$ is the free Hamiltonian of the pointer. Most of the cases, we might ignore the effect of the pointer Hamiltonian to the total system because the spreading of pointer wavepacket can be neglected due to the massive pointer [26]. The time-dependent coupling $g(t)$ is assumed to be nonzero over the interaction time interval $t \in [0, T]$.

Generally, if $\hat{\boldsymbol{A}}$ does not commute with $\hat{\boldsymbol{H}}_0$, then we have to take into account the evolution of the observable during the measurement. However, for simplicity, let us adopting that $\hat{\boldsymbol{A}}$ and $\hat{\boldsymbol{H}}_0$ commute, i.e., $[\hat{\boldsymbol{A}}, \hat{\boldsymbol{H}}_0] = 0$, or we assume that the measurement is implemented so quick that we can neglect the free evolution of the system during the measurement time [26]. Then, the total Hamiltonian reduces to

$$\hat{\boldsymbol{H}} = \hbar g(t)\hat{\boldsymbol{A}} \otimes \hat{\boldsymbol{P}}, \tag{1.2}$$

where we have added $\hbar$ to the formula for later convenience. We also note that during the rest of this dissertation, we usually use this Hamiltonian as the total interaction Hamiltonian.

1.2.2 The evolution operator

In the Schrödinger picture, the time evolution of a quantum state $|\psi\rangle$ is governed by the Schrödinger equation

$$i\hbar\frac{\partial}{\partial t}|\psi(t)\rangle = \hat{\boldsymbol{H}}|\psi(t)\rangle. \tag{1.3}$$

Suppose that $|\psi(t)\rangle = \hat{\boldsymbol{U}}|\psi(0)\rangle$ for some operators $\hat{\boldsymbol{U}}$. Then submitting this formula into the Schrödinger equation (1.3) we obtain

$$i\hbar\frac{\partial\hat{\boldsymbol{U}}}{\partial t} = \hat{\boldsymbol{H}}\hat{\boldsymbol{U}}. \tag{1.4}$$

The solution is straightforwardly given by

$$\hat{\boldsymbol{U}} = e^{-ig\hat{\boldsymbol{A}}\otimes\hat{\boldsymbol{P}}}\ ,\ \text{with}\ g = \int_0^T g(t)dt\ , \tag{1.5}$$

where we have used the initial condition $\hat{\boldsymbol{U}}(t=0) = \hat{\boldsymbol{I}}$. In an arbitrarily strong measurement, the coupling constant g is no need to require to be weak.

1.2.3 The pointer shift as a measurement result

The measured observable $\hat{\boldsymbol{A}}$ can be expanded on the diagonal basis as

$$\hat{\boldsymbol{A}} = \sum_n a_n|a_n\rangle\langle a_n|, \tag{1.6}$$

with the eigenvalue a_n corresponding to the eigenfunction $|a_n\rangle$. We then recast the evolution operator $\hat{\boldsymbol{U}}$ as

$$\hat{\boldsymbol{U}} = \sum_n e^{-iga_n\hat{\boldsymbol{P}}}|a_n\rangle\langle a_n|. \tag{1.7}$$

Now, if the pointer operator is the momentum, i.e., $\hat{\boldsymbol{P}} = -i\hbar\frac{\partial}{\partial x}$, and if the quantum state is the superposition of $\hat{\boldsymbol{A}}$ eigenvalues, initially uncorrelated with the pointer wavepacket $\xi(x) \equiv \langle x|\xi\rangle$, such that

$$|\psi\rangle\otimes\xi(x) = \sum_n \psi_n|a_n\rangle\otimes\xi(x), \tag{1.8}$$

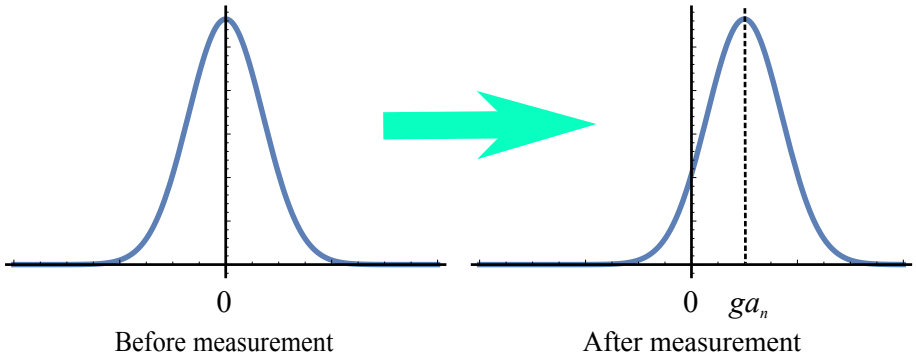

Figure 1.1: The shift of the pointer position before and after the measurement. The amount of shift corresponds to the eigenvalue of the measured observable.

where $\psi_n \equiv \langle a_n|\psi\rangle$, then the action of the evolution operator upon this state gives

$$\hat{\boldsymbol{U}}|\psi\rangle \otimes \xi(x) = \sum_n \psi_n |a_n\rangle \otimes \xi(x - ga_n), \tag{1.9}$$

where the position of the pointer is now shifted an amount corresponding to the eigenvalue of the observable $\hat{\boldsymbol{A}}$ as illustrated in Fig. 1.1.

1.2.4 POVM measurements

Suppose that quantum measurements are described by a collection $\{\hat{\boldsymbol{\Omega}}_\mu\}$ of measured operators. These operators act upon the quantum state $|\psi\rangle$ and the measurement outcome that may occur in the experiment is assigned as μ with a probability

$$P(\mu) = \langle\psi|\hat{\boldsymbol{\Omega}}_\mu^\dagger \hat{\boldsymbol{\Omega}}_\mu|\psi\rangle. \tag{1.10}$$

If the initial quantum state is a mixed state, which is described by a density matrix $\hat{\boldsymbol{\rho}}$, then the probability is given by

$$P(\mu) = \mathrm{Tr}(\hat{\boldsymbol{\Omega}}_\mu^\dagger \hat{\boldsymbol{\Omega}}_\mu \hat{\boldsymbol{\rho}}). \tag{1.11}$$

Then, the system state after the measurement is updated to

$$|\psi\rangle \to \frac{\hat{\boldsymbol{\Omega}}_\mu|\psi\rangle}{\sqrt{P(\mu)}} \text{ and } \hat{\boldsymbol{\rho}} \to \frac{\hat{\boldsymbol{\Omega}}_\mu \hat{\boldsymbol{\rho}} \hat{\boldsymbol{\Omega}}_\mu^\dagger}{P(\mu)}, \tag{1.12}$$

for pure and mixed states, respectively.

The measurement operators satisfy the completeness relation

$$\sum_{\mu} \hat{\boldsymbol{\Omega}}_{\mu}^{\dagger} \hat{\boldsymbol{\Omega}}_{\mu} = \hat{\boldsymbol{I}}, \tag{1.13}$$

then, as a result, the probabilities sum to unity

$$\sum_{\mu} P(\mu) = \sum_{\mu} \langle \psi | \hat{\boldsymbol{\Omega}}_{\mu}^{\dagger} \hat{\boldsymbol{\Omega}}_{\mu} | \psi \rangle = 1. \tag{1.14}$$

Furthermore, we define by $\hat{\boldsymbol{E}}_{\mu} \equiv \hat{\boldsymbol{\Omega}}_{\mu}^{\dagger} \hat{\boldsymbol{\Omega}}_{\mu}$, a positive operator, and hence, from (1.13) $\sum_{\mu} \hat{\boldsymbol{E}}_{\mu} = \hat{\boldsymbol{I}}$. This complete set of operators $\hat{\boldsymbol{E}}_{\mu}$ allows us to determine the probabilities of the measurement outcomes and is known as the *Positive-Operator Valued Measure* (POVM).

As an example, let us illustrate how to employ the theorem of POVM to distinguish non-orthogonal states. Assume that we are given a qubit prepared in one of two non-orthogonal states, $|\psi_1\rangle = |0\rangle$ and $|\psi_2\rangle = (|0\rangle + |1\rangle)/\sqrt{2}$. Since they are not orthogonal, no measurement completely distinguishes them. For example, if we get $|1\rangle$ in the measurement result, then we can assert that the given state is $|\psi_2\rangle$. However, if the result is in $|0\rangle$, then the given state could be either $|\psi_1\rangle$ or $|\psi_2\rangle$.

Nevertheless, it is possible for us to proceed a measurement that discriminates between the two states, such as using a POVM containing three elements as in Ref. [27]

$$\hat{\boldsymbol{E}}_1 = \frac{\sqrt{2}}{1+\sqrt{2}} |1\rangle\langle 1|, \tag{1.15}$$

$$\hat{\boldsymbol{E}}_2 = \frac{\sqrt{2}}{1+\sqrt{2}} \frac{(|0\rangle - |1\rangle)(\langle 0| - \langle 1|)}{2}, \tag{1.16}$$

$$\hat{\boldsymbol{E}}_3 = \hat{\boldsymbol{I}} - \hat{\boldsymbol{E}}_1 - \hat{\boldsymbol{E}}_2. \tag{1.17}$$

Obviously, in this example, $\hat{\boldsymbol{E}}_1$ is orthogonal to $|\psi_1\rangle$ and $\hat{\boldsymbol{E}}_2$ is orthogonal to $|\psi_2\rangle$. Or, in other words, $\langle \psi_i | \hat{\boldsymbol{E}}_i | \psi_i \rangle = 0$, for $i = 1, 2$. Therefore, if the measurement result is $\hat{\boldsymbol{E}}_1$ (or $\hat{\boldsymbol{E}}_2$), then we make sure that the given state must in $|\psi_2\rangle$ (or $|\psi_1\rangle$). However, if the result corresponds to $\hat{\boldsymbol{E}}_3$, then this measurement tells us nothing about the discrimination of the state [27].

1.3 A brief to weak measurements and weak values

1.3.1 Weak interactions

To describe weak measurements, we pursue a weak coupling between a measured system and a pointer, where the interaction Hamiltonian and the corresponding evolution operator are given as in Eqs. (1.2, 1.5), such that

$$\hat{\boldsymbol{H}} = \hbar g(t)\hat{\boldsymbol{A}} \otimes \hat{\boldsymbol{P}}, \text{ and } \hat{\boldsymbol{U}} = e^{-ig\hat{\boldsymbol{A}}\otimes\hat{\boldsymbol{P}}} , \tag{1.18}$$

where $\hat{\boldsymbol{A}}$ is the measured observable and $\hat{\boldsymbol{P}}$ is the pointer momentum. For a weak measurement, the coupling constant g is chosen to be *infinitely small*. How small is weak enough? There are few ways to determine the weak coupling. Ideally, the limit case is taken place, i.e., taking the limit $g \to 0$. However, it seems not enough to consider only $g \ll 1$ since g might have a dimension or with unbounded variables in the interaction (1.18), then the effect of the interaction can be large even small g [28]. In this case, it is better to consider the weakness of the integration of the Hamiltonian as [28]

$$\left|\left\langle \int \hat{\boldsymbol{H}} dt \right\rangle\right| \ll 1, \text{ or, equivalent } \left|g\langle\hat{\boldsymbol{A}}\rangle\langle\hat{\boldsymbol{P}}\rangle\right| \ll 1. \tag{1.19}$$

where $\langle ... \rangle$ is the expectation value, assume that the measured system and the pointer are initially uncorrelated. Another way to defined the weak interaction is that the measured state after the interaction does not collapse. In other words, the back action of the pointer to the measured system is mall, following [28] such that

$$|\langle\psi'|\psi\rangle|^2 \to 1, \tag{1.20}$$

where $|\psi'\rangle \equiv e^{-ig\hat{\boldsymbol{A}}\otimes\hat{\boldsymbol{P}}}|\psi\rangle$ is the system state after the interaction.

1.3.2 Weak values

For weak interactions, we can expand the evolution operator in Eq. (1.18) up to the first order of g as

$$\hat{\boldsymbol{U}} = \hat{\boldsymbol{I}} - ig\hat{\boldsymbol{A}} \otimes \hat{\boldsymbol{P}} + O(g^2). \tag{1.21}$$

For simplicity, we also assume that the system state is pure and denoted as $|\psi\rangle$, initially uncorrelated to the pointer state $|\xi\rangle$. Then the composite state is given by $|\psi\rangle \otimes |\xi\rangle$. After the interaction, the state evolves to

$$\hat{\boldsymbol{U}}|\psi\rangle \otimes |\xi\rangle = (\hat{\boldsymbol{I}} - ig\hat{\boldsymbol{A}} \otimes \hat{\boldsymbol{P}})|\psi\rangle \otimes |\xi\rangle, \tag{1.22}$$

where we have used the approximation (1.21).

In the manner of conditional weak measurement, the system is postselected onto a final state $|\phi\rangle$ after the interaction. Then the remain pointer state is calculated to be

$$\begin{aligned} |\eta\rangle &= \langle\phi|\hat{\boldsymbol{U}}|\psi\rangle \otimes |\xi\rangle \\ &= \langle\phi|\psi\rangle e^{-ig\langle\hat{\boldsymbol{A}}\rangle_{\mathrm{w}}\hat{\boldsymbol{P}}}|\xi\rangle, \end{aligned} \tag{1.23}$$

where

$$\langle\hat{\boldsymbol{A}}\rangle_{\mathrm{w}} \equiv \frac{\langle\phi|\hat{\boldsymbol{A}}|\psi\rangle}{\langle\phi|\psi\rangle}\ , \tag{1.24}$$

is named as "weak value," $|\psi\rangle$ and $|\phi\rangle$ are known as pre- and postselection states, respectively. The subscript "w" stands for "weak."

1.3.3 Properties of weak values

Counter to conventional expectation values, weak values have many intriguing properties. Particularly, weak values can lie far outside the range of eigenvalues of the measured observable and can even be complex. Of course, they also can be reduced to expectation values or eigenvalues in some cases. Following are some of properties.

(i) Weak values as transition amplitudes

Naively, from the definition (1.24), a weak value can be understood as the ratio of the transition amplitude from the preselection state to the postselection state for the measured observables $\hat{\boldsymbol{A}}$ and $\hat{\boldsymbol{I}}$, respectively. This ratio sometimes can be viewed as the "relative change" in the detection probabilities [29, 30].

(ii) Without postselection case

If there is no postselection, or in other words, $|\phi\rangle = |\psi\rangle$, then the weak value mathematically reduces to the ordinary expectation value

$$\langle\hat{\boldsymbol{A}}\rangle_{\mathrm{w}} = \frac{\langle\psi|\hat{\boldsymbol{A}}|\psi\rangle}{\langle\psi|\psi\rangle} = \langle\hat{\boldsymbol{A}}\rangle\ . \tag{1.25}$$

(iii) Eigenstate case

If the preselection state is an eigenstate of the measured observable, i.e., $\hat{\boldsymbol{A}}|\psi\rangle = a|\psi\rangle$, where a is the corresponding eigenvalue, then the straightforward calculation weak value gives

$$\langle \hat{\boldsymbol{A}} \rangle_{\mathrm{w}} = \frac{\langle \phi | a | \psi \rangle}{\langle \phi | \psi \rangle} = a \ . \tag{1.26}$$

Roughly speaking, the weak value becomes the eigenvalue that corresponds to the preselection eigenstate regardless the postselection state. This result is also valid for the case that the postselection is chosen to be an eigenstate of the measured observable.

(iv) Anomalous weak values

Weak values can describe a quantum system with pre- and postselection states which can be chosen independently with each other. Their values, therefore, depend on the choice of the states for a fixed measured observable and cause some anomalous results. One of the strange features is that the weak value amplitudes can go far away from the standard eigenvalues of the measured observable. This effect occurs when the inner product, $\langle \phi | \psi \rangle$, is tiny, which implies that the pre- and postselection states are closely orthonormal. Another anomalous property, which contracts to the original expectation values, is that weak values can be complex. Usually, if the transition amplitudes are real, then the weak values are also real. However, if the transition amplitudes are complex, then, in general, the weak values are complex. The meaning of complex weak values has been discussed so far [31, 32].

1.4 Dissertation overview and key results

1.4.1 Dissertation overview

Chapter 2 presents the concept of quantum modular values. Therein, at first, we review a von Neumann approach to postselection quantum measurements for the case of qubit pointers. We also demonstrate how modular values can be obtained from the outcomes of the pointers. After that, we propose and implement a simple quantum circuit using a control-Z gate for such a *modular-value measurement*.

In Chapter 3, we will provide full relationships between modular values and weak values and also the applications of modular values to quantum paradoxes. To do this,

we proceed the Lagrange interpolation of an exponential function to the case of modular values. We study detail for two and three dimensional Hilbert space cases, and then infer the results to finite-dimensional Hilbert spaces. Later in this chapter, we describe the applications of modular values to the EPR-Bohm paradox, the Hardy paradox, and the Cheshire-cat paradox.

We then generalize the quantum modular values in Chapter 4. By "general," we mean the pointer is treated both finial-dimensional discrete and continuous, and the measured system is generally prepared and postselected in mixed states. The relation of generalized modular values and generalized weak values is also figured out in this Chapter. We finally discuss the usage of the generalized pointer states by analyzing the cases of a spin-s particle pointer, a semiclassical pointer state, and a continuous pointer state as examples.

Time-dependent weak values and modular values will be described in Chapter 5 from the viewpoint of enlarged Hilbert spaces. By introducing an enlarged quantum state which engaged to both preselection and the postselection states, the quantum weak and modular values become the expectation values, which can be measured dynamically.

In Chapter 6, we will express the concept of quantum modular values in the probabilistic representation by using the spectral decomposition. Later in this chapter, we also derive the chain rule of the quantum modular values in term of the conditional probabilities.

Chapter 7 will explain the meaning of quantum modular values as complex values and derive their polar representations. Therein, we demonstrate that the modulus and phase of a modular value are associated with some physical properties. A modulus-phase relation is also discussed and illustrated on a Bloch sphere.

Finally, we will give the conclusions and outlook in Chapter 8. Therein, we extend the possible usages and various applications of the modular values. Our proposal also could motivate and guide further various exciting experiments.

1.4.2 Key results

In this dissertation, we theoretically analyze the concept of quantum modular values for both of the generalized characterization and complex behaviors fundamental understanding. We show generalized relationships between modular and weak values for

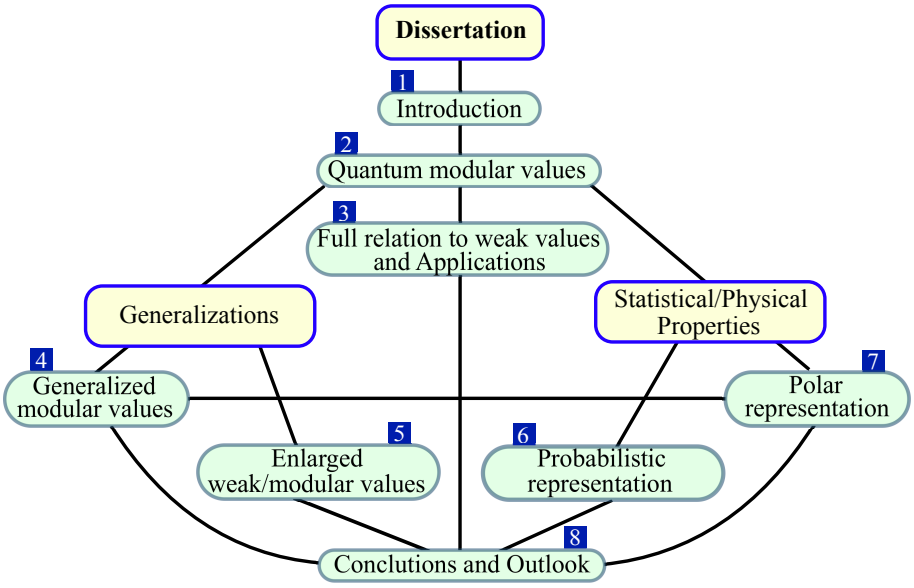

Figure 1.2: "Ship-like" structure of the dissertation.

finite-dimensional systems by analyzing the Lagrange interpolation of the exponential form of the measured observable. One of the important consequences of these relationships is that weak values can be easily deduced from the corresponding measurement results of modular values, which are, in principle, more accessible to measure than weak values. Another critical result is that the *modular-value amplification effect* (MVA), similar to the weak-value case, is also observed in the case of the generalized modular value. Furthermore, the time-dependent enlarged weak and modular values can be entirely interpreted as expectation values of a linear combination of given operators by introducing the enlarged Hilbert space, proposed in this thesis, which might enable us to obtain the weak and modular values at any time dynamically. Finally, this dissertation also provides the significance of complex modular values, where the meaning of the modulus and phase of a modular value in the polar form are connected to primary concepts, such as the conditional probabilities and Pancharatnam phases.

Chapter 2

Quantum modular values

This chapter presents the concept of quantum modular values by analyzing von Neumann measurements for a simple case of a qubit pointer. Particularly, starting from a von Neumann measurement approach, we analyze a postselection measurement of a quantum system with a qubit pointer. The resultant in the qubit pointer, after the postselected in the quantum system, relates to a complex measurement quantity which is named as "modular value." Later in this chapter, we also propose and discuss a simple quantum circuit for modular-value measurement using a control-rotate-Z gate. Even though the primary purpose of this chapter is just to introduced the concept of modular values under the original motivation with the qubit pointer, we will extend this concept to the finite-dimensional discrete pointer (qudit pointer) and the continuous pointer in Chap. 4.

2.1 A brief review to quantum modular values

2.1.1 A von Neumann measurement approach

Following the standard von Neumann treatment [33], an operator $\hat{\boldsymbol{A}}$ on a system Hilbert space $\mathcal{H}_s$ is coupled to an operator $\hat{\boldsymbol{P}}$ on an apparatus Hilbert space $\mathcal{H}_p$ via a time-dependent interaction Hamiltonian of the form

$$\hat{\boldsymbol{H}} = \hbar g(t) \hat{\boldsymbol{A}} \otimes \hat{\boldsymbol{P}}. \tag{2.1}$$

The time-dependent interaction strength $g(t)$ is assumed to be nonzero over the interaction time interval $t \in [0, T]$. For simplicity, we neglect the free evolution of both the system and the pointer by assuming that the measurement is carried out quickly enough as discussed in Chap 1. The interaction Hamiltonian (2.1), therefore is also the total Hamiltonian.

We remind that the Schrödinger equation for the unitary operator $\hat{\boldsymbol{U}}$ is given by

$$i\hbar \frac{\partial \hat{\boldsymbol{U}}}{\partial t} = \hat{\boldsymbol{H}}\hat{\boldsymbol{U}}. \tag{2.2}$$

The solution is straightforwardly given

$$\hat{\boldsymbol{U}} = e^{-ig\hat{\boldsymbol{H}}\otimes\hat{\boldsymbol{P}}} \ , \ \text{with } g = \int_0^T g(t)dt \ , \tag{2.3}$$

where the initial condition $\hat{\boldsymbol{U}}(t = 0) = \hat{\boldsymbol{I}}$, and the coupling constant g is arbitrarily large.

2.1.2 A postselection measurement with a qubit pointer

For more precisely, we consider the apparatus is a two-dimensional discrete pointer which named as *qubit pointer*. The pointer operator $\hat{\boldsymbol{P}}$ is chosen to be a projection operator as

$$\hat{\boldsymbol{P}} \equiv |1\rangle\langle 1|, \tag{2.4}$$

where we have assumed the qubit pointer is spanned by the computation basis $\{|0\rangle, |1\rangle\}$. The initial state of the qubit pointer is chosen to be a superposition state of the two states on the basis as

$$|\xi\rangle = \gamma|0\rangle + \bar{\gamma}|1\rangle, \tag{2.5}$$

where γ and $\bar{\gamma}$ are complex numbers satisfying $|\gamma|^2 + |\bar{\gamma}|^2 = 1$.

The quantum system, which does not have to be a qubit, is conditioned by an initial state vector $|\psi\rangle$. After the interaction as described above, the quantum system is postselected into a final state vector $|\phi\rangle$. The result of the measurement is readout from the qubit pointer as schematically shown in Fig. 2.1 and is given as

$$|\eta\rangle = \langle\phi|e^{-ig\hat{\boldsymbol{A}}\otimes\hat{\boldsymbol{P}}}|\psi\rangle|\xi\rangle. \tag{2.6}$$

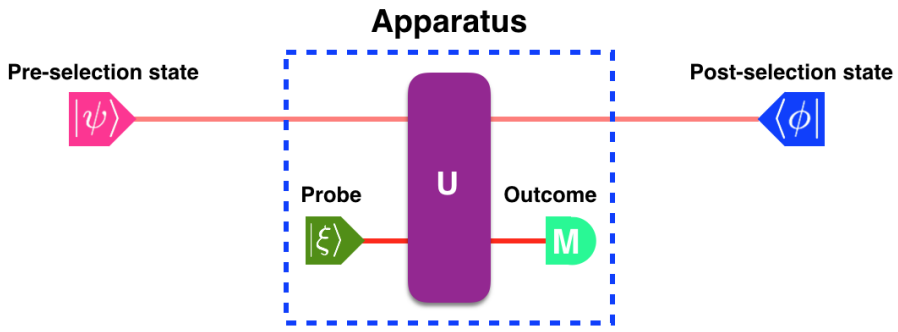

Figure 2.1: A postselection measurement scheme. The system (not necessary being a qubit but could be in a higher dimensional Hilbert space) is conditioned by a preselection state vector $|\psi\rangle$ and a postselection state vector $|\phi\rangle$. The system arbitrarily couples to an apparatus with its initial probe state $|\xi\rangle$. After the postselection in the system, the outcome M in the probe is measured, which gives the result of the measured observable $\hat{\boldsymbol{A}}$ in the system.

The Taylor series expansion for the unitary operator gives

$$e^{-ig\hat{\boldsymbol{A}}\otimes|1\rangle\langle 1|} = \hat{\boldsymbol{I}} + \frac{(-ig\hat{\boldsymbol{A}})}{1!}\otimes|1\rangle\langle 1| + \frac{(-ig\hat{\boldsymbol{A}})^2}{2!}\otimes|1\rangle\langle 1| + ... \tag{2.7}$$

The action on the initial qubit pointer state $|\xi\rangle$ shows that

$$\begin{aligned} e^{-ig\hat{\boldsymbol{A}}\otimes|1\rangle\langle 1|}|\xi\rangle &= \gamma|0\rangle + \bar{\gamma}|1\rangle + \bar{\gamma}\frac{(-ig\hat{\boldsymbol{A}})}{1!}|1\rangle + \bar{\gamma}\frac{(-ig\hat{\boldsymbol{A}})^2}{2!}|1\rangle + ... \\ &= \gamma|0\rangle + \bar{\gamma}e^{-ig\hat{\boldsymbol{A}}}|1\rangle. \end{aligned} \tag{2.8}$$

Submitting Eq. (2.8) into Eq. (2.6), the final pointer state yields

$$|\eta\rangle = \langle\phi|\psi\rangle\left[\gamma|0\rangle + \bar{\gamma}\,\frac{\langle\phi|e^{-ig\hat{\boldsymbol{A}}}|\psi\rangle}{\langle\phi|\psi\rangle}|1\rangle\right]. \tag{2.9}$$

The complex number $\dfrac{\langle\phi|e^{-ig\hat{\boldsymbol{A}}}|\psi\rangle}{\langle\phi|\psi\rangle}$ was named the "modular value" of operator $\hat{\boldsymbol{A}}$ [25], which is written as $(\hat{\boldsymbol{A}})_{\rm m}$

$$(\hat{\boldsymbol{A}})_{\rm m} \equiv \frac{\langle\phi|e^{-ig\hat{\boldsymbol{A}}}|\psi\rangle}{\langle\phi|\psi\rangle}\,. \tag{2.10}$$

2.1.3 Modular values and weak values

Modular values have the same amplification factor $1/\langle\phi|\psi\rangle$ as weak values. Therefore, their values also might lay outside the usual boundaries of measured observables. Apparently, a weak value of an observable is related to the corresponding modular value through

$$\langle\hat{\boldsymbol{A}}\rangle_{\rm w} = i\frac{\partial(\hat{\boldsymbol{A}})_{\rm m}}{\partial g}\Big|_{g\to 0}\,. \tag{2.11}$$

Nevertheless, in some particular cases, the modular value can be related to the weak value. Let us give an example of spin operators $\hat{\boldsymbol{\sigma}}_x, \hat{\boldsymbol{\sigma}}_y$ and $\hat{\boldsymbol{\sigma}}_z$ with $g = -\pi/2$. We have [25]

$$(\hat{\boldsymbol{\sigma}})_{\rm m} \equiv \frac{\langle\phi|e^{i\frac{\pi}{2}\hat{\boldsymbol{\sigma}}}|\psi\rangle}{\langle\phi|\psi\rangle} = i\langle\hat{\boldsymbol{\sigma}}\rangle_{\rm w} \quad (\hat{\boldsymbol{\sigma}} = \hat{\boldsymbol{\sigma}}_x, \hat{\boldsymbol{\sigma}}_y \text{ or } \hat{\boldsymbol{\sigma}}_z)\,. \tag{2.12}$$

Therefore, the modular value of a spin component is directly related to its weak value in this specific case, i.e., $\hat{\boldsymbol{A}} = \hat{\boldsymbol{\sigma}}$ and $g = -\pi/2$ [25].

From the measurement point of view, a modular value is easily obtained because one can just perform the tomography using the binary outcomes of the qubit pointer. On top of it, a modular value can be measured more efficiently than a weak value because the measurement coupling constant g can be made large. To obtain the modular value, we perform a tomography measurement of the final state of the qubit pointer. Assume that the outcome is found to be

$$|\eta\rangle = \alpha|0\rangle + \beta|1\rangle. \tag{2.13}$$

Then comparing with Eq. (2.9) we obtain,

$$(\hat{\boldsymbol{A}})_{\rm m} = \frac{\gamma\beta}{\bar{\gamma}\alpha}. \tag{2.14}$$

2.2 A quantum circuit for modular-value measurements

2.2.1 Controlled-R_Z gate

We present a controlled-rotate-Z gate (= C-$R_{\rm z}(\theta)$ gate) as a simple quantum circuit that possibly implements a modular-value measurement. However, in our scheme, the

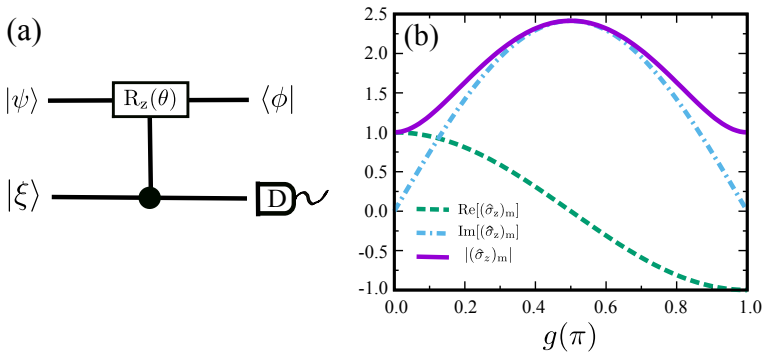

Figure 2.2: (a) Quantum circuit simulates the modular-value measurement. The system is prepared in state $|\psi\rangle$ and postselected to $|\phi\rangle$. The qubit pointer state is prepared as $|\xi\rangle = \gamma|0\rangle + \bar{\gamma}|1\rangle$, and measured on the $\hat{\boldsymbol{\sigma}}_z$ basis. The qubit pointer controls the system whenever its input is $|1\rangle$. The system is rotated θ angle around the z-axis. (b) The modular value as a function of coupling constant $g = \theta/2$. The highest position corresponds to weak value when $g = \pi/2$.

qubit system is controlled by the qubit pointer as is shown in Fig 2.2(a). The rotation $R_z(\theta)$ around the z-axis has the form [27]

$$R_z(\theta) = e^{-i\theta\hat{\boldsymbol{\sigma}}_z/2} = \begin{pmatrix} e^{-i\theta/2} & 0 \\ 0 & e^{i\theta/2} \end{pmatrix} . \tag{2.15}$$

Then, the C-$R_z(\theta)$ gate is given as

$$\hat{\boldsymbol{U}} = \hat{\boldsymbol{I}} \otimes |0\rangle\langle 0| + e^{-i\theta\hat{\boldsymbol{\sigma}}_z/2} \otimes |1\rangle\langle 1| , \tag{2.16}$$

which means the qubit system will rotate iff the qubit pointer is in state $|1\rangle$. Let us choose $\hat{\boldsymbol{P}} = 0|0\rangle\langle 0| + 1|1\rangle\langle 1|$, then this formula can be recast as

$$\hat{\boldsymbol{U}} = e^{-i\theta\hat{\boldsymbol{\sigma}}_z \otimes \hat{\boldsymbol{P}}/2} , \tag{2.17}$$

which is also the unitary operator of a modular-value measurement with $g = \theta/2$ and $\hat{\boldsymbol{A}} = \hat{\boldsymbol{\sigma}}_z$. We, therefore, can extendedly conclude that controlled-rotate gates can simulate modular-value measurements.

2.2.2 Example

As an example, let us choose the pre- and postselected states for the system following [4] as

$$|\psi\rangle = \frac{|\uparrow\rangle + |\downarrow\rangle}{\sqrt{2}} , \tag{2.18}$$

$$|\phi\rangle = \frac{\sqrt{2+\sqrt{2}}|\uparrow\rangle - \sqrt{2-\sqrt{2}}|\downarrow\rangle}{2} , \tag{2.19}$$

where we have used the eigenvalues 1 and -1, and eigenvectors $|\uparrow\rangle$ and $|\downarrow\rangle$ of Pauli matrix $\hat{\boldsymbol{\sigma}}_z$, respectively. The weak value and modular value of $\hat{\boldsymbol{\sigma}}_z$ for arbitrary value of $\theta(=2g)$ can be straightforwardly calculated, which yield

$$\langle\hat{\boldsymbol{\sigma}}_z\rangle_{\mathrm{w}} = 1+\sqrt{2} , \text{ and} \tag{2.20}$$

$$(\hat{\boldsymbol{\sigma}}_z)_{\mathrm{m}} = \cos\frac{\theta}{2} - i(1+\sqrt{2})\sin\frac{\theta}{2} . \tag{2.21}$$

Obviously, in this example, the modular value is complex and its modulus lies outside the range of eigenvalues of $\hat{\boldsymbol{\sigma}}_z$, the same as the weak value, as we can see from Fig. 2.2(b). Moreover, the modulus of the modular value lies between the expectation values and the weak value of observable $\hat{\boldsymbol{\sigma}}_z$, that is, $1 \le |(\hat{\boldsymbol{\sigma}}_z)_{\mathrm{m}}| \le 1+\sqrt{2}$, and coincides with the weak value when $g = \pi/2$ (the center peak in Fig. 2.2(b)). This boundary still holds for all Pauli matrices in this particular example. This example might be tested in the laboratory with the help of the current quantum information technology, which can be implemented by a controlled-rotation gate and might also motive and guide further various exciting experiments.

Chapter 3

Quantum modular values and weak values: full relations and applications to quantum paradoxes

In this chapter, we characterize full relations of modular values to weak values. We apply the Lagrange interpolation approach to a power series function of a given matrix, which later becomes an operator. We also analyze detail for the cases of two- and three-dimensional Hilbert space, and then extend to an arbitrary n-dimension. Afterwards, we present some implications of quantum modular values to the concept of nonlocal joint measurements. We first mathematically demonstrate that a nonlocal joint measurement can be easily described by a modular value. Particularly, the modular value of a sum of measured observables is related to the weak value of the product of these observables. Finally, we apply this result to the quantum paradoxes, i.e., the EPR-Bohm paradox, the Hardy paradox, the Cheshire-cat paradox.

3.1 Full relations of modular values to weak values

In this section, we characterize the full relations of modular values to weak values. When the dimension of the system Hilbert space is two, the modular value of an arbitrary observable is linearly related to the corresponding weak value, for any quantity of the coupling constant. Also, when the dimension n of the Hilbert space is larger than two, the modular value can be expressed in term of weak values up to $(n-1)^{\text{th}}$ order. At first, let us introduce the Lagrange interpolation, which is the main tool for analyzing these relationships.

3.1.1 The Lagrange interpolation

Suppose that we are given a square matrix $\boldsymbol{A} \in \mathbb{C}^{n\times n}$, where n is the range of the matrix $\boldsymbol{A}$, and we want to find $f(\boldsymbol{A})$ for some functions f; e.g., $f(\boldsymbol{A}) = e^{-ig\boldsymbol{A}}$, being defined as a power series. We also assume that the matrix $\boldsymbol{A}$ has n non-degeneracy eigenvalues λ_k $(k = 1, 2, ..., n)$, which are known. The Lagrange interpolation of the matrix form is given, following the theorem in Ref. [34], as

$$e^{-ig\boldsymbol{A}} = \sum_{k=1}^{n} e^{-ig\lambda_k} L_k(\boldsymbol{A}) \,, \tag{3.1}$$

where $L_k(\boldsymbol{A})$ is a Lagrange interpolation coefficient, which is given by a polynomial in $\mathbf{A}$ of degree $n-1$ as

$$L_k(\boldsymbol{A}) = \prod_{\ell=1,\ell\neq k}^{n} \frac{\boldsymbol{A} - \lambda_\ell \boldsymbol{I}}{\lambda_k - \lambda_\ell}, \quad \text{for } k = 1, 2, ..., n \,, \tag{3.2}$$

where $\boldsymbol{I}$ the identity matrix. The proof of this theorem is given in Appendix A.

Taking the eigenvectors of an operator $\hat{\boldsymbol{A}}$ as the orthonormal bases for the matrix expression, i.e., $|a_1\rangle, |a_2\rangle, \cdots, |a_n\rangle$, it is easy to show that

$$\mathrm{e}^{-\mathrm{i}g\hat{\boldsymbol{A}}} = \begin{pmatrix} |a_1\rangle \\ |a_2\rangle \\ \vdots \\ |a_n\rangle \end{pmatrix} \mathrm{e}^{-\mathrm{i}g\boldsymbol{A}} \Big(\langle a_1|, \langle a_2|, \cdots, \langle a_n| \Big) \,, \tag{3.3}$$

where $\boldsymbol{A}$ is the matrix expression of the operator $\hat{\boldsymbol{A}}$. Similarly, it is also straightforward to obtain

$$\prod_{\ell=1,\ell\neq k}^{n}\frac{\hat{\boldsymbol{A}}-\lambda_\ell\hat{\boldsymbol{I}}}{\lambda_k-\lambda_\ell}=\begin{pmatrix}|a_1\rangle\\|a_2\rangle\\:\\|a_n\rangle\end{pmatrix}\prod_{\ell=1,\ell\neq k}^{n}\frac{\boldsymbol{A}-\lambda_\ell\boldsymbol{I}}{\lambda_k-\lambda_\ell}\Big(\langle a_1|,\langle a_2|,\cdots,\langle a_n|\Big)\,. \tag{3.4}$$

Comparing these two Eqs. (3.3) and (3.4) with the help of Eqs. (3.1, 3.2), we obtain the interpolation of operator form as

$$e^{-ig\hat{\boldsymbol{A}}}=\sum_{k=1}^{n}e^{-ig\lambda_k}\prod_{\ell=1,\ell\neq k}^{n}\frac{\hat{\boldsymbol{A}}-\lambda_\ell\hat{\boldsymbol{I}}}{\lambda_k-\lambda_\ell}\,. \tag{3.5}$$

In the following, we apply this decomposition to modular values for particularly two- and three-dimensional system Hilbert space cases. The results then can be expressed to n-dimensional system Hilbert space case.

3.1.2 Two-dimensional Hilbert space

Two-dimensional systems are the simplest non-trivial cases in many physical systems, such as two-level atoms, spin-$\frac{1}{2}$ particles, and attract the most studies on them. For $n=2$, let us assume that an arbitrary observable $\hat{\boldsymbol{A}}$ has two distinguishable eigenvalues λ_1 and λ_2, and then Eq. (3.5) explicitly gives

$$\begin{aligned}e^{-ig\hat{\boldsymbol{A}}}&=e^{-ig\lambda_1}\frac{\hat{\boldsymbol{A}}-\lambda_2\hat{\boldsymbol{I}}}{\lambda_1-\lambda_2}+e^{-ig\lambda_2}\frac{\hat{\boldsymbol{A}}-\lambda_1\hat{\boldsymbol{I}}}{\lambda_2-\lambda_1}\\&=\frac{\lambda_1e^{-ig\lambda_2}-\lambda_2e^{-ig\lambda_1}}{\lambda_1-\lambda_2}\hat{\boldsymbol{I}}+\frac{e^{-ig\lambda_1}-e^{-ig\lambda_2}}{\lambda_1-\lambda_2}\hat{\boldsymbol{A}}\\&=\Lambda\hat{\boldsymbol{I}}+\Lambda'\hat{\boldsymbol{A}}\,,\end{aligned} \tag{3.6}$$

where

$$\Lambda=\frac{\lambda_1e^{-ig\lambda_2}-\lambda_2e^{-ig\lambda_1}}{\lambda_1-\lambda_2}\quad\text{and}\quad\Lambda'=\frac{e^{-ig\lambda_1}-e^{-ig\lambda_2}}{\lambda_1-\lambda_2}$$

are complex numbers.

From the left-hand side of Eq.(3.6), applying pre- and postselection states, $|\psi\rangle$ and $\langle\phi|$, and dividing a nonzero inner product, $\langle\phi|\psi\rangle$, we obtain the modular value of $\hat{\boldsymbol{A}}$.

Repeating the same procedures from the right-hand side, we obtain the corresponding weak value. Then the expression (3.6) yields a linear relation

$$(\hat{\boldsymbol{A}})_{\mathrm{m}} = \Lambda + \Lambda' \langle \hat{\boldsymbol{A}} \rangle_{\mathrm{w}} \ . \tag{3.7}$$

The weak value of $\hat{\boldsymbol{A}}$ can be straightforwardly expressed by inverting its modular value such that

$$\langle \hat{\boldsymbol{A}} \rangle_{\mathrm{w}} = \frac{(\hat{\boldsymbol{A}})_{\mathrm{m}} - \Lambda}{\Lambda'} \ . \tag{3.8}$$

As an illustration, let us consider the case of a spin-$\frac{1}{2}$ operator $\hat{\boldsymbol{\sigma}}$ ($= \hat{\boldsymbol{\sigma}}_x, \hat{\boldsymbol{\sigma}}_y$, or $\hat{\boldsymbol{\sigma}}_z$) with $g = -\pi/2$. In this case, the spin operator has two eigenvalues $\lambda_1 = 1$ for $|\uparrow\rangle$ and $\lambda_2 = -1$ for $|\downarrow\rangle$. Then, the modular value of $\hat{\boldsymbol{\sigma}}$ calculated from Eq. (3.7) immediately yields

$$\begin{aligned} (\hat{\boldsymbol{\sigma}})_{\mathrm{m}} &= \frac{e^{i\frac{\pi}{2}} - e^{-i\frac{\pi}{2}}}{2} \langle \hat{\boldsymbol{\sigma}} \rangle_{\mathrm{w}} + \frac{e^{i\frac{\pi}{2}} + e^{-i\frac{\pi}{2}}}{2} \\ &= i \langle \hat{\boldsymbol{\sigma}} \rangle_{\mathrm{w}} \ . \end{aligned} \tag{3.9}$$

This result is precisely the result obtained by [25] as shown in Eq. (2.12) of this dissertation.

Another example is the projection operator $\hat{\boldsymbol{\Pi}} = |1\rangle\langle 1|$, which has two eigenvalues $\lambda_1 = 1$ for $|1\rangle$ and $\lambda_2 = 0$ for $|0\rangle$. Then for $g = \pi$, we have

$$\begin{aligned} (\hat{\boldsymbol{\Pi}})_{\mathrm{m}} &= \frac{e^{i\pi} - 1}{1} \langle \hat{\boldsymbol{\Pi}} \rangle_{\mathrm{w}} + 1 \\ &= 1 - 2 \langle \hat{\boldsymbol{\Pi}} \rangle_{\mathrm{w}} \ , \end{aligned} \tag{3.10}$$

which is also the same result as [25]. Obviously, our method can reproduce the previous study results.

3.1.3 Three-dimensional Hilbert space

Along with the two-dimensional systems, three-dimensional systems are also well studies which can be realized such as three-level atoms, spin-1 systems. For $n = 3$, a straightforward calculation of Eq. (3.5) for an arbitrary observable $\hat{\boldsymbol{A}}$, which has three distinguishable eigenvalues λ_1, λ_2, and λ_3, yields the result

$$e^{-ig\hat{\boldsymbol{A}}} = \Lambda \hat{\boldsymbol{I}} + \Lambda' \hat{\boldsymbol{A}} + \Lambda'' \hat{\boldsymbol{A}}^2 \ . \tag{3.11}$$

where

$$\Lambda = \frac{-1}{\prod_{\{i,j\}}(\lambda_i - \lambda_j)} \sum_{\{k,l,m\}} e^{-ig\lambda_k} \lambda_l \lambda_m (\lambda_l - \lambda_m) \ ,$$

$$\Lambda' = \frac{1}{\prod_{\{i,j\}}(\lambda_i - \lambda_j)} \sum_{\{k,l,m\}} e^{-ig\lambda_k} (\lambda_l^2 - \lambda_m^2) \ ,$$

$$\text{and} \quad \Lambda'' = \sum_{k=1}^{3} e^{-ig\lambda_k} \prod_{l=1, l\neq k}^{3} \frac{1}{\lambda_k - \lambda_l} \ ,$$

are complex numbers, and $\{i, j\}$ takes $\{1, 2\}$, $\{2, 3\}$, and $\{3, 1\}$, whereas $\{k, l, m\}$ takes $\{1, 2, 3\}$, $\{2, 3, 1\}$, and $\{3, 1, 2\}$. Applying the pre- and postselected states into Eq. (3.11), similarly two-dimensional case, we have the expression for the modular value as

$$(\hat{\boldsymbol{A}})_{\mathrm{m}} = \Lambda + \Lambda' \langle \hat{\boldsymbol{A}} \rangle_{\mathrm{w}} + \Lambda'' \langle \hat{\boldsymbol{A}}^2 \rangle_{\mathrm{w}} \ . \tag{3.12}$$

As an example, let us consider a spin-1 particle with the eigenvalues -1, 0, and 1, which yields $\Lambda = 1$, $\Lambda' = -i\sin(g)$, and $\Lambda'' = \cos(g) - 1$. In this case, Eq.(3.11) becomes

$$e^{-ig\hat{\boldsymbol{A}}} = 1 - i\sin(g)\hat{\boldsymbol{A}} + \big[\cos(g) - 1\big]\hat{\boldsymbol{A}}^2 \ , \tag{3.13}$$

which is also clarified in [35]. And hence Eq. (3.12) yields

$$(\hat{\boldsymbol{A}})_{\mathrm{m}} = 1 - i\sin(g)\langle \hat{\boldsymbol{A}} \rangle_{\mathrm{w}} + \big(\cos(g) - 1\big)\langle \hat{\boldsymbol{A}}^2 \rangle_{\mathrm{w}} \ . \tag{3.14}$$

For n-dimensional Hilbert space, the modular value can be expressed in terms of weak values up to the $(n-1)^{\mathrm{th}}$ order as

$$(\hat{\boldsymbol{A}})_{\mathrm{m}} = \Lambda + \Lambda' \langle \hat{\boldsymbol{A}} \rangle_{\mathrm{w}} + \Lambda'' \langle \hat{\boldsymbol{A}}^2 \rangle_{\mathrm{w}} + ... + \Lambda^{(n-1)\prime} \langle \hat{\boldsymbol{A}}^{n-1} \rangle_{\mathrm{w}} \ . \tag{3.15}$$

As can be seen in this equation, when the dimension of the Hilbert space of the system is finite, the expression for the modular value becomes a finite series of weak values. The advantage of this method is clear when comparing this to a Taylor series expansion, i.e., $e^{-ig\hat{\boldsymbol{A}}} = \hat{I} + (-ig)\hat{\boldsymbol{A}} + ...$, which is, in general, an infinite series.

3.2 Nonlocal joint measurements induced by modular values

3.2.1 Nonlocal observables

Given a set of nonlocal observables $\{\mathbf{\Gamma}\}$ on a multipartite system such that

$$\mathbf{\Gamma} = \{\hat{\mathbf{\Gamma}}_1, \hat{\mathbf{\Gamma}}_2, ..., \hat{\mathbf{\Gamma}}_k, ...\} \,, \tag{3.16}$$

and denoted by $\hat{\mathbf{\Gamma}}_k$ the k^{th} component, for $k = 1, 2, \cdots, N$, in N-partite. $\hat{\mathbf{\Gamma}}_k$ is a Hermitian operator on each $\mathcal{H}_k$ Hilbert subspace. Without loss of generality in assuming $\hat{\mathbf{\Gamma}}_k$ and $\hat{\mathbf{\Gamma}}_l$ commute with each other even for $k \neq l$ since they act in the different subspaces in the total Hilbert space $\mathcal{H} = \otimes_k \mathcal{H}_k$. Therefore, we have

$$e^{\hat{\mathbf{\Gamma}}_k + \hat{\mathbf{\Gamma}}_l} = e^{\hat{\mathbf{\Gamma}}_k} e^{\hat{\mathbf{\Gamma}}_l} \,, \tag{3.17}$$

for N variables. More precisely, we should write this expression as $e^{\hat{\mathbf{\Gamma}}_k \otimes \hat{\boldsymbol{I}}_l + \hat{\boldsymbol{I}}_k \otimes \hat{\mathbf{\Gamma}}_l} = e^{\hat{\mathbf{\Gamma}}_k \otimes \hat{\boldsymbol{I}}_l} e^{\hat{\boldsymbol{I}}_k \otimes \hat{\mathbf{\Gamma}}_l}$, but we avoid this complexity unless things become confusing.

3.2.2 Lagrange interpolation for nonlocal observables

Let $f\{\mathbf{\Gamma}\}$ is a function such that

$$f\{\mathbf{\Gamma}\} \equiv e^{-ig\sum_{k=1}^{N} \hat{\mathbf{\Gamma}}_k}, \tag{3.18}$$

is the exponential function of a sum nonlocal observables. Thus we obtain, with the help of Eq. (3.5)

$$\begin{aligned} e^{-ig\sum_{k=1}^{N} \hat{\mathbf{\Gamma}}_k} &= \prod_{k=1}^{N} e^{-ig\hat{\mathbf{\Gamma}}_k} \\ &= \prod_{k=1}^{N} \left[\sum_{j=1}^{n} e^{-ig\lambda_{j,k}} \prod_{l=1, l\neq j}^{n} \frac{\hat{\mathbf{\Gamma}}_j - \lambda_{j,l}\hat{\boldsymbol{I}}}{\lambda_{k,j} - \lambda_{j,l}} \right] , \end{aligned} \tag{3.19}$$

where we have assumed that the dimension n is the same for all N subsystems. Then, considering the case that the rank of each observable is two, i.e., $n = 2$ for all of k, the modular value of the sum is obtained as

$$\left(\sum_{k}^{N} \hat{\mathbf{\Gamma}}_k \right)_{\text{m}} = \frac{\langle \phi | \prod_{k}^{N} \left(\Lambda_k \hat{\boldsymbol{I}}_k + \Lambda'_k \hat{\mathbf{\Gamma}}_k \right) | \psi \rangle}{\langle \phi | \psi \rangle} \,. \tag{3.20}$$

where

$$\Lambda_k = \frac{\lambda_{k,1}e^{-ig\lambda_{k,2}} - \lambda_{k,2}e^{-ig\lambda_{k,1}}}{\lambda_{k,1} - \lambda_{k,2}} ,$$
$$\text{and} \quad \Lambda'_k = \frac{e^{-ig\lambda_{k,1}} - e^{-ig\lambda_{k,2}}}{\lambda_{k,1} - \lambda_{k,2}} .$$

The expression (3.20) shows the general relation between *the modular value of the sum* and *the weak value of the product* for two-dimensional system operators, $\hat{\mathbf{\Gamma}}_k$. A particular example for N-spin particles (N Pauli matrices) has been shown in Ref. [25]. Now, we calculate the modular value of the sum of two arbitrary system operators $\hat{\boldsymbol{A}}$ and $\hat{\boldsymbol{B}}$. From Eq. (3.20), we have

$$\begin{aligned}(\hat{\boldsymbol{A}} + \hat{\boldsymbol{B}})_{\rm m} &= \frac{\langle\phi|\Big((\Lambda_A\hat{\boldsymbol{I}} + \Lambda'_A\hat{\boldsymbol{A}})(\Lambda_B\hat{\boldsymbol{I}} + \Lambda'_B\hat{\boldsymbol{B}})\Big)|\psi\rangle}{\langle\phi|\psi\rangle} \\ &= \Lambda_A\Lambda_B + \Lambda_A\Lambda'_B\langle\hat{\boldsymbol{B}}\rangle_{\rm w} + \Lambda'_A\Lambda_B\langle\hat{\boldsymbol{A}}\rangle_{\rm w} + \Lambda'_A\Lambda'_B\langle\hat{\boldsymbol{A}}\hat{\boldsymbol{B}}\rangle_{\rm w} . \end{aligned} \tag{3.21}$$

Inversely solving this, we obtain

$$\langle\hat{\boldsymbol{A}}\hat{\boldsymbol{B}}\rangle_{\rm w} = \frac{(\hat{\boldsymbol{A}} + \hat{\boldsymbol{B}})_{\rm m} - \Lambda_B(\hat{\boldsymbol{A}})_{\rm m} - \Lambda_A(\hat{\boldsymbol{B}})_{\rm m} + \Lambda_A\Lambda_B}{\Lambda'_A\Lambda'_B} , \tag{3.22}$$

where we have used $\Lambda'_X\langle\hat{\boldsymbol{X}}\rangle_{\rm w} = (\hat{\boldsymbol{X}})_{\rm m} - \Lambda_X$ ($\hat{\boldsymbol{X}} \equiv \hat{\boldsymbol{A}}$ or $\hat{\boldsymbol{B}}$), which is derived from Eq. (3.7). This relation can be generalized for arbitrary $N > 2$, by repeating the same procedures.

Hereafter, we analyze the EPR paradox, the Hardy paradox and the Cheshire-cat paradox one by one using the relations between modular values and weak values, i.e., Eqs. (3.7, 3.8) and the relations between the modular value of the sum observables and the weak value of the product observables, i.e., Eqs. (3.21, 3.22). Joint weak values can be obtained using Eqs. (3.22), where the modular values on the right-hand side are experimentally obtained. As can be seen in the three examples below, it can be said, from Eq. (3.40), the modular value of the sum observables is easier to measure because one can directly perform the tomography from the outcomes of the qubit pointer. This point has also been claimed by Kedem and Vaidman [25]. It is, therefore, easier to obtain the joint weak values via modular values using our method than to use the previous methods [36–38].

3.3 Applications to quantum paradoxes

3.3.1 The EPR paradox

The paradox

To describe the EPR paradox, we consider the EPR-Bohm experiment with postselection [4, 5, 39]. In this experiment, assuming a pair of spin-$\frac{1}{2}$ particles 1 and 2 in an initial state $|\psi\rangle_{1,2}$ at time t_1 are passed to Alice and Bob, where

$$|\psi\rangle_{1,2} = \frac{1}{\sqrt{2}}\Big(|\uparrow_z\rangle_1|\downarrow_z\rangle_2 - |\downarrow_z\rangle_1|\uparrow_z\rangle_2\Big)\,, \tag{3.23}$$

where the subscript $k(=1,2)$ means particle k, and $|\uparrow_j\rangle$ ($|\downarrow_j\rangle$) denotes the spin up (down) in j direction. At a final time t_2, Alice and Bob perform a post-measurement with $\hat{\boldsymbol{\sigma}}_{1,y}$ and $\hat{\boldsymbol{\sigma}}_{2,x}$, respectively, and obtain certain results (postselection states). At an arbitrary moment t in between t_1 and t_2, let us consider the following three cases as are shown in Fig. 3.1

(i) Only Alice measures $\hat{\boldsymbol{\sigma}}_x$ of particle 1. (Measurement of $\hat{\boldsymbol{\sigma}}_{1,x}$), or

(ii) Only Bob measures $\hat{\boldsymbol{\sigma}}_y$ of particle 2. (Measurement of $\hat{\boldsymbol{\sigma}}_{2,y}$), or

(iii) Alice and Bob make a joint measurement on $\hat{\boldsymbol{\sigma}}_{1,x}\hat{\boldsymbol{\sigma}}_{2,y}$.

It is important that the *joint measurement* is a single measurement $\hat{\boldsymbol{\sigma}}_{1,x}\hat{\boldsymbol{\sigma}}_{2,y}$ without measuring each observable independently. When Alice and Bob perform strong measurements, it is straightforward to calculate the result, which shows [4, 5, 39]

(i) The single measurement of $\hat{\boldsymbol{\sigma}}_{1,x}(t)$ yields $-\hat{\boldsymbol{\sigma}}_{2,x}(t_2)$.

(ii) The single measurement of $\hat{\boldsymbol{\sigma}}_{2,y}(t)$ yields $-\hat{\boldsymbol{\sigma}}_{1,y}(t_2)$.

(iii) The joint measurement of $\hat{\boldsymbol{\sigma}}_{1,x}\hat{\boldsymbol{\sigma}}_{2,y}$, in principle, different from the measurement of both (i) and (ii) separately [39]. However, the product of the single-measurement results for two observables is not equal to the joint-measurement result of the product of the observables. That is the paradox.

Weak values interpretation

This paradox can be expressed by the weak values, with the preselection state is given in Eq. (3.23) and the postselection state is $|\phi\rangle_{1,2} = |\uparrow_y\rangle_1|\uparrow_x\rangle_2$ at time $t_2(> t_1)$, the

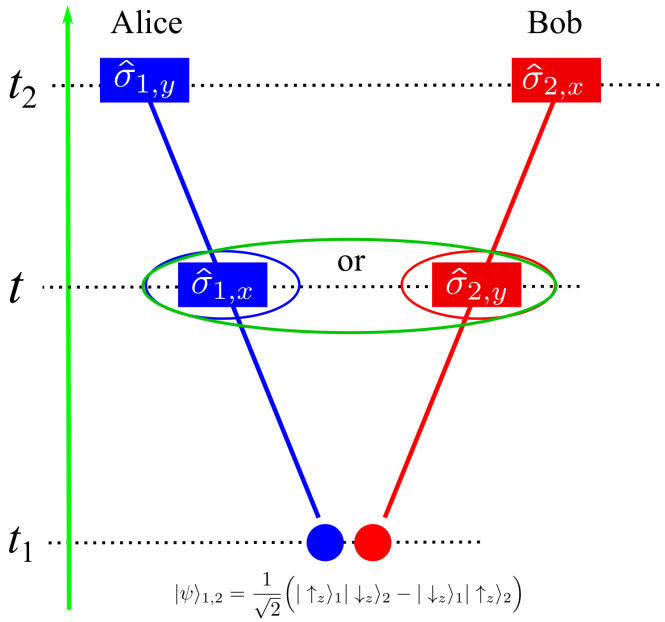

Figure 3.1: The schematic description of EPR-Bohm experiment. At time t_1, a pair of spin-$\frac{1}{2}$ particles, maximally entangled singlet state, is separated to Alice and Bod. They measure their particle with certain results at time t_2. Supporting that at time t ($t_1 < t < t_2$) only Alice measures her particle, or only Bob measures his particle, or they perform a joint measurement as shown in the figure. The paradox here is that the product of single measurements does not equal to the joint measurement.

weak values yield

$$\langle \hat{\boldsymbol{\sigma}}_{1,x} \rangle_{\rm w} = -1, \ \langle \hat{\boldsymbol{\sigma}}_{2,y} \rangle_{\rm w} = -1, \ \text{and} \ \langle \hat{\boldsymbol{\sigma}}_{1,x} \hat{\boldsymbol{\sigma}}_{2,y} \rangle_{\rm w} = -1 \ . \tag{3.24}$$

Obviously, by using the weak values, the measurement results well agree with the above prediction, and it also explains the strange result of the joint measurement.

Modular values interpretation

It is not so easy to experimentally obtain weak values since the measurement strength should be made infinitesimally small (but should not be exactly zero for meaningful measurement). It might be, however, easier to use the modular values since the coupling constant g needs not to be infinitesimally small but can be arbitrarily large. The

modular values are related to weak values as

$$(\hat{\boldsymbol{\sigma}}_{1,x})_{\mathrm{m}} = \cos(g) - i\sin(g)\langle\hat{\boldsymbol{\sigma}}_{1,x}\rangle_{\mathrm{w}} \ , \tag{3.25a}$$

$$(\hat{\boldsymbol{\sigma}}_{2,y})_{\mathrm{m}} = \cos(g) - i\sin(g)\langle\hat{\boldsymbol{\sigma}}_{2,y}\rangle_{\mathrm{w}} \ , \tag{3.25b}$$

$$(\hat{\boldsymbol{\sigma}}_{1,x} + \hat{\boldsymbol{\sigma}}_{2,y})_{\mathrm{m}} = \cos^2(g) - \frac{i}{2}\sin(2g)\big(\langle\hat{\boldsymbol{\sigma}}_{2,y}\rangle_{\mathrm{w}} + \langle\hat{\boldsymbol{\sigma}}_{1,x}\rangle_{\mathrm{w}}\big) - \sin^2(g)\langle\hat{\boldsymbol{\sigma}}_{1,x}\hat{\boldsymbol{\sigma}}_{2,y}\rangle_{\mathrm{w}} \ . \tag{3.25c}$$

Here, Eqs.(3.25a) and (3.25b) are derived from Eq.(3.7) by putting $\lambda_1 = 1$ and $\lambda_2 = -1$, and Eq.(3.25c) is obtained from Eq. (3.21). It should be noted that the "sum rule" does not hold, i.e., the sum of Eqs.(3.25a) and (3.25b) is not equal to (3.25c). The weak values can be obtained from the modular values by reversing Eqs. (3.25). Therefore, the paradox is also explained via modular values.

3.3.2 The Hardy paradox

The paradox

The second example is Hardy's paradox experiment [6–9]. In this setup (Fig.3.2), a monochromatic electron and a positron are respectively put into each Mach-Zehnder interferometer. Each interferometer is independently adjusted so that the monochromatic electron goes out the upper exit without being detected and the monochromatic positron goes out the right exit without being detected. When the two interferometers are overlapped as is shown in the figure, then strange things happen, that is, the electron is sometimes detected by the detector and the positron is sometimes detected by the detector. It is not strange if we know quantum mechanics because it is due to the electron-positron destruction at the overlapping point, whose probability is easily calculated by quantum mechanics. Now we consider only those cases when we have the coincidence counting by the two detectors, that is, we do not register the other events.

In this case, if we try to consider the path of each particle, then we encounter the following paradox. First of all, we cannot assume that the electron took the $|NO_-\rangle$ path because if we assume it, the positron-Mach-Zehnder interferometer is independent on the electron, and in this case, the positron could not be detected since we set the interferometer as such. So, we conclude that the electron took $|O_-\rangle$ path. The same thing can be drawn for the positron, and we conclude that the positron took $|O_+\rangle$ path. Then we encounter the paradox that they should disappear by the collision, which

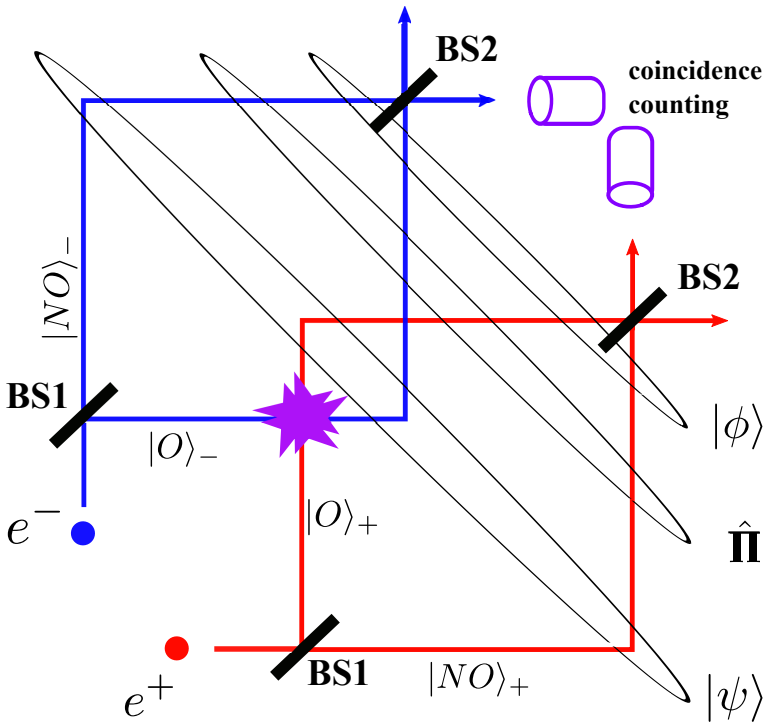

Figure 3.2: The setup for the Hardy paradox, where a monochromatic electron (e^-) and a positron (e^+) are respectively put into each Mach-Zehnder interferometer. Here, state $|O\rangle_-$ (or $|O\rangle_+$) denotes the electron (or positron) that goes to the overlapping region, and the state $|NO\rangle_-$ (or $|NO\rangle_+$) denotes the electron (or positron) that goes to the non-overlapping region. BS means the beam splitter.

contradicts to the fact that we picked up only such cases when we have the coincidence counting. This is the Hardy paradox, and the experiments have been performed using photons instead of an electron and a positron. In this case, Hong-Ou-Mandel interference is used instead of pairwise extinction of a particle and an anti-particle.

Weak values interpretation

We now review the Aharonov's calculations and then use our general theory of the sum of the modular values described in Sec. 3.2. The initial condition (we put a positron from the left and an electron from the bottom) is expressed regarding the states inside

the interferometer as

$$|\psi_0\rangle = \frac{1}{\sqrt{4}}\Big(|O\rangle_+|NO\rangle_- + |NO\rangle_+|O\rangle_- + |NO\rangle_+|NO\rangle_- + |O\rangle_+|O\rangle_-\Big)\,, \tag{3.26}$$

just after passing through BS1. Here, state $|O\rangle_-$ (or $|O\rangle_+$) denotes the electron (or positron) that goes to the overlapping region, and the state $|NO\rangle_-$ (or $|NO\rangle_+$) denotes the electron (or positron) that goes to the non-overlapping region. The subsystem subscript k thus represents $k = +$ (positron) or $-$ (electron). After the pairwise-extinction point, the possibility of $|O\rangle_+|O\rangle_-$ vanishes, which leads to the recalculated state

$$|\psi\rangle = \frac{1}{\sqrt{3}}\Big(|O\rangle_+|NO\rangle_- + |NO\rangle_+|O\rangle_- + |NO\rangle_+|NO\rangle_-\Big)\,, \tag{3.27}$$

where the denominator $\sqrt{4}$ is renormalized into $\sqrt{3}$. Now, we postselect the case that two detectors in Fig. 3.2 click simultaneously. By inversely calculating this back to the point before BS2s, the post-projection state $|\phi\rangle$ is expressed as

$$|\phi\rangle = \frac{1}{2}\Big(|O\rangle_+ - |NO\rangle_+\Big)\Big(|O\rangle_- - |NO\rangle_-\Big)\,. \tag{3.28}$$

Using the prepared state Eq. (3.27) and the postselected state Eq. (3.28), one can calculate the weak value for the "which path?" measurement between $|\psi\rangle$ and $|\phi\rangle$, which leads to

$$\langle\hat{\mathbf{\Pi}}_{+,O}\rangle_{\rm w} = 1,\ \langle\hat{\mathbf{\Pi}}_{-,O}\rangle_{\rm w} = 1,\ \text{and}\ \langle\hat{\mathbf{\Pi}}_{+,O}\hat{\mathbf{\Pi}}_{-,O}\rangle_{\rm w} = 0\,, \tag{3.29}$$

where, $\hat{\mathbf{\Pi}}_{\pm,O} = |O\rangle_\pm\langle O|_\pm$. This means the probability of each case is 1, whereas the joint probability of the two cases is 0. This strange result was predicted by Aharonov *et al.*, [7] and experimentally verified by Lundeen *et al.*, [8] and Yokota *et al.*, [9]. These studies show the significance of the weak values. Weak values adequately explain the paradoxical behavior of the individual probabilities and their joint probability.

Modular values interpretation

Now, we relate weak values to modular values to this case. By performing the same procedure as the first example (EPR paradox), it is easy to obtain the modular values

as follows

$$(\hat{\mathbf{\Pi}}_{+,O})_{\mathrm{m}} = (e^{-ig}-1)\langle\hat{\mathbf{\Pi}}_{+,O}\rangle_{\mathrm{w}} + 1\ , \tag{3.30a}$$

$$(\hat{\mathbf{\Pi}}_{-,O})_{\mathrm{m}} = (e^{-ig}-1)\langle\hat{\mathbf{\Pi}}_{-,O}\rangle_{\mathrm{w}} + 1\ , \quad \text{and} \tag{3.30b}$$

$$(\hat{\mathbf{\Pi}}_{+,O}+\hat{\mathbf{\Pi}}_{-,O})_{\mathrm{m}} = (e^{-ig}-1)\Big[(e^{-ig}-1)\langle\hat{\mathbf{\Pi}}_{+,O}\hat{\mathbf{\Pi}}_{-,O}\rangle_{\mathrm{w}} + \langle\hat{\mathbf{\Pi}}_{+,O}\rangle_{\mathrm{w}} + \langle\hat{\mathbf{\Pi}}_{-,O}\rangle_{\mathrm{w}}\Big] + 1\ . \tag{3.30c}$$

It is easy to express the weak values using the modular values by solving the above equations inversely.

3.3.3 The Cheshire-cat paradox

The paradox

The Cheshire-cat paradox in nature is suggested by the Cheshire cat story in Alice in Wonderland [40]: "Well! I've often seen a cat without a grin," thought Alice; "but a grin without a cat! It's the most curious thing I ever saw in all my life!" In the quantum world, the concept of quantum Cheshire cat was first introduced in [10] and was experimentally verified in [11]. In this paradox, a quantum particle along with a particular property is compared to the Cheshire cat. A Mach-Zehnder interferometer is prepared for the particle, and the particle has the two possibilities in its paths, $|L\rangle$ and $|R\rangle$ and also the same for its property. The "which path?" information reflects the position of the cat's body, and the particle's property is considered to be the cat's grin. For example, Aharonov *et al.*, [10] have considered a photon as the cat's body while its polarization ($|H\rangle$ and $|V\rangle$ polarizations) is the cat's grin. Experientially, by putting a particle-beam attenuator in path L or R, or applying a magnetic field which changes the neutron's spin, Hasegawa's group succeeded in observing that the neutron (the body of the cat) goes through one path whereas its spin (the cat's grin) goes through the other path [11]. This is the paradox.

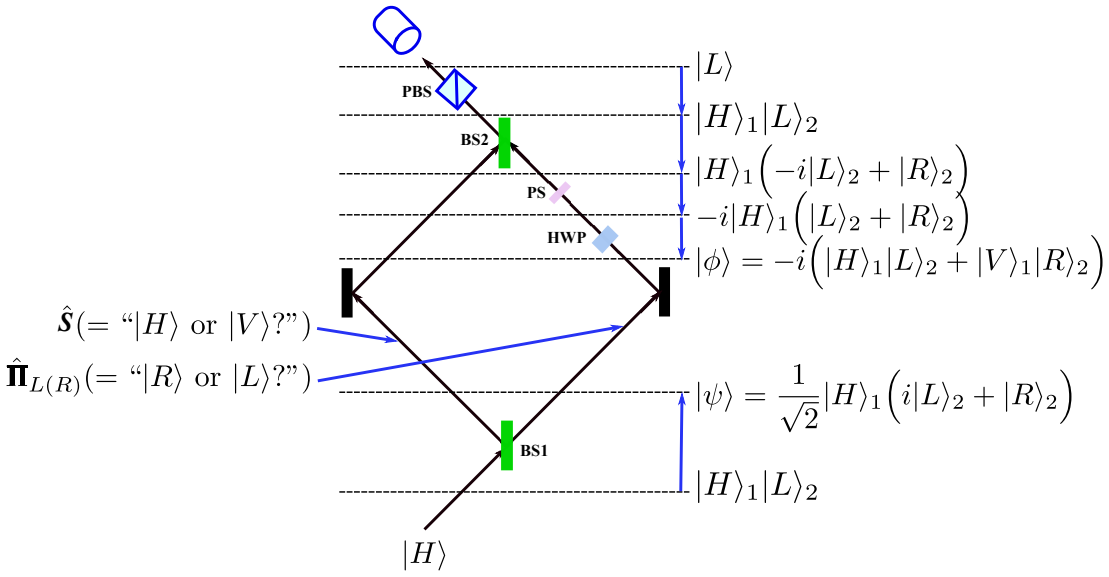

Figure 3.3: Setup for the Cheshire cat, where a horizontally polarized photon is put toward a Mach-Zehnder interferometer. The state $|H\rangle$ ($|V\rangle$) represents horizontally (vertically) polarized photon state, state $|L\rangle$ ($|R\rangle$) is the left (right) of photon path. These other notations are BS: beam splitter, PBS: polarized beam splitter, HWP: half waveplate, PS: phase splitter.

Weak values interpretation

We follow the notation of [10], that is, we assume the initial state of the single photon to be

$$|\psi\rangle=\frac{1}{\sqrt{2}}|H\rangle_1\left(i|L\rangle_2+|R\rangle_2\right), \tag{3.31}$$

which can be prepared by sending a horizontally polarized photon toward a 50/50 beam splitter (BS1 in Fig. 3.3). Here, subscript 1 ($k=1$) denotes the polarization degree of freedom, and 2 ($k=2$) denotes that of the "which path?", and state $|H\rangle$ represents the horizontally polarized photon state. The quantum Cheshire cat is observed when we perform weak measurement on "which-path?" in one arm and weak measurement on the polarization in the other arm conditioned by the subsequent postselection of the projection onto state $|\phi\rangle$

$$|\phi\rangle\equiv\frac{-i}{\sqrt{2}}\left(|H\rangle_1|L\rangle_2+|V\rangle_1|R\rangle_2\right), \tag{3.32}$$

where $|V\rangle$ is the vertically polarized photon state. The result of the weak measurement, as is described below, suggests that the particle travels along one path, whereas its polarization goes along the other. This strange result can be well expressed by the weak values of the measurement. The calculations of the weak values for projection operators $\hat{\mathbf{\Pi}}_{2,k} = |k\rangle\langle k|$ $(k = L, R)$ yield

$$\langle \hat{\mathbf{\Pi}}_{2,L} \rangle_{\mathrm{w}} = 1, \text{ and } \langle \hat{\mathbf{\Pi}}_{2,R} \rangle_{\mathrm{w}} = 0 \, . \tag{3.33}$$

It means that the particle just travels on the left side. Note that these local weak measurements can be performed simultaneously and the measurement at one location does not affect the measurement result at the other location. Next, we carry out the calculations for the nonlocal weak measurement to determine the location of polarization component which yield

$$\langle \hat{\boldsymbol{S}}_1 \hat{\mathbf{\Pi}}_{2,L} \rangle_{\mathrm{w}} = 0, \text{ and } \langle \hat{\boldsymbol{S}}_1 \hat{\mathbf{\Pi}}_{2,R} \rangle_{\mathrm{w}} = 1 \, , \tag{3.34}$$

where $\hat{\boldsymbol{S}} = i(|V\rangle\langle H| - |H\rangle\langle V|)$ [10]. This result implies that the polarization component of the quantum particle located on the right side. The Cheshire cat really exist in the quantum world!

Modular values interpretation

Now, we relate weak values to modular values to this case. Using Eqs. (3.9, 3.10) and Eq. (3.21) for arbitrary g, we have,

$$(\hat{\mathbf{\Pi}}_{2,L(R)})_{\mathrm{m}} = (e^{-ig} - 1)\langle \hat{\mathbf{\Pi}}_{2,L(R)} \rangle_{\mathrm{w}} + 1 \tag{3.35a}$$

$$(\hat{\boldsymbol{S}}_1)_{\mathrm{m}} = \cos(g) - i \sin(g) \langle \hat{\boldsymbol{S}}_1 \rangle_{\mathrm{w}} \tag{3.35b}$$

$$\begin{aligned}(\hat{\boldsymbol{S}}_1 + \hat{\mathbf{\Pi}}_{2,L(R)})_{\mathrm{m}} = \cos(g) - i \sin(g) \langle \hat{\boldsymbol{S}}_1 \rangle_{\mathrm{w}} + \cos(g)(e^{-ig} - 1)\langle \hat{\mathbf{\Pi}}_{2,L(R)} \rangle_{\mathrm{w}} \\ - i \sin(g)(e^{-ig} - 1)\langle \hat{\boldsymbol{S}}_1 \hat{\mathbf{\Pi}}_{2,L(R)} \rangle_{\mathrm{w}} \, .\end{aligned} \tag{3.35c}$$

Substituting Eqs. (3.33) and (3.34) into Eqs.(3.35a)(3.35b)(3.35c), with a specific value of g, such as $g = \pi$ we obtain

$$(\hat{\mathbf{\Pi}}_{2,L})_{\mathrm{m}} = -1 \, , \text{ and } (\hat{\mathbf{\Pi}}_{2,R})_{\mathrm{m}} = 1 \, , \tag{3.36}$$

and

$$(\hat{\boldsymbol{S}}_1 + \hat{\boldsymbol{\Pi}}_{2,L})_{\rm m} = 1 \ , \ \text{ and } \ (\hat{\boldsymbol{S}}_1 + \hat{\boldsymbol{\Pi}}_{2,R})_{\rm m} = -1 \ , \tag{3.37}$$

These expressions give the modular-value expression of the paradox.

3.3.4 Measurements on the two-qubit pointer

In this subsection, we show how to realize such modular-value measurements for these three examples above following the proposed scheme in Ref. [25]. Let us consider the Hamiltonian that describes the interaction between a two-qubit pointer with the two nonlocal observables $\hat{\boldsymbol{A}}$ and $\hat{\boldsymbol{B}}$ as

$$\hat{\boldsymbol{H}} = \hbar g(t) \Big[|1\rangle\langle 1|_1 \otimes \hat{\boldsymbol{A}} + |1\rangle\langle 1|_2 \otimes \hat{\boldsymbol{B}} \Big] \ , \tag{3.38}$$

where both qubits of the pointer are always chosen to be the projection operators in the state $|1\rangle$ of the computation basis. Of course, it also can be a projection onto spin down in the z-direction or a projection onto the vertical polarization. The system observables $\hat{\boldsymbol{A}}$ and $\hat{\boldsymbol{B}}$ are the measured modular values. For example, $\hat{\boldsymbol{A}} = \hat{\boldsymbol{\sigma}}_{1,x}$ and $\hat{\boldsymbol{B}} = \hat{\boldsymbol{\sigma}}_{2,y}$ as in Eq. (3.25); $\hat{\boldsymbol{A}} = \hat{\boldsymbol{\Pi}}_{+,O}$ and $\hat{\boldsymbol{B}} = \hat{\boldsymbol{\Pi}}_{-,O}$ as in Eq. (3.30); and $\hat{\boldsymbol{A}} = \hat{\boldsymbol{S}}_1$ and $\hat{\boldsymbol{B}} = \hat{\boldsymbol{\Pi}}_{2,L(R)}$ as in Eq. (3.35).

Furthermore, the initial state of the two-qubit pointer is prepared in an entangled state

$$\gamma|00\rangle + \bar{\gamma}\Big[|01\rangle + |10\rangle + |11\rangle\Big] \ , \tag{3.39}$$

where $|\gamma|^2 + 3|\bar{\gamma}|^2 = 1$. Then, after the measurement interaction and the postselection of the system state, the final state of the qubits pointer becomes

$$\langle\phi|\psi\rangle \Big\{ \gamma|00\rangle + \bar{\gamma}\Big[(\hat{\boldsymbol{A}})_{\rm m}|01\rangle + (\hat{\boldsymbol{B}})_{\rm m}|10\rangle + \big(\hat{\boldsymbol{A}} + \hat{\boldsymbol{B}}\big)_{\rm m}|11\rangle \Big] \Big\} \ . \tag{3.40}$$

By performing full state tomography on the two-qubit pointer, the modular values of $\hat{\boldsymbol{A}}$, $\hat{\boldsymbol{B}}$, and sum $\hat{\boldsymbol{A}} + \hat{\boldsymbol{B}}$ are well obtained from the tomography states $|01\rangle$, $|10\rangle$, and $|11\rangle$, respectiverly. Then, the weak values can be obtained correspondingly.

Chapter 4

Generalized modular-value-based schemes and generalized modular values

This chapter presents the concept of generalized modular values for both cases of finite-dimensional discrete pointers and continuous pointers. We first generalize the concept of modular values from a qubit pointer in Chap. 2 to a finite-dimensional discrete pointer by introducing a generalized modular-value-based scheme, which is based on the theory of POVM. We also explicitly derive the analytical expressions of the conditional probability, the expectation value, and the average displacement in the measured value of a pointer observable, which we name the pointer quantities. We provide an expression for an adjoint-form modular value and a generalized modular value and discuss the relationship between the generalized modular value and generalized weak values. Subsequently, the adjoint-form modular value also will be given and discussed for the continuous pointer case. Finally, we apply our proposal to the cases of a spin-s particle pointer, a semiclassical pointer state, and a continuous Gaussian pointer state. One of the key results is that the amplification effect, similar to the weak-value case, is also observed in the case of modular values. Our study thus can also apply to the cases of nonclassical pointer states.

4.1 Finite-dimensional pointer states

4.1.1 A POVM approach to postselection measurements

We consider the arbitrarily large interaction of the system observable $\hat{\boldsymbol{A}}$ and the pointer observable $\hat{\boldsymbol{P}}$ via the interaction Hamiltonian and the corresponding evolution operator

$$\hat{\boldsymbol{H}}_I = \hbar\, g(t)\hat{\boldsymbol{A}} \otimes \hat{\boldsymbol{P}}\ ,\ \hat{\boldsymbol{U}} = e^{-ig\hat{\boldsymbol{A}}\otimes\hat{\boldsymbol{P}}}, \text{with } g = \int_0^T g(t)dt. \tag{4.1}$$

as described in Chap. 1 and 2.

We also assume the system is initially prepared in state $\hat{\boldsymbol{\rho}}_i$ while the pointer state is $|\xi\rangle$. The initial joint state of the system and the pointer is given as

$$\hat{\boldsymbol{\rho}} = \hat{\boldsymbol{\rho}}_{\boldsymbol{i}} \otimes |\xi\rangle\langle\xi|\ . \tag{4.2}$$

After the interaction, the joint state evolves in the Schrödinger picture under the unitary interaction to

$$\hat{\boldsymbol{\rho}}' = \hat{\boldsymbol{U}}\hat{\boldsymbol{\rho}}\hat{\boldsymbol{U}}^\dagger\ . \tag{4.3}$$

For a postselection measurement, after the interaction, the system is postselected onto the final state $\hat{\boldsymbol{\rho}}_f \equiv |\phi\rangle\langle\phi|$ and leaves the pointer in $|\mu\rangle$ ($|\mu\rangle$ can be any of the bases). We denote by $P(\mu, f)$ the joint probability, where μ and f are the obtained outcomes indicating that the pointer is found in the state $|\mu\rangle$ and the system in $\hat{\boldsymbol{\rho}}_f$, respectively. By using the theory of the POVM, the joint probability of the system and the pointer reads

$$P(\mu, f) = \mathrm{Tr}\Big[\big(\hat{\boldsymbol{\rho}}_f \otimes |\mu\rangle\langle\mu|\big)\hat{\boldsymbol{\rho}}'\Big] = \mathrm{Tr}_{\mathrm{s}}\Big[\hat{\boldsymbol{\rho}}_f\hat{\boldsymbol{\Omega}}_\mu\hat{\boldsymbol{\rho}}_i\hat{\boldsymbol{\Omega}}_\mu^\dagger\Big]\ , \tag{4.4}$$

where "Tr" denotes the total trace and "Tr_{s}" means the partial trace over the system "s." We denote by $\hat{\boldsymbol{\Omega}}_\mu$ the *Kraus operator* such that

$$\hat{\boldsymbol{\Omega}}_\mu \equiv \langle\mu|e^{-ig\hat{\boldsymbol{A}}\otimes\hat{\boldsymbol{P}}}|\xi\rangle\ , \tag{4.5}$$

which is acting on the system Hilbert space only. It is easy to check that the operators $\hat{\boldsymbol{\Omega}}$ obey the completeness relation $\sum_\mu \hat{\boldsymbol{\Omega}}_\mu^\dagger\hat{\boldsymbol{\Omega}}_\mu = \hat{\boldsymbol{I}}$.

Taking the sum over all μ's in the joint probability, we get the probability for obtaining the postselection outcome $\hat{\boldsymbol{\rho}}_f$ with

$$P(f) = \sum_{\mu} P(\mu, f) = \mathrm{Tr_s}\left[\hat{\boldsymbol{\rho}}_f \hat{\boldsymbol{\rho}}'_i\right] , \tag{4.6}$$

where $\hat{\boldsymbol{\rho}}'_i$ is the system state right after the interaction (before the postselection), which can be obtained by taking the partial trace on the pointer "p" as shown in the following

$$\hat{\boldsymbol{\rho}}'_i = \sum_{\mu} \hat{\boldsymbol{\Omega}}_\mu \hat{\boldsymbol{\rho}}_i \hat{\boldsymbol{\Omega}}^\dagger_\mu = \mathrm{Tr_p}\left[\hat{\boldsymbol{\rho}}'\right] . \tag{4.7}$$

By using the Bayesian rule, the conditional probability for obtaining the outcome μ in the pointer takes the form

$$P(\mu|f) = \frac{P(\mu, f)}{P(f)} = \frac{\mathrm{Tr_s}\left[\hat{\boldsymbol{\rho}}_f \hat{\boldsymbol{\Omega}}_\mu \hat{\boldsymbol{\rho}}_i \hat{\boldsymbol{\Omega}}^\dagger_\mu\right]}{\mathrm{Tr_s}\left[\hat{\boldsymbol{\rho}}_f \hat{\boldsymbol{\rho}}'_i\right]}. \tag{4.8}$$

Particularly, without post-section, i.e., $\hat{\boldsymbol{\rho}}_f = \hat{\boldsymbol{I}}$, the conditional probably reduces to $P(\mu|f) = \mathrm{Tr_s}\left[\hat{\boldsymbol{\Omega}}_\mu \hat{\boldsymbol{\rho}}_i \hat{\boldsymbol{\Omega}}^\dagger_\mu\right]$ and leaves the back action state $\hat{\boldsymbol{\rho}}_i \to \hat{\boldsymbol{\Omega}}_\mu \hat{\boldsymbol{\rho}}_i \hat{\boldsymbol{\Omega}}^\dagger_\mu / P(\mu|f)$ for the outcome μ [27].

We next consider the expectation value of an arbitrary pointer operator and its average displacement. The expectation value of an arbitrary pointer operator, $\hat{\boldsymbol{O}}_\mathrm{p}$, is given by

$$\langle \hat{\boldsymbol{O}}_\mathrm{p} \rangle_\eta = \frac{\mathrm{Tr}[(\hat{\boldsymbol{\rho}}_f \otimes \hat{\boldsymbol{O}}_\mathrm{p})\hat{\boldsymbol{\rho}}']}{\mathrm{Tr}[(\hat{\boldsymbol{\rho}}_f \otimes \hat{\boldsymbol{I}}_\mathrm{p})\hat{\boldsymbol{\rho}}']} , \tag{4.9}$$

where $\langle ... \rangle_\eta$ denotes the expectation value for the final pointer state (denoted as $|\eta\rangle$). After tracing out the pointer Hilbert space and using the spectral decomposition, i.e., $\hat{\boldsymbol{O}}_\mathrm{p} = \sum_k o_k |k\rangle\langle k|$, where o_k denotes the k^{th} eigenvalue of the operator $\hat{\boldsymbol{O}}_\mathrm{p}$ with $\hat{\boldsymbol{O}}_\mathrm{p}|k\rangle = o_k|k\rangle$, we have [see Appendix B.1]

$$\langle \hat{\boldsymbol{O}}_\mathrm{p} \rangle_\eta = \sum_k o_k \frac{\mathrm{Tr_s}[\hat{\boldsymbol{\rho}}_f \hat{\boldsymbol{\Omega}}_k \hat{\boldsymbol{\rho}}_i \hat{\boldsymbol{\Omega}}^\dagger_k]}{\mathrm{Tr_s}[\hat{\boldsymbol{\rho}}_f \hat{\boldsymbol{\rho}}'_i]} = \sum_k o_k P(k|f) , \tag{4.10}$$

where we have used the basis $\{|k\rangle\}$ of the discrete Hilbert space $\mathcal{H}_\mathrm{p}$. We define and calculate the average displacement in the measured value of the pointer observable $\hat{\boldsymbol{O}}_\mathrm{p}$ as

$$\Delta\langle \hat{\boldsymbol{O}}_\mathrm{p} \rangle \equiv \langle \hat{\boldsymbol{O}}_\mathrm{p} \rangle_\eta - \langle \hat{\boldsymbol{O}}_\mathrm{p} \rangle_\xi = \sum_k o_k \Big[P(k|f) - |c_k|^2\Big], \tag{4.11}$$

where $\langle \hat{\boldsymbol{O}}_{\rm p} \rangle_\xi \equiv \langle \xi | \hat{\boldsymbol{O}}_{\rm p} | \xi \rangle$ is the expectation of the pointer observable for the initial pointer state $|\xi\rangle$, and we have defined $c_k \equiv \langle k|\xi\rangle$. The term inside the bracket [...] is the *average displacement* of the probability, which is the difference between probabilities after and before the interaction in the pointer. So, Eq. (4.11) implies that the average displacement in the measured value of the pointer observable is proportional to the average displacement of the probability. The same as weak-value case, an amplification effect appears whenever the average displacement of the pointer observable is very large.

4.1.2 Adjoint-form modular values

Before analyzing the adjoint-form modular values, we also introduce an adjoint operation $({\rm ad}\hat{\boldsymbol{A}})(\cdot) \equiv [\hat{\boldsymbol{A}}, \cdot]$, which is the adjoint action of $\hat{\boldsymbol{A}}$ on its Lie algebra. We are interested in, [32]

$$e^{-ig({\rm ad}\hat{\boldsymbol{A}})}(\cdot) = e^{-ig\hat{\boldsymbol{A}}}(\cdot)e^{ig\hat{\boldsymbol{A}}} \ , \tag{4.12}$$

that we will use for some calculations below.

We consider the case that the initial pointer state is $|\xi\rangle = \sum_k c_k |k\rangle$, where $c_k = \langle k|\xi\rangle$ and $\sum_k |c_k|^2 = 1$, where $k = 0, 1, ..., n-1$, for n-dimensional of the discrete pointer Hilbert space. Furthermore, in the context of the modular measurements, we also choose the pointer operator $\hat{\boldsymbol{P}} = |\lambda\rangle\langle\lambda| = \sum_k \delta_{k\lambda} |k\rangle\langle k|$, is the projection operator into one of the bases of the pointer, where $\delta_{k\lambda}$ is the Kronecker delta function. Then the action of the evolution operator on the pointer state yields $\hat{\boldsymbol{U}}|\xi\rangle = \sum_k c_k e^{-ig\hat{\boldsymbol{A}}\delta_{k\lambda}}|k\rangle$. The Klaus operator reads [see Appendix B.2]

$$\hat{\boldsymbol{\Omega}}_\mu = c_\mu e^{-ig\hat{\boldsymbol{A}}\delta_{\mu\lambda}} \ . \tag{4.13}$$

Then $\hat{\boldsymbol{\rho}}_i'$ straightforwardly yields

$$\hat{\boldsymbol{\rho}}_i' = \sum_\mu \hat{\boldsymbol{\Omega}}_\mu \hat{\boldsymbol{\rho}}_i \hat{\boldsymbol{\Omega}}_\mu^\dagger = \hat{\boldsymbol{\rho}}_i \Big(1 - |c_\lambda|^2\Big)\Big|_{\forall \mu \neq \lambda} + |c_\lambda|^2 e^{-ig\hat{\boldsymbol{A}}} \hat{\boldsymbol{\rho}}_i e^{ig\hat{\boldsymbol{A}}}\Big|_{\mu=\lambda} \ , \tag{4.14}$$

where we have used the completeness relation $\sum_\mu |c_\mu|^2 = 1$, and we also assume $\hat{\boldsymbol{A}}$ is a Hermitian operator during the rest of this chapter. Applying (4.12), the above equation can be recast as

$$\hat{\boldsymbol{\rho}}_i' = \hat{\boldsymbol{\rho}}_i \Big(1 - |c_\lambda|^2\Big)\Big|_{\forall \mu \neq \lambda} + |c_\lambda|^2 e^{-ig({\rm ad}\hat{\boldsymbol{A}})} \hat{\boldsymbol{\rho}}_i\Big|_{\mu=\lambda} \ . \tag{4.15}$$

Substituting Eqs. (4.13) and (4.15) into Eq. (4.8), we obtain

$$P(\mu|f) = \frac{|c_\mu|^2 \mathrm{Tr_s}\left[\hat{\boldsymbol{\rho}}_f e^{-ig(\mathrm{ad}\hat{\boldsymbol{A}})\delta_{\mu\lambda}}\hat{\boldsymbol{\rho}}_i\right]}{\left(1-|c_\lambda|^2\right)\mathrm{Tr_s}\left[\hat{\boldsymbol{\rho}}_f\hat{\boldsymbol{\rho}}_i\right]\Big|_{\forall\mu\neq\lambda} + |c_\lambda|^2\mathrm{Tr_s}\left[\hat{\boldsymbol{\rho}}_f e^{-ig(\mathrm{ad}\hat{\boldsymbol{A}})}\hat{\boldsymbol{\rho}}_i\right]\Big|_{\mu=\lambda}}. \tag{4.16}$$

Particularly, for $\mu \neq \lambda$, we divide a non-zero term $\mathrm{Tr_s}\left[\hat{\boldsymbol{\rho}}_f\hat{\boldsymbol{\rho}}_i\right]$ to both the numerator and denominator, then the conditional probability gives

$$P(\mu \neq \lambda|f) = \frac{|c_\mu|^2}{1-|c_\lambda|^2+|c_\lambda|^2(\mathrm{ad}\hat{\boldsymbol{A}})_\mathrm{m}}\,, \tag{4.17}$$

where we have defined the *adjoint-form modular value* as

$$(\mathrm{ad}\hat{\boldsymbol{A}})_\mathrm{m} \equiv \frac{\mathrm{Tr_s}\left[\hat{\boldsymbol{\rho}}_f e^{-ig(\mathrm{ad}\hat{\boldsymbol{A}})}\hat{\boldsymbol{\rho}}_i\right]}{\mathrm{Tr_s}\left[\hat{\boldsymbol{\rho}}_f\hat{\boldsymbol{\rho}}_i\right]}\,. \tag{4.18}$$

For $\mu = \lambda$, we have

$$P(\mu = \lambda|f) = \frac{|c_\lambda|^2(\mathrm{ad}\hat{\boldsymbol{A}})_\mathrm{m}}{1-|c_\lambda|^2+|c_\lambda|^2(\mathrm{ad}\hat{\boldsymbol{A}})_\mathrm{m}}\,. \tag{4.19}$$

It is easy to prove that the sum of the conditional probabilities of all possible outcomes μ must be $\sum_\mu P(\mu|f) = \sum_{\mu\neq\lambda}[P(\mu\neq\lambda|f)] + P(\mu=\lambda|f) = 1$.

4.1.3 Generalized modular values

In this subsection, we introduce a generalized modular value and connect it to the postselection conditional probability [Eq. (4.8)], the expectation value [Eq. (4.10)] and the average displacement of the measured values of the pointer observable [Eq. (4.11)]. We first introduce an analytic function, which is based on the joint probability and the Kraus operator (4.13), defined by

$$Z(\mu,\nu|\lambda) \;\equiv\; \mathrm{Tr_s}\left[\hat{\boldsymbol{\rho}}_f e^{-ig\hat{\boldsymbol{A}}\delta_{\mu\lambda}}\hat{\boldsymbol{\rho}}_i e^{ig\hat{\boldsymbol{A}}\delta_{\nu\lambda}}\right], \tag{4.20}$$

where the vertical bar "|" means "conditioned by," and ν is an extra integer suffix, which will be used to express the density matrix elements like $\hat{\boldsymbol{\rho}}_{\mu\nu}$. This similar characteristic function for weak values has been introduced and analyzed by Lorenzo [41]. We will show that this analytic function, $Z(\mu,\nu|\lambda)$, is used to express a generalized modular value as below.

The generalized modular value is defined as

$$(\hat{\boldsymbol{A}})_{\rm m}^{\mu,\nu|\lambda} \equiv \frac{Z(\mu,\nu|\lambda)}{Z(\mu'\neq\lambda,\nu'\neq\lambda|\lambda)} = \frac{{\rm Tr_s}\left[\hat{\boldsymbol{\rho}}_f e^{-ig\hat{\boldsymbol{A}}\delta_{\mu\lambda}}\hat{\boldsymbol{\rho}}_i e^{ig\hat{\boldsymbol{A}}\delta_{\nu\lambda}}\right]}{{\rm Tr_s}\left[\hat{\boldsymbol{\rho}}_f\hat{\boldsymbol{\rho}}_i\right]}, \tag{4.21}$$

where, same as before, $\hat{\boldsymbol{\rho}}_i$ is the prepared state, $\hat{\boldsymbol{\rho}}_f$ is the postselected state, μ and ν are the suffixes of density matrix components used in the below. We classify the generalized modular value in the following three cases:

(**i**) $\mu\neq\lambda$ and $\nu\neq\lambda$ case, which both $\mu=\nu$ and $\mu\neq\nu$ are allowed. In this case, the generalized modular value $(\hat{\boldsymbol{A}})_{\rm m}^{\mu,\nu|\lambda}$ becomes unity.

(**ii**) $\mu=\lambda$ and $\nu\neq\lambda$ (or, $\nu=\lambda$ and $\mu\neq\lambda$) case. For $\mu=\lambda$ and $\nu\neq\lambda$, Eq. (4.21) gives

$$(\hat{\boldsymbol{A}})_{\rm m}^{\lambda,\nu|\lambda} \equiv \frac{Z(\mu=\lambda,\nu\neq\lambda|\lambda)}{Z(\mu'\neq\lambda,\nu'\neq\lambda|\lambda)} = \frac{{\rm Tr_s}\left[\hat{\boldsymbol{\rho}}_f e^{-ig\hat{\boldsymbol{A}}}\hat{\boldsymbol{\rho}}_i\right]}{{\rm Tr_s}\left[\hat{\boldsymbol{\rho}}_f\hat{\boldsymbol{\rho}}_i\right]}. \tag{4.22}$$

This expression is reduced to the original definition of the standard modular value [Eq. (2.10)] when both pre- and postselected states are pure states, i.e., $\hat{\boldsymbol{\rho}}_i=|\psi\rangle\langle\psi|$, and $\hat{\boldsymbol{\rho}}_f=|\phi\rangle\langle\phi|$. For $\nu=\lambda$ and $\mu\neq\lambda$, on the other hand, the generalized modular value becomes

$$(\hat{\boldsymbol{A}})_{\rm m}^{\mu,\lambda|\lambda} = \frac{{\rm Tr_s}\left[\hat{\boldsymbol{\rho}}_f\hat{\boldsymbol{\rho}}_i e^{ig\hat{\boldsymbol{A}}}\right]}{{\rm Tr_s}\left[\hat{\boldsymbol{\rho}}_f\hat{\boldsymbol{\rho}}_i\right]} = \left[(\hat{\boldsymbol{A}})_{\rm m}^{\lambda,\mu|\lambda}\right]^* . \tag{4.23}$$

(**iii**) $\mu=\nu=\lambda$ case. Then, we have

$$(\hat{\boldsymbol{A}})_{\rm m}^{\lambda,\lambda|\lambda} \equiv \frac{Z(\mu=\lambda,\nu=\lambda|\lambda)}{Z(\mu'\neq\lambda,\nu'\neq\lambda|\lambda)} = \frac{{\rm Tr_s}\left[\hat{\boldsymbol{\rho}}_f e^{-ig\hat{\boldsymbol{A}}}\hat{\boldsymbol{\rho}}_i e^{ig\hat{\boldsymbol{A}}}\right]}{{\rm Tr_s}\left[\hat{\boldsymbol{\rho}}_f\hat{\boldsymbol{\rho}}_i\right]}, \tag{4.24}$$

which will reduce to the square of the modulus of the standard modular value $|(\hat{\boldsymbol{A}})_{\rm m}|^2$ when the system states are pure. Using $(\hat{\boldsymbol{A}})_{\rm m}^{\mu,\nu|\lambda}=[(\hat{\boldsymbol{A}})_{\rm m}^{\nu,\mu|\lambda}]^*$, $(\hat{\boldsymbol{A}})_{\rm m}^{\lambda,\lambda|\lambda}$ becomes real. We note that there is a similar "generalized" concept for weak values [41, 42], but the way of generalization is very different. This particular case is also the adjoint-form modular value Eq. (4.18) as discussed in the above subsection.

To indices μ and ν explicitly, we consider the final state of the pointer, which is given by

$$\hat{\boldsymbol{\rho}}_{\mathrm{p}}^{\mathrm{out}} = \frac{\mathrm{Tr}_{\mathrm{s}}\left[(\hat{\boldsymbol{\rho}}_f \otimes \hat{\boldsymbol{I}}_{\mathrm{p}})\hat{\boldsymbol{\rho}}'_{\mathrm{sp}}\right]}{\mathrm{Tr}_{\mathrm{sp}}\left[(\hat{\boldsymbol{\rho}}_f \otimes \hat{\boldsymbol{I}}_{\mathrm{p}})\hat{\boldsymbol{\rho}}'_{\mathrm{sp}}\right]} , \tag{4.25}$$

where the denominator is the normalization factor, which equals to the success probability of the postselected of $\hat{\boldsymbol{\rho}}_f$, which is $P(f)$. We can proceed the calculation, as is seen in Appendix B.3, resulting in

$$\begin{aligned}\frac{\mathrm{Tr}_{\mathrm{s}}[(\hat{\boldsymbol{\rho}}_f \otimes \hat{\boldsymbol{I}}_{\mathrm{p}})\hat{\boldsymbol{\rho}}'_{\mathrm{sp}}]}{\mathrm{Tr}_{\mathrm{sp}}[(\hat{\boldsymbol{\rho}}_f \otimes \hat{\boldsymbol{I}}_{\mathrm{p}})\hat{\boldsymbol{\rho}}'_{\mathrm{sp}}]} &= \frac{\sum_{\mu,\nu} c_\mu c_\nu^* (\hat{\boldsymbol{A}})_{\mathrm{m}}^{\mu,\nu|\lambda} |\mu\rangle\langle\nu|}{\sum_\mu |c_\mu|^2 (\hat{\boldsymbol{A}})_{\mathrm{m}}^{\mu,\mu|\lambda}} \\ &= \sum_{\mu,\nu} \left(\hat{\boldsymbol{\rho}}_{\mathrm{p}}^{\mathrm{out}}\right)_{\mu\nu} |\mu\rangle\langle\nu| , \end{aligned} \tag{4.26}$$

where we define $\left(\hat{\boldsymbol{\rho}}_{\mathrm{p}}^{\mathrm{out}}\right)_{\mu\nu} \equiv \dfrac{c_\mu c_\nu^* (\hat{\boldsymbol{A}})_{\mathrm{m}}^{\mu,\nu|\lambda}}{P(f)}$. In this form, we can see that the indicators μ and ν indicate the elements of the pointer density matrix outcome.

We now show the usage of the generalized modular value in the pointer, which gives the attainable outcomes. First, it can be used to express the conditional probabilities. The R.H.S. of Eq. (4.8) is rewritten, using Eqs. (4.13), (4.21), as

$$P(\mu|f) = \frac{|c_\mu|^2 (\hat{\boldsymbol{A}})_{\mathrm{m}}^{\mu,\mu|\lambda}}{1 - |c_\lambda|^2 + |c_\lambda|^2 (\hat{\boldsymbol{A}})_{\mathrm{m}}^{\lambda,\lambda|\lambda}} . \tag{4.27}$$

Clearly, the conditional probabilities satisfy the normalization condition $\sum_\mu P(\mu|f) = 1$.

Since these conditional probabilities appear in Eqs.(4.10) and (4.11), this means that the generalized modular value also characterizes the expectation value of an arbitrary operator $\hat{\boldsymbol{O}}_{\mathrm{p}}$ and its average displacement $\Delta\langle\hat{\boldsymbol{O}}_{\mathrm{p}}\rangle$.

4.1.4 Generalized modular values and generalized weak values

As we mentioned in Chap. 3, the standard modular value and the standard weak value are closely related even for an arbitrarily large coupling g, which allows us to obtain the weak value from the modular value. Here we show that this relation is still valid in the generalized case. Let us illustrate this for cases (**ii**) and (**iii**), while ignoring the trivial

case (**i**) in subsection 4.1.3. Following Chap. 3, for the two-dimensional nondegenerate case, the corresponding exponential term $e^{-ig\hat{\boldsymbol{A}}}$ is given by

$$e^{-ig\hat{\boldsymbol{A}}} = \Lambda\hat{\boldsymbol{I}} + \Lambda'\hat{\boldsymbol{A}}, \tag{4.28}$$

where $\Lambda \equiv \frac{\lambda_1 e^{-ig\lambda_2} - \lambda_2 e^{-ig\lambda_1}}{\lambda_1 - \lambda_2}$, and $\Lambda' \equiv \frac{e^{-ig\lambda_1} - e^{-ig\lambda_2}}{\lambda_1 - \lambda_2}$, with λ_1 and λ_2 are two distinct eigenvalues of the operator $\hat{\boldsymbol{A}}$ (see Chap. 3). Inserting Eq. (4.28) into Eq. (4.22), we have

$$(\hat{\boldsymbol{A}})_{\mathrm{m}}^{\lambda,\nu|\lambda} = \Lambda + \Lambda'\langle\hat{\boldsymbol{A}}\rangle_{\mathrm{w}}, \tag{4.29}$$

where we have used $\langle\hat{\boldsymbol{A}}\rangle_{\mathrm{w}} = \frac{\mathrm{Tr_s}[\hat{\boldsymbol{\rho}}_f\hat{\boldsymbol{A}}\hat{\boldsymbol{\rho}}_i]}{\mathrm{Tr_s}[\hat{\boldsymbol{\rho}}_f\hat{\boldsymbol{\rho}}_i]}$, which is the *generalized weak value* [42]. Similarly, Eq. (4.24) gives

$$(\hat{\boldsymbol{A}})_{\mathrm{m}}^{\lambda,\lambda|\lambda} = \Lambda\Lambda_+ + \Lambda'\Lambda_+\langle\hat{\boldsymbol{A}}\rangle_{\mathrm{w}} + \Lambda\Lambda'_1(\langle\hat{\boldsymbol{A}}\rangle_{\mathrm{w}})^* + \Lambda'\Lambda'_+|\langle\hat{\boldsymbol{A}}\rangle_{\mathrm{w}}|^2, \tag{4.30}$$

where we have also used $\Lambda_+ \equiv \frac{\lambda_1 e^{ig\lambda_2} - \lambda_2 e^{ig\lambda_1}}{\lambda_1 - \lambda_2}$, and $\Lambda'_+ \equiv \frac{e^{ig\lambda_1} - e^{ig\lambda_2}}{\lambda_1 - \lambda_2}$. The last term in Eq. (4.30) can be viewed as a *generalized high-order weak value* [42].

Note that for higher-dimensional Hilbert space, the relation between the generalized modular value and the generalized weak value is still valid, which allows for the measurement of the generalized weak values and generalized high-order weak values from the generalized modular values with an arbitrarily coupling constant g.

In nonlocal observables cases, for simplicity, we consider two nonlocal observables $\hat{\boldsymbol{A}}$ and $\hat{\boldsymbol{B}}$ of the system. The rank of each observable is two. Following Chap. 3, we have

$$e^{-ig(\hat{\boldsymbol{A}}+\hat{\boldsymbol{B}})} = \big(\Lambda_A\hat{\boldsymbol{I}} + \Lambda'_A\hat{\boldsymbol{A}}\big)\big(\Lambda_B\hat{\boldsymbol{I}} + \Lambda'_B\hat{\boldsymbol{B}}\big), \tag{4.31}$$

where $\Lambda_{A(B)}$ and $\Lambda'_{A(B)}$ are the same as Λ and Λ' above for $\hat{\boldsymbol{A}}(\hat{\boldsymbol{B}})$. Inserting this equation into Eq.(4.22), we obtain

$$\begin{aligned}(\hat{\boldsymbol{A}}+\hat{\boldsymbol{B}})_{\mathrm{m}}^{\lambda,\nu|\lambda} &= \Lambda_A\Lambda_B + \Lambda_A\Lambda'_B\frac{\mathrm{Tr_s}[\hat{\boldsymbol{\rho}}_f\hat{\boldsymbol{B}}\hat{\boldsymbol{\rho}}_i]}{\mathrm{Tr_s}[\hat{\boldsymbol{\rho}}_f\hat{\boldsymbol{\rho}}_i]} + \Lambda'_A\Lambda_B\frac{\mathrm{Tr_s}[\hat{\boldsymbol{\rho}}_f\hat{\boldsymbol{A}}\hat{\boldsymbol{\rho}}_i]}{\mathrm{Tr_s}[\hat{\boldsymbol{\rho}}_f\hat{\boldsymbol{\rho}}_i]} + \Lambda'_A\Lambda'_B\frac{\mathrm{Tr_s}[\hat{\boldsymbol{\rho}}_f\hat{\boldsymbol{A}}\hat{\boldsymbol{B}}\hat{\boldsymbol{\rho}}_i]}{\mathrm{Tr_s}[\hat{\boldsymbol{\rho}}_f\hat{\boldsymbol{\rho}}_i]} \\ &= \Lambda_A\Lambda_B + \Lambda_A\Lambda'_B\langle\hat{\boldsymbol{B}}\rangle_{\mathrm{w}} + \Lambda'_A\Lambda_B\langle\hat{\boldsymbol{A}}\rangle_{\mathrm{w}} + \Lambda'_A\Lambda'_B\langle\hat{\boldsymbol{A}}\hat{\boldsymbol{B}}\rangle_{\mathrm{w}},\end{aligned} \tag{4.32}$$

where $(\hat{\boldsymbol{A}}+\hat{\boldsymbol{B}})_{\mathrm{m}}^{\lambda,\nu|\lambda}$ is the generalized modular value of the sum of $\hat{\boldsymbol{A}}$ and $\hat{\boldsymbol{B}}$. The denotation $\langle\boldsymbol{A}\rangle_{\mathrm{w}}$ (or $\langle\hat{\boldsymbol{B}}\rangle_{\mathrm{w}}$) represents the generalized weak value of $\hat{\boldsymbol{A}}$ (or $\hat{\boldsymbol{B}}$), which is related to the generalized modular value $(\hat{\boldsymbol{A}})_{\mathrm{m}}$ (or $(\hat{\boldsymbol{B}})_{\mathrm{m}}$) via Eq. (4.29). $\langle\hat{\boldsymbol{A}}\hat{\boldsymbol{B}}\rangle_{\mathrm{w}}$ is

the generalized weak value of the product of $\hat{\boldsymbol{A}}$ and $\hat{\boldsymbol{B}}$. Equation (4.32) implies that one can measure the generalized weak value of the product of nonlocal observables by measuring the corresponding generalized modular values.

4.2 Continuous pointer states

4.2.1 Momentum-dependent modular values

Now let us consider the continuous pointer states case. We first assume the initial pointer state is a zero-mean Gaussian in position, such that

$$\xi(x) \equiv \langle x|\xi\rangle = (2\pi\sigma^2)^{-1/4}\exp(-x^2/4\sigma^2). \tag{4.33}$$

Using the Fourier transform, we have

$$\xi(p) \equiv \langle p|\xi\rangle = \left(\frac{2\sigma^2}{\pi}\right)^{1/4}\exp(-p^2\sigma^2), \tag{4.34}$$

where we have used $\hbar = 1$. In addition, the pointer operator is chosen to be the momentum

$$\hat{\boldsymbol{P}} \equiv \hat{\boldsymbol{p}}\,. \tag{4.35}$$

Similar the qubit pointer case, the final state of the pointer is

$$|\eta\rangle = \langle\phi|e^{-ig\hat{\boldsymbol{A}}\otimes\hat{\boldsymbol{p}}}|\psi\rangle|\xi\rangle. \tag{4.36}$$

The Taylor series expansion for the unitary operator yields

$$e^{-ig\hat{\boldsymbol{A}}\otimes\hat{\boldsymbol{p}}} = \hat{\boldsymbol{I}} + \frac{(-ig\hat{\boldsymbol{A}})}{1!}\otimes\hat{\boldsymbol{p}} + \frac{(-ig\hat{\boldsymbol{A}})^2}{2!}\otimes\hat{\boldsymbol{p}}^2 + ... \tag{4.37}$$

The action on the initial qubit pointer state $|\xi\rangle \equiv \int dp\,\xi(p)|p\rangle$ gives

$$e^{-ig\hat{\boldsymbol{A}}\otimes\hat{\boldsymbol{p}}}|\xi\rangle = \int dp\,\xi(p)|p\rangle e^{-igp\hat{\boldsymbol{A}}}\,, \tag{4.38}$$

where p is the eigenvalue of $\hat{\boldsymbol{p}}$ such that $\hat{\boldsymbol{p}}|p\rangle = p|p\rangle$. Submitting Eq. (4.38) into Eq. (4.36), the final pointer state yields

$$|\eta\rangle = \langle\phi|\psi\rangle\int dp\,\xi(p)|p\rangle(\hat{\boldsymbol{A}})^p_{\rm m}\,. \tag{4.39}$$

where the modular value, in this case, is given as

$$(\hat{\boldsymbol{A}})^{p}_{\mathrm{m}} \equiv \frac{\langle\phi|e^{-igp\hat{\boldsymbol{A}}}|\psi\rangle}{\langle\phi|\psi\rangle} \ , \tag{4.40}$$

where we have used the superscript p for p-dependent of the modular value. In the following, we will consider a POVM approach for this modular value.

4.2.2 A POVM approach to postselection measurements

We consider the same situation as the finite-discrete pointer state as above section. The Kraus operator is also given as $\hat{\boldsymbol{\Omega}}_{\mu} \equiv \langle\mu|e^{-ig\hat{\boldsymbol{A}}\otimes\hat{\boldsymbol{P}}}|\xi\rangle$ and satisfies the completeness relation $\int \hat{\boldsymbol{\Omega}}^{\dagger}_{\mu}\hat{\boldsymbol{\Omega}}_{\mu}d\mu = \hat{\boldsymbol{I}}$. Here, μ is a continuous variable, such as position x or momentum p. The probability for obtaining the postselection outcome $\hat{\boldsymbol{\rho}}_f$ and the probability for obtaining the postselection conditional pointer outcome μ are given

$$P(f) = \int P(\mu, f)d\mu = \mathrm{Tr_s}\big[\hat{\boldsymbol{\rho}}_f\hat{\boldsymbol{\rho}}'_i\big] \ , \tag{4.41}$$

where

$$\hat{\boldsymbol{\rho}}'_i = \int \hat{\boldsymbol{\Omega}}_{\mu}\hat{\boldsymbol{\rho}}_i\hat{\boldsymbol{\Omega}}^{\dagger}_{\mu}d\mu = \mathrm{Tr_p}[\hat{\boldsymbol{\rho}}'] \ , \tag{4.42}$$

and

$$P(\mu|f) = \frac{P(\mu, f)}{P(f)} = \frac{\mathrm{Tr_s}\big[\hat{\boldsymbol{\rho}}_f\hat{\boldsymbol{\Omega}}_{\mu}\hat{\boldsymbol{\rho}}_i\hat{\boldsymbol{\Omega}}^{\dagger}_{\mu}\big]}{\mathrm{Tr_s}\big[\hat{\boldsymbol{\rho}}_f\hat{\boldsymbol{\rho}}'_i\big]}, \tag{4.43}$$

respectively.

4.2.3 Adjoint-form modular values

The starting point comes from the fact that the pointer momentum $\hat{\boldsymbol{p}}$ does not evolve in the Heisenberg picture $[\hat{\boldsymbol{U}}, \hat{\boldsymbol{I}} \otimes \hat{\boldsymbol{p}}]$, therefore, the Kraus operator yields [32]

$$\hat{\boldsymbol{\Omega}}_p = \langle p|e^{-ig\hat{\boldsymbol{A}}\otimes\hat{\boldsymbol{p}}}|\xi\rangle = e^{-igp\hat{\boldsymbol{A}}}\langle p|\xi\rangle. \tag{4.44}$$

Substituting (4.34) into (4.44), we recast the expression

$$\hat{\boldsymbol{\Omega}}_p = \Big(\frac{2\sigma^2}{\pi}\Big)^{1/4}\exp(-p^2\sigma^2)e^{-igp\hat{\boldsymbol{A}}}. \tag{4.45}$$

As in the discrete case, the system state after the interaction yields

$$\hat{\boldsymbol{\rho}}_i' = \int \hat{\boldsymbol{\Omega}}_p \hat{\boldsymbol{\rho}}_i \hat{\boldsymbol{\Omega}}_p^\dagger dp = \left(\frac{2\sigma^2}{\pi}\right)^{1/2} \int \exp(-2p^2\sigma^2) e^{-igp(\mathrm{ad}\hat{\boldsymbol{A}})} \hat{\boldsymbol{\rho}}_i \, dp \, . \tag{4.46}$$

Then the conditional probability Eq. (4.43) reads

$$P(p|f) = \frac{\exp(-2p^2\sigma^2)(\mathrm{ad}\hat{\boldsymbol{A}})^p_{\mathrm{m}}}{\int \exp(-2p^2\sigma^2)(\mathrm{ad}\hat{\boldsymbol{A}})^p_{\mathrm{m}} \, dp} \, , \tag{4.47}$$

where the adjoint-form modular value is

$$(\mathrm{ad}\hat{\boldsymbol{A}})^p_{\mathrm{m}} = \frac{\mathrm{Tr_s}\left[\hat{\boldsymbol{\rho}}_f e^{-igp(\mathrm{ad}\hat{\boldsymbol{A}})} \hat{\boldsymbol{\rho}}_i\right]}{\mathrm{Tr_s}\left[\hat{\boldsymbol{\rho}}_f \hat{\boldsymbol{\rho}}_i\right]} \, , \tag{4.48}$$

here we have added a superscript p to the adjoint-form modular value to emphasize that it depends on p. It is easy to see that $\int P(p)dp = 1$ since the denominator does not depend on p.

4.3 Applications

In this section, we apply our proposal to the cases of a spin-s particle pointer, a semi-classical pointer state, and a continuous pointer state.

4.3.1 Spin-s particle pointer

We first consider a spin-s particle pointer. We investigate the conditional probability, the expectation value, and the average displacement of an arbitrary operator of the pointer. We also examine the signal-to-noise ratio (SNR) of the spin operator $\hat{\boldsymbol{S}}^z$ to discuss the enhancement of the signal-to-noise ratio.

We represent the spin state in the Zeeman basis with states $|s,k\rangle$, where s takes values 0, $\frac{1}{2}$, 1, $\frac{3}{2}$,..., which corresponds to the $(2s{+}1)$-dimensional Hilbert space, and k takes values $-s, -s+1, \cdots, s$, for a fixed s, which is an integer or a half-integer with the natural unit $\hbar = 1$ [43]. Notable that k are also the eigenvalues of $\hat{\boldsymbol{S}}^z$. Hereafter, we omit the trivial case of $s = 0$.

Next, we choose the initial pointer state (for a fixed s) as

$$|\xi\rangle = \frac{\gamma}{\sqrt{2s}} \sum_{k=-s}^{s-1} |s,k\rangle + \sqrt{1-\gamma^2}|s,s\rangle \, . \tag{4.49}$$

For simplicity, we assume γ is real ($0 \leq \gamma \leq 1$). Also, the projection operator is selected to be $\hat{\boldsymbol{P}} = |s,s\rangle\langle s,s|$; i.e., $|\eta_\lambda\rangle = |s,s\rangle$.

In the system, we also assume that the system is chosen to be a spin-$\frac{1}{2}$ particle and described by the pure pre- and postselected states

$$|\psi\rangle = \frac{1}{\sqrt{2}}\Big(|\uparrow\rangle + |\downarrow\rangle\Big), \tag{4.50}$$

$$|\phi\rangle = \frac{1}{\sqrt{2\epsilon^2 - 2\epsilon + 1}}\Big(\epsilon|\uparrow\rangle - (\epsilon-1)|\downarrow\rangle\Big), \tag{4.51}$$

where we have used the spin orientations $\uparrow$ (up) and $\downarrow$ (down) for z-direction. It should be noted that the choice of the system is not relevant to the pointer, where the dimension can be chosen arbitrarily. We then also choose $\hat{\boldsymbol{A}} \equiv \hat{\boldsymbol{S}}^z = \frac{1}{2}\hat{\boldsymbol{\sigma}}_z$ to be the system observable and $g = \pi$. A straightforward calculation the modular value Eq. (4.24) gives $(\hat{\boldsymbol{A}})^s_{\rm m} = (2\epsilon - 1)^2$. To change the modular value, e.g., from 0 to 9, we vary the parameter ϵ from 0.5 to 2.0 as shown in the Inset Fig. 4.1. Notable that $|\phi\rangle = |\psi\rangle$ when $\epsilon = 0.5$, and they are orthogonal when $\epsilon \to \pm\infty$.

We now calculate the conditional probabilities Eq. (4.27) for the outcomes $\mu = s$ and $\mu \neq s$, which yields

$$P(\mu = s|f) = \frac{(1-\gamma^2)(\hat{\boldsymbol{A}})^s_{\rm m}}{\gamma^2 + (1-\gamma^2)(\hat{\boldsymbol{A}})^s_{\rm m}}, \tag{4.52a}$$

$$P(\mu \neq s|f) = \frac{\gamma^2}{2s\Big[\gamma^2 + (1-\gamma^2)(\hat{\boldsymbol{A}})^s_{\rm m}\Big]}, \tag{4.52b}$$

where we have introduced for short the symbol $(\hat{\boldsymbol{A}})^s_{\rm m} \equiv (\hat{\boldsymbol{A}})^{s,s|s}_{\rm m}$. To see the effect of the modular values to the conditional probability, we calculate the probability displacement $\Delta P(\mu|f) \equiv P(\mu|f) - |c_\mu|^2$, which is the difference between the probabilities after and before the interaction in the pointer. The resultants give

$$\Delta P(\mu = s|f) = \frac{\gamma^2(1-\gamma^2)\big[(\hat{\boldsymbol{A}})^s_{\rm m} - 1\big]}{\gamma^2 + (1-\gamma^2)(\hat{\boldsymbol{A}})^s_{\rm m}}, \tag{4.53a}$$

$$\Delta P(\mu \neq s|f) = \frac{\gamma^2(1-\gamma^2)\big[1 - (\hat{\boldsymbol{A}})^s_{\rm m}\big]}{2s\Big[\gamma^2 + (1-\gamma^2)(\hat{\boldsymbol{A}})^s_{\rm m}\Big]}. \tag{4.53b}$$

Obviously, $\Delta P(\mu = s|f)$(4.53a) is positive when $(\hat{\boldsymbol{A}})^s_{\rm m} > 1$, and negative when $(\hat{\boldsymbol{A}})^s_{\rm m} < 1$, while the behavior for $\Delta P(\mu \neq s|f)$ (4.53b) is opposite.

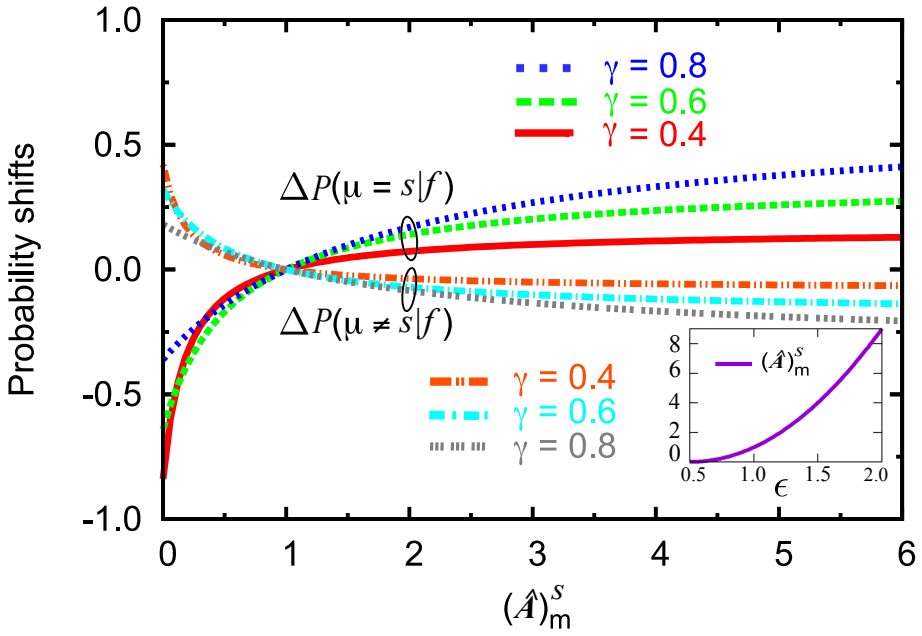

Figure 4.1: The probability displacements $\Delta P(\mu = s|f)$ and $\Delta P(\mu \neq s|f)$ in Eqs. (4.53) as functions of $(\hat{\boldsymbol{A}})^s_{\rm m}$ for $\gamma = 0.4$, 0.6 and 0.8, and $s = 1$, i.e., spin-1 pointer. Inset: the modular value of the system observable $\hat{\boldsymbol{\sigma}}_z/2$ varies as a function of ϵ, where the quantum system states are chosen as in Eqs. (4.50, 4.51), also we fix the value of $g = \pi$.

The main Fig. 4.1 shows the results of $\Delta P(\mu = s|f)$ and $\Delta P(\mu \neq s|f)$ in Eqs. (4.53) as functions of $(\hat{\boldsymbol{A}})^s_{\rm m}$ for $\gamma = 0.4$, 0.6 and 0.8. Here we assumed a three-level pointer, that is, $s = 1$. In general, with increasing $(\hat{\boldsymbol{A}})^s_{\rm m}$ from 1, the probability displacements $\Delta P(\mu = s|f)$ smoothly rise, while the probability displacements $\Delta P(\mu \neq s|f)$ gradually descend. In other words, the modular value plays a significant role in the probability displacements. It can be used to design the measurement interaction to increase the probability of getting the desired outcome, e.g., getting $|s, s\rangle$ after the interaction.

We next examine the expectation value and the average displacement in the measured value of the pointer observable $\hat{\boldsymbol{S}}^z_{\rm p}$, whose eigenvalues are $k = -s, ..., s$. The expectation value, Eq.(4.10), straightforwardly yields

$$\langle \hat{\boldsymbol{S}}^z_{\rm p} \rangle_\eta = \frac{2s(1-\gamma^2)(\hat{\boldsymbol{A}})^s_{\rm m} - \gamma^2}{2\left[\gamma^2 + (1-\gamma^2)(\hat{\boldsymbol{A}})^s_{\rm m}\right]} , \tag{4.54}$$

where we have applied the expressions in Eq. (4.52). The average displacement in the

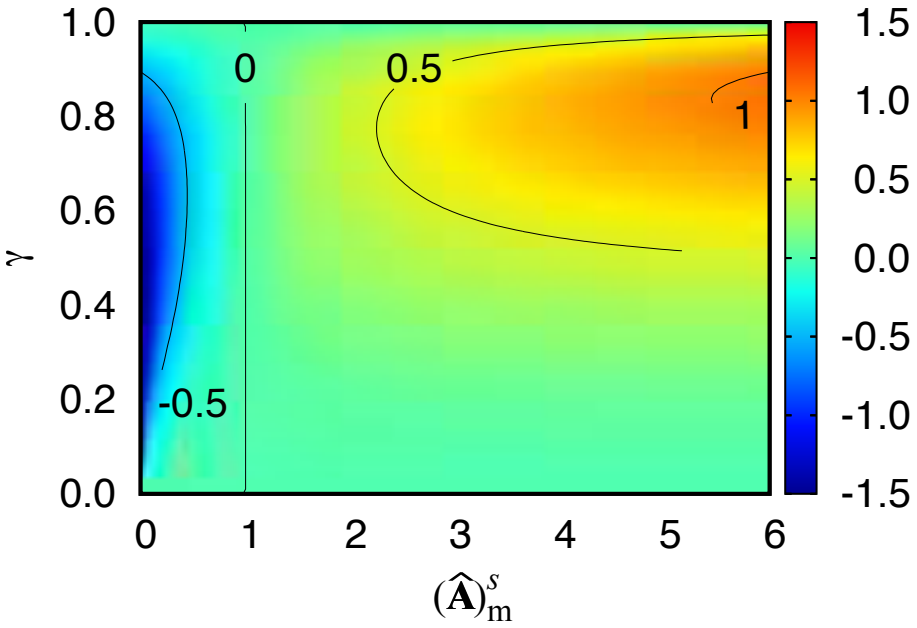

Figure 4.2: Contour plot of the average displacement in the measured value of the pointer observable $\hat{\boldsymbol{S}}^z_{\mathrm{p}}$ of spin-2 ($s = 2$) particle. The vertical line at $(\hat{\boldsymbol{A}})^s_{\mathrm{m}} = 1$ indicates the value zero, which means no "displacement". The quantum system is chosen the same as in Fig. 4.1.

pointer observable is given by Eq. (4.11), being

$$\begin{aligned}\Delta\langle\hat{\boldsymbol{S}}^z_{\mathrm{p}}\rangle &= \sum_k k\Delta P(k|f) \\ &= \frac{(2s+1)\gamma^2(1-\gamma^2)\big[(\hat{\boldsymbol{A}})^s_{\mathrm{m}} - 1\big]}{2\big[\gamma^2 + (1-\gamma^2)(\hat{\boldsymbol{A}})^s_{\mathrm{m}}\big]} \,. \end{aligned} \tag{4.55}$$

Fig. 4.2 presents the result of the average displacement of the pointer observable $\hat{\boldsymbol{S}}^z_{\mathrm{p}}$ of spin-2 ($s = 2$) particle. It shows that, for $(\hat{\boldsymbol{A}})^s_{\mathrm{m}} = 1$ (indicated by the vertical line), the average displacement of $\hat{\boldsymbol{S}}^z_{\mathrm{p}}$ is 0 regardless of the γ value. The figure also shows that, by increasing (or decreasing) $(\hat{\boldsymbol{A}})^s_{\mathrm{m}}$, the amount of displacement can be made large toward positive (or negative) sign direction, and the effect of the increase can be made even greater by choice of γ. Obviously, this tendency can be seen in Eqs. (4.11) and (4.55). This effect can be viewed as the amplification effect in postselected modular-value measurement. This amplification effect has been extensively studied in weak-value measurement both theoretically [1, 12, 29, 44] and experimentally [13, 14], but still lack

in the context of modular-value measurement. Here we first show the existence of this effect in the above example. Notable, in this example, $\hat{\boldsymbol{S}}_{\rm p}^{z}$ does not play a major role in the amplification effect. Instead, the effect might appear for any pointer observable as we showed in Eq. (4.11) with a suitable choice of pre- and postselected states.

Interestingly, all the above results depend on s, which means that the amplification effect depends on the dimension of the pointer Hilbert space $2s+1$. For more investigation regarding the dimension, we next investigate the signal-to-noise ratio (SNR), which is defined by the ratio between the expectation value $\langle\hat{\boldsymbol{S}}_{\rm p}^{z}\rangle_{\eta}$ and the square root of the variance $\sqrt{\mathrm{Var}(\hat{\boldsymbol{S}}_{\rm p}^{z})}$, as follows [45]

$$\mathrm{SNR}=\frac{\left|\langle\hat{\boldsymbol{S}}_{\rm p}^{z}\rangle_{\eta}\right|}{\sqrt{\mathrm{Var}(\hat{\boldsymbol{S}}_{\rm p}^{z})}}, \tag{4.56}$$

where the variance $\mathrm{Var}(\hat{\boldsymbol{S}}_{\rm p}^{z})$ is defined and given by

$$\mathrm{Var}(\hat{\boldsymbol{S}}_{\rm p}^{z})\equiv\langle[\hat{\boldsymbol{S}}_{\rm p}^{z}]^{2}\rangle_{\eta}-\langle\hat{\boldsymbol{S}}_{\rm p}^{z}\rangle_{\eta}^{2}, \tag{4.57}$$

where

$$\langle[\hat{\boldsymbol{S}}_{\rm p}^{z}]^{2}\rangle_{\eta}=\frac{\gamma^{2}\Big[s^{2}+2s^{3}(1-\gamma^{2})(\hat{\boldsymbol{A}})_{\rm m}^{s}+\sum_{k=-s+1}^{s-1}k^{2}\Big]}{2s\big[\gamma^{2}+(1-\gamma^{2})(\hat{\boldsymbol{A}})_{\rm m}^{s}\big]}, \tag{4.58}$$

and $\langle\hat{\boldsymbol{S}}_{\rm p}^{z}\rangle_{\eta}^{2}$ is given in Eq. (4.54). We remind that $\langle...\rangle_{\eta}$ denotes an expectation value for the final pointer state throughout this chapter. Fig. 4.3 presents the signal-to-noise ratio (SNR) for $s=\frac{1}{2},2,\frac{7}{2}$ and 5. It shows that the SNR increase significantly for the larger s cases.

4.3.2 Semiclassical pointer state

In this subsection, we illustrate the usage of our model to the case of the semiclassical pointer state. Here, the initial state of the pointer is a coherent state of bosons as [46]

$$|\xi\rangle\equiv|\alpha\rangle=e^{-\frac{1}{2}|\alpha|^{2}}\sum_{n=0}^{\infty}\frac{\alpha^{n}}{\sqrt{n!}}|n\rangle. \tag{4.59}$$

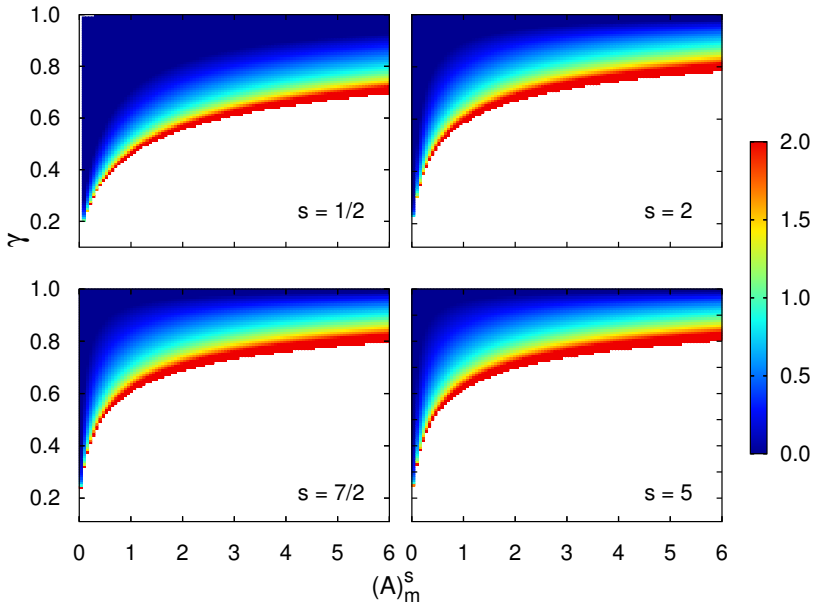

Figure 4.3: The SNRs are shown as functions of $(\hat{\boldsymbol{A}})^s_{\rm m}$ and γ for $s = \frac{1}{2}, 2, \frac{7}{2}$ and 5 as can be seen in each panel. The quantum system is chosen the same as in Fig. 4.1.

The system-pointer interaction is given as $\hat{\boldsymbol{H}} = g(t)\hat{\boldsymbol{A}} \otimes |n\rangle\langle n|$, where $|n\rangle$ is a specifically chosen number state for the pointer, i.e., $|\eta_\lambda\rangle \equiv |n\rangle$. After the interaction, we postselect the system state $\hat{\boldsymbol{\rho}}_f$ and measure the boson number of the pointer and select the case that the final state is $|n\rangle$. So, the outcome μ is chosen to be n, which will be seen in Eq. (4.61).

Before the interaction, the probability of finding the number n is given by the Poisson distribution,

$$P(n) = |\langle n|\alpha\rangle|^2 = \frac{e^{-|\alpha|^2}|\alpha|^{2n}}{n!}\,, \tag{4.60}$$

however, after the interaction, the conditional probability of finding the boson number n is given in Eq. (4.27) as

$$P(n|f) = \frac{P(n)(\hat{\boldsymbol{A}})^n_{\rm m}}{1 - P(n) + P(n)(\hat{\boldsymbol{A}})^n_{\rm m}}\,, \tag{4.61}$$

where $(\hat{\boldsymbol{A}})^n_{\rm m}$ stands for $(\hat{\boldsymbol{A}})^{\mu,\nu|\lambda}_{\rm m}$ with $\mu = \nu = \lambda = n$. In this way, the conditional probability is expressed by the generalized modular value even in this semiclassical

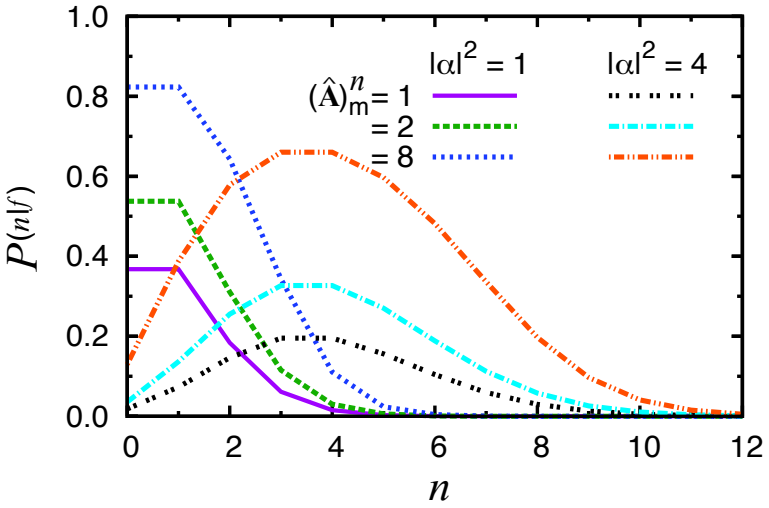

Figure 4.4: The conditional probability-versus-n curves with different modular values $(\hat{\boldsymbol{A}})^n_{\rm m}$ and $|\alpha|^2$. All curves show the increasing with $(\hat{\boldsymbol{A}})^n_{\rm m}$ for each $|\alpha|^2$. This phenomenon can be regarded as the amplification effect of the modular value. The quantum system can be chosen the same as in Fig. 4.1, i.e., interactions between spin and photon.

pointer-state case.

Equation (4.61) can be used, by designing the pre- or postselected states, to increase the measurement signal, e.g., the conditional probability. When the modular value takes 1, Eq. (4.61) tells that $P(n|f) = P(n)$. Now there is a possibility to increase $P(n|f)$ by changing the value of $(\hat{\boldsymbol{A}})^n_{\rm m}$ [47]. To see this, we plotted the conditional probabilities for different modular values $(\hat{\boldsymbol{A}})^n_{\rm m}$ and different values of $|\alpha|^2$ in Fig. 4.4. The results apparently tell that we can increase the conditional probability by increasing the modular value. Furthermore, we predict that our study can be applied to various kind of nonclassical pointer states such as squeezed vacuum state, Schrödinger cat state.

4.3.3 Continuous Gaussian pointer state

We consider the preselection and postselection system states as

$$|\psi\rangle = \frac{1}{\sqrt{2}}\Big[e^{i\theta}|\uparrow\rangle + e^{-i\theta}|\downarrow\rangle\Big]\,, \tag{4.62}$$

$$|\phi\rangle = \frac{1}{\sqrt{2}}\Big[|\uparrow\rangle - |\downarrow\rangle\Big]\,. \tag{4.63}$$

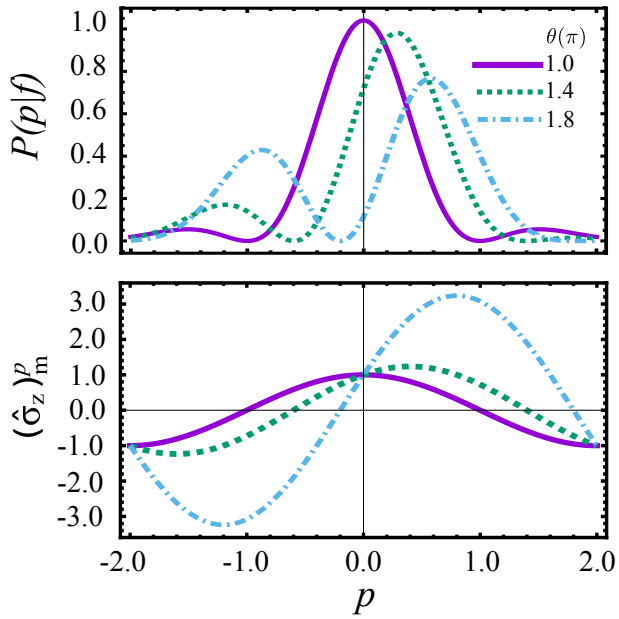

Figure 4.5: The conditional probabilities and modular values as functions of momentum p for fixed $g = \pi/2$ and several values of θ as shown in the figure.

The modular value of $\hat{\boldsymbol{\sigma}}_z$ of the system is calculated to be

$$(\hat{\boldsymbol{\sigma}}_z)^p_{\rm m} = \frac{\sin(\frac{\theta}{2} - gp)}{\sin(\frac{\theta}{2})} \,. \tag{4.64}$$

The corresponding adjoint-form modular value reads

$$({\rm ad}\hat{\boldsymbol{\sigma}}_z)^p_{\rm m} = |(\hat{\boldsymbol{\sigma}}_z)^p_{\rm m}|^2 = \Big|\frac{\sin(\frac{\theta}{2} - gp)}{\sin(\frac{\theta}{2})}\Big|^2 \,, \tag{4.65}$$

which is the square of the modular value. Then the conditional probability (4.47) yields,

$$P(p|f) = 2\sqrt{\frac{2\sigma^2}{\pi}}\exp\big(\frac{g^2}{2\sigma^2} - 2p^2\sigma^2\big)\frac{\sin^2(\theta/2 - gp)}{e^{g^2/2\sigma^2} - \cos\theta}. \tag{4.66}$$

The conditional probabilities and modular values as functions of p for fixed $g = \pi/2$ and several values θ are given in Fig. 4.5. In this subsection, we also fix $\sigma^2 = 0.5$. For each θ, the result shows that the peaks of the probability locate at p's that around the maximum (positive and negative) modular values. Especially, the lower modular value gives the higher probability. This is because the numerator and denominator of (4.47)

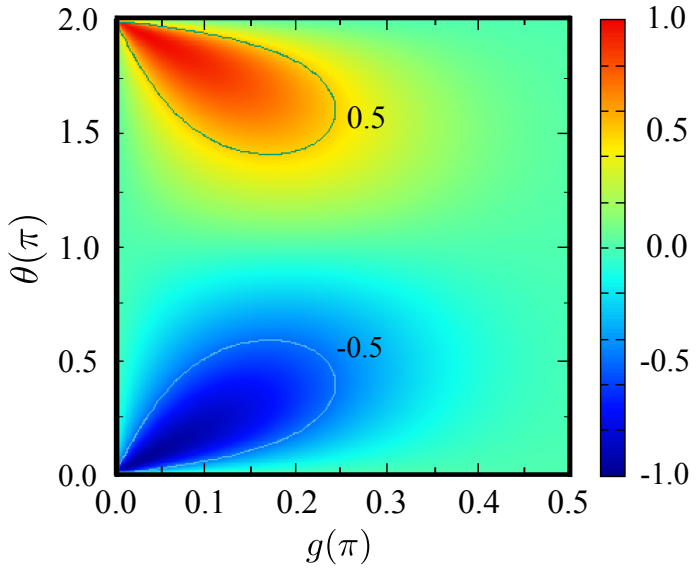

Figure 4.6: The contour plot of the momentum displacement $\Delta\langle\hat{\boldsymbol{p}}\rangle$.

are both dependent on the modular value, and the denominator is varied faster than the numerator as p changes.

We next calculate the momentum displacement $\Delta\langle\hat{\boldsymbol{p}}\rangle$, which is defined and given as

$$\Delta\langle\hat{\boldsymbol{p}}\rangle \equiv \langle\hat{\boldsymbol{p}}\rangle' - \langle\hat{\boldsymbol{p}}\rangle = \frac{g\sin\theta}{2\sigma^2(-e^{g^2/2\sigma^2}+\cos\theta)}\,, \tag{4.67}$$

where the average momentum over the final state is given by

$$\langle\hat{\boldsymbol{p}}\rangle' = \int \hat{\boldsymbol{p}}\; P(p|f)dp, \tag{4.68}$$

and the average momentum over the initial state, $\langle\hat{\boldsymbol{p}}\rangle$, is zero.

In Fig. 4.6, the contour plot of the momentum displacement $\Delta\langle\hat{\boldsymbol{p}}\rangle$ is shown. The result shows that the momentum displacement can change toward from negative to positive when θ changes from 0 to 2π and the value is greater for weak coupling region (small g).

Next, we examine the signal-to-noise ratio which is defined by

$$\mathrm{SNR} \equiv \frac{|\langle\hat{\boldsymbol{p}}\rangle'|}{\sqrt{\mathrm{Var}[\hat{\boldsymbol{p}}]}}\,, \tag{4.69}$$

where $\mathrm{Var}[\hat{\boldsymbol{p}}] \equiv \langle\hat{\boldsymbol{p}}^2\rangle' - \langle\hat{\boldsymbol{p}}\rangle'^2$. Figure 4.7 shows the SNRs as functions of the measurement strength for several θ. For each fixed θ, as g increases, the SNR increases, reaches the

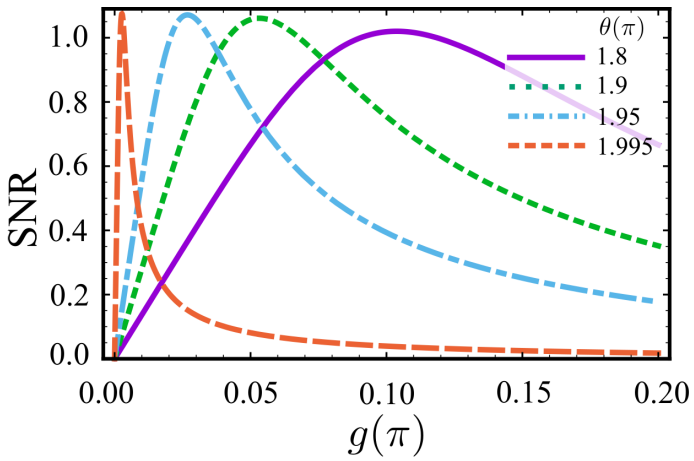

Figure 4.7: The SNRs as functions of the measurement strength for several θ.

maximum value at a certain g and then decreases to zero. The maximum value increases as θ increasing toward to 2π or decreasing toward to 0 due to the symmetry of the initial system state.

Finally, we evaluate the optimal g for a given θ. To do this, we calculate the condition $\partial_g \mathrm{SNR} = 0$, where $\partial_g \equiv \frac{\partial}{\partial g}$. The result gives,

$$g_{\mathrm{opt}} \approx \frac{2\sigma \sin\frac{\theta}{2}}{(2+\cos\theta)^{1/4}} \ , \tag{4.70}$$

that well agrees with results in Fig. 4.7.

Chapter 5

Weak and modular values in enlarged Hilbert spaces

This chapter describes the enlarged forms of time-dependent weak values and modular values. The main idea carries on a way of thinking about an enlarged state, which combines both the pre- and postselection states at a given time t in between the pre- and postselection. Particularly, we first introduce a mapping process of a given quantum state and an arbitrary state onto an enlarged state. The dynamical evolution process of the enlarged system is also discussed. After that, we apply this formalism to the quantum weak and modular values and show that they can be expressed as expectation values in the enlarged space. This formalism thus potentially allows for the description of the weak and modular values at any time dynamically. An example of a single spin under an external magnetic field is also given. We finally propose an efficient method for implementing an enlarged Hamiltonian and applied to the above example.

5.1 Uncausal weak/modular measurements problem

Traditionally, it is believed that the state of a system at time t is solely determined by the initial condition at time t_{i}, both for classical mechanics and quantum mechanics. This fact can be understood by adopting equations of motion with initial conditions. In this manner, the final condition is not relevant since it is merely the result of the natural evolution of the system. However, in the concept of quantum weak values and

modular values, a final condition at time t_f ($> t$) is taken into account via a projection measurement. In this case, the final state plays a role of the posterior condition and affects, together with the initial state, the statistics of the observed values [1]. Thus the initial and final states are equally important to give a complete description of the quantum system [48]. Such kind of theory is known as the two-state vector formalism (see p. 1-8 Ref. [49], and Chap. 13 Ref. [50]).

A weak value can be operationally obtained by weak measurements [1, 29, 51], whereas a modular value can be acquired by arbitrarily strong measurements [25]. In any case, the time t when the measurement is done does not matter if the system stays in the same state during $t_\mathrm{i} \leq t \leq t_\mathrm{f}$. In cases of time-dependent weak values and modular values, however, to obtain a weak (or modular) value at time t, we need to prepare $|\psi\rangle$ at time t_i, wait until t_f, and postselect $|\phi\rangle$ at time t_f, for each choice of t. This can be seen as the uncausal problem in weak/modular measurements.

To solve this problem, in the following, we will propose an enlarged-Hilbert-space method, that enables us to construct a quantum simulator that simulates the original system in such a way that a time-dependent weak (or modular) value in the original scheme is expressed as a one-way evolving expectation value in the enlarged scheme. This means that, by causally running this simulator, we can simulate the time dependence of the weak value, which does not evolve causally but merely is a function of time t that will be known only after the postselection at the final time t_f.

5.2 Enlarged Hilbert space method

An *enlarged Hilbert space formalism* that can be implemented in a quantum simulator is a concept that has been proposed by Solano and his colleagues and has been extensively studied recently both theoretically and experimentally [52–61]. In this method, a given quantum state in a Hilbert space (usually named as *simulated space*) is embedded onto an enlarged state in an *enlarged Hilbert space*. Several manners of mapping have been suggested for different purposes. For example, a mapping that maps a pair of conjugate wave functions (ψ, ψ^*) onto an enlarged real wave function $\tilde{\psi}$ allows us to implement some unphysical operators, such as charge conjugation $\mathcal{C}$, parity inversion $\mathcal{P}$, and time reversal $\mathcal{T}$ [52–55]. It is also applicable to Majorana particles [52–54]. It is

also successfully applied to measurements of the entanglement monotone [56–59]. Using another way of mapping, correlation functions in different reference frames, which are not directly measured, become observables that are directly measured [60]. A noncausal kinematic transformation and time/spatial parity transformations can also be discussed by an expectation value of the enlarged state [60,61].

5.2.1 The enlarged state

We introduce a way of mapping, where a given quantum state, $\psi(t)$, is mapped together with an arbitrary state $\phi(t)$, which we name as a *partner state*, onto an enlarged state $\Psi(t)$. Assume that the given quantum state $|\psi(t)\rangle$ and its partner state $|\phi(t)\rangle$ are live in an n-dimensional Hilbert space $\mathscr{H}_n$, these two states are mapped onto an enlarged state $|\Psi(t)\rangle$ in an enlarged Hilbert space $\mathbb{C}_2 \otimes \mathscr{H}_n$. The mapping $\mathcal{M} : \mathscr{H}_n \to \mathbb{C}_2 \otimes \mathscr{H}_n$, following [60], is

$$\psi(t) \xrightarrow{\mathcal{M}} \Psi(t) = \frac{1}{2}\begin{pmatrix} \psi(t) + \phi(t) \\ \psi(t) - \phi(t) \end{pmatrix}. \tag{5.1}$$

Here we omit ket $|\ \rangle$ vectors for short. Notable, the mapping can be done by adding an extra qubit to the given system that contains the given state and its partner state. This mapping can always be implemented due to the fact that any wave function can be expressed as

$$\psi(t) = \frac{1}{2}\Big(\big[\psi(t) + \phi(t)\big] + \big[\psi(t) - \phi(t)\big] \Big) , \tag{5.2}$$

and therefore, the quantum state and its partner can be decoded by the inverses

$$\psi(t) = \hat{\boldsymbol{M}}\Psi(t) \ , \ \text{and} \ \ \phi(t) = \hat{\boldsymbol{M}}(\hat{\boldsymbol{\sigma}}_z \otimes \hat{\boldsymbol{I}}_n)\Psi(t) \ , \tag{5.3}$$

where $\hat{\boldsymbol{M}} \equiv (1,1) \otimes \hat{\boldsymbol{I}}_n$, with $\hat{\boldsymbol{I}}_n$ is the n-dimensional identity matrix.

5.2.2 The enlarged Schrödinger equation

We now treat the dynamics of the Schrödinger equation in the enlarged Hilbert space. Notable that the quantum state satisfies the Schrödinger equation

$$(i\partial_t - \hat{\boldsymbol{H}})\psi(t) = 0 \ , \tag{5.4}$$

with the initial condition $\psi(t=0)$, and $\hat{\boldsymbol{H}}$ is the system Hamiltonian in the original Hilbert space $\mathscr{H}_n$. We want to map this equation onto the one in the enlarged Hilbert space that satisfies

$$(i\partial_t - \widetilde{\hat{\boldsymbol{H}}})\Psi(t) = 0\ , \tag{5.5}$$

as proposed in Ref. [56]. Here $\widetilde{\hat{\boldsymbol{H}}}$ is the enlarged Hamiltonian in the enlarged Hilbert space $\mathbb{C}_2 \otimes \mathscr{H}_n$. Following [56], if the state $\Psi(t)$ is the solution of Eq.(5.5) with the initial condition $\Psi(t=0)$, then the state $\hat{\boldsymbol{M}}\Psi(t)$ is the solution of the Schrödinger equation (5.4) with the initial condition $\hat{\boldsymbol{M}}\Psi(t=0)$. Here, in our mapping (5.1), they are both satisfied, such that

$$\psi(t=0) = \hat{\boldsymbol{M}}\Psi(t=0), \text{ and } \psi(t) = \hat{\boldsymbol{M}}\Psi(t). \tag{5.6}$$

Applying $\hat{\boldsymbol{M}}$ into Eq. (5.5), we have

$$\begin{aligned} i\partial_t \hat{\boldsymbol{M}}\Psi(t) =& \hat{\boldsymbol{M}}\widetilde{\hat{\boldsymbol{H}}}\Psi(t) \\ i\partial_t \psi(t) \overset{(5.6)}{=}& \\ \hat{\boldsymbol{H}}\psi(t) \overset{(5.4)}{=}& \\ \hat{\boldsymbol{H}}\hat{\boldsymbol{M}}\Psi(t) \overset{(5.6)}{=}& \end{aligned} \tag{5.7}$$

Or, we obtain the condition $\hat{\boldsymbol{M}}\widetilde{\hat{\boldsymbol{H}}} = \hat{\boldsymbol{H}}\hat{\boldsymbol{M}}$. With this condition we obtain

$$\widetilde{\hat{\boldsymbol{H}}} = \begin{pmatrix} \hat{\boldsymbol{C}} & \hat{\boldsymbol{B}} \\ \hat{\boldsymbol{B}} & \hat{\boldsymbol{C}} \end{pmatrix} = \hat{\boldsymbol{I}}_2 \otimes \hat{\boldsymbol{C}} + \hat{\boldsymbol{\sigma}}_x \otimes \hat{\boldsymbol{C}}\ , \tag{5.8}$$

where $\hat{\boldsymbol{B}}$ is an arbitrary $n \times n$ matrix and $\hat{\boldsymbol{C}} \equiv \hat{\boldsymbol{H}} - \hat{\boldsymbol{B}}$, and $\hat{\boldsymbol{I}}_2$ is the 2-dimensional identity matrix.

We next discuss the initial state of the enlarged expression. In fact, any $\Psi(0)$ that gives $\psi(0) = \hat{\boldsymbol{M}}\Psi(0)$ is not enough. This is different from the case of [60], because, here we can freely choose the partner state independent from the initial state of the system. Therefore, a proper choice would take into account to the partner state at the initial time. The proper choice depends on each problem, and later we will show that we choose the initial partner state $\phi(t=0)$ as the backwardly propagated state from the postselected state $\phi(t_{\mathrm{f}}) \equiv |\phi\rangle$.

5.3 Time-dependent quantum weak and modular values

Most of the studies on weak values and modular values have focused on the interaction Hamiltonian between a quantum system and a measuring device for the case without the time evolution of the system. There are only a few studies on time-dependent weak values [62–64]. These studies, however, mainly focused on the time evolutions of the pre- and postselection states. They were lacking in discussion on how to measure (or obtain) time-dependent weak values. They instead mathematically consider the related effects caused by time-dependent weak values. Here, we also consider the evolution of the quantum system in describing the weak values and modular values. The main scope is to express them as expectation values evolving only by an enlarged initial condition in the enlarged system. Therefore, the enlarged weak values and modular values could be measured directly (measurements of expectation values) at the given time t.

5.3.1 Time-dependent weak values in a normal Hilbert space

We first introduce the process for time-dependent weak values in normal Hilbert spaces, i.e., not enlarged spaces. The process can be described as follows. A quantum system was prepared at time t_i in the identical quantum states $|\psi(t_\mathrm{i})\rangle$. The initial state propagates from time t_i by the unitary propagator $\hat{\boldsymbol{U}}(t,t_\mathrm{i}) = \exp(-\frac{i}{\hbar}\int_{t_\mathrm{i}}^{t}\hat{\boldsymbol{H}}d\tau)$ to time t ($> t_\mathrm{i}$) when the weak measurement is performed. Here, $\hat{\boldsymbol{H}}$ is the free Hamiltonian of the system, which takes place in the Hilbert space $\mathscr{H}_n$. The state just before the measurement is thus $\hat{\boldsymbol{U}}(t,t_\mathrm{i})|\psi(t_\mathrm{i})\rangle$. After weak interaction at time t, the system again evolves freely towards the final time t_f ($> t$) under the same propagator and then postselects in state $|\phi(t_\mathrm{f})\rangle$ at that time. In general, the postselection state does not need to be the freely evolved preselection state, i.e., $|\phi(t_\mathrm{f})\rangle \neq |\psi(t_\mathrm{f})\rangle$. The postselection state at time t can be obtained from the backward propagation of the postselection state from time t_f to time t. The connection between the forward and backward evolutions is given by $\hat{\boldsymbol{U}}(t_\mathrm{f},t) = \hat{\boldsymbol{U}}^{-1}(t,t_\mathrm{f}) = \hat{\boldsymbol{U}}^{\dagger}(t,t_\mathrm{f})$ [65]. Therefore, the final state of the system propagates toward the past with $\langle\phi(t)| = \langle\phi(t_\mathrm{f})|\hat{\boldsymbol{U}}^{\dagger}(t,t_\mathrm{f})$. Then, the quantum weak value of a Hermitian operator $\hat{\boldsymbol{A}}$ at time t ($t_\mathrm{i} < t < t_\mathrm{f}$), is expressed as

$$\langle\hat{\boldsymbol{A}}(t)\rangle_\mathrm{w} = \frac{\langle\phi(t_\mathrm{f})|\hat{\boldsymbol{U}}^{\dagger}(t,t_\mathrm{f})|\hat{\boldsymbol{A}}\hat{\boldsymbol{U}}(t,t_\mathrm{i})|\psi(t_\mathrm{i})\rangle}{\langle\phi(t_\mathrm{f})|\hat{\boldsymbol{U}}^{\dagger}(t,t_\mathrm{f})\hat{\boldsymbol{U}}(t,t_\mathrm{i})|\psi(t_\mathrm{i})\rangle}\,. \tag{5.9}$$

We next introduce "retarded" and "advanced" states at any time t, with $t_\mathrm{i} < t < t_\mathrm{f}$, that satisfy [66]:

$$|\psi_r(t)\rangle = \hat{\boldsymbol{U}}(t, t_\mathrm{i})|\psi(t_\mathrm{i})\rangle \ , \quad \text{and} \tag{5.10a}$$

$$|\phi_a(t)\rangle = \hat{\boldsymbol{U}}(t, t_\mathrm{f})|\phi(t_\mathrm{f})\rangle \ . \tag{5.10b}$$

These expressions describe the forward evolution of the preselection state from t_i to t and the backward evolution of the postselection state from t_f to t, respectively. By using Eqs.(5.10), the weak value can be rewritten as follows

$$\langle \hat{\boldsymbol{A}}(t)\rangle_\mathrm{w} = \frac{\langle \phi_a(t)|\hat{\boldsymbol{A}}|\psi_r(t)\rangle}{\langle \phi_a(t)|\psi_r(t)\rangle} \ . \tag{5.11}$$

5.3.2 Time-dependent weak values in an enlarged Hilbert space: expectation-value forms

In this subsection, we aim to express weak values, which are conventionally defined with so-called two-state vector formalism, by single-state formalism such as expectation values. It can be done by embedding the retarded and advanced states, onto an enlarged state by using our mapping method described in section 5.2. Indeed, the mapping (5.1), would give

$$\Psi(t) = \frac{1}{2}\begin{pmatrix} \psi_r(t) + \phi_a(t) \\ \psi_r(t) - \phi_a(t) \end{pmatrix}, \tag{5.12}$$

where we have chosen $\psi(t) = \psi_r(t)$ and $\phi(t) = \phi_a(t)$ in (5.1). The retarded and advanced states, of course, can be decoded by

$$\psi_r(t) = \hat{\boldsymbol{M}}\Psi(t), \ \text{and} \ \phi_a(t) = \hat{\boldsymbol{M}}(\hat{\boldsymbol{\sigma}}_z \otimes \hat{\boldsymbol{I}}_n)\Psi(t). \tag{5.13}$$

Then, the weak value in the enlarged Hilbert space is given, using Eqs. (5.11) and (5.13) as

$$\langle \hat{\boldsymbol{A}}(t)\rangle_\mathrm{w} = \frac{\langle \Psi(t)|(\hat{\boldsymbol{\sigma}}_z + i\hat{\boldsymbol{\sigma}}_y) \otimes \hat{\boldsymbol{A}}|\Psi(t)\rangle}{\langle \Psi(t)|(\hat{\boldsymbol{\sigma}}_z + i\hat{\boldsymbol{\sigma}}_y) \otimes \hat{\boldsymbol{I}}_n|\Psi(t)\rangle} \ , \tag{5.14}$$

which completes the description of the weak value of the system observable $\hat{\boldsymbol{A}}$ by the time dependence of the enlarged state $|\Psi(t)\rangle$. Furthermore, the weak value now has

the form of a causal dynamics of the *expectation value*, i.e., the ordinary single-state formalism for an enlarged system operator, $\hat{\boldsymbol{\sigma}}_z \otimes \hat{\boldsymbol{A}} + i\hat{\boldsymbol{\sigma}}_y \otimes \hat{\boldsymbol{A}}$. Note that, although this operator is not a Hermitian operator, its expectation value is experimentally obtainable since it is a linear combination of two Hermitian operators.

In the enlarged system, if an appropriate initial enlarged state is prepared at time t_i as $|\Psi(t_\mathrm{i})\rangle$, then it evolves to $|\Psi(t)\rangle$ under an appropriate enlarged evolution operator $\widetilde{\hat{\boldsymbol{U}}}(t, t_\mathrm{i}) \equiv \exp(-\frac{i}{\hbar}\int_{t_\mathrm{i}}^{t} \widetilde{\hat{\boldsymbol{H}}} d\tau)$. The weak value at time t then is given by the expectation value of the linear combination of Hermitian operators as above in Eq. (5.14). Of course, the enlarged evolution operator $\widetilde{\hat{\boldsymbol{U}}}(t, t_\mathrm{i})$ should give the state evolution

$$\Psi\Big(\psi(t_\mathrm{i}), \phi(t_\mathrm{i}), t_\mathrm{i}\Big) \xrightarrow{\widetilde{\hat{\boldsymbol{U}}}(t,t_\mathrm{i})} \Psi\Big(\psi(t), \phi(t), t\Big). \tag{5.15}$$

For this $\phi(t)$, the following relation

$$|\phi(t)\rangle = \hat{\boldsymbol{U}}(t, t_\mathrm{f})|\phi(t_\mathrm{f})\rangle \tag{5.16}$$

must also hold.

One possible way to satisfy both Eqs. (5.15) and (5.16) is to choose $\hat{\boldsymbol{B}} = 0$ and $\hat{\boldsymbol{C}} = \hat{\boldsymbol{H}}$ in Eq. (5.8). Then the backward evolution $\hat{\boldsymbol{U}}(t_\mathrm{i}, t_\mathrm{f})|\phi(t_\mathrm{f})\rangle$, satisfies the requirement and thus,

$$|\phi(t_\mathrm{i})\rangle = \hat{\boldsymbol{U}}(t_\mathrm{i}, t_\mathrm{f})|\phi(t_\mathrm{f})\rangle. \tag{5.17}$$

So that, if we know both the system free evolution $\hat{\boldsymbol{U}}(t_\mathrm{i}, t_\mathrm{f})$ and the postselected state $|\phi(t_\mathrm{f})\rangle$ beforehand, then $|\phi(t_\mathrm{i})\rangle$ also becomes well defined at the initial time t_i.

Remarkably, other than $\hat{\boldsymbol{B}} = 0$ and $\hat{\boldsymbol{C}} = \hat{\boldsymbol{H}}$, we can also freely choose $\hat{\boldsymbol{B}}$ and $\hat{\boldsymbol{C}}$ in Eq. (5.8). In this case, however, the backward evolution $\hat{\boldsymbol{U}}(t_\mathrm{i}, t_\mathrm{f})|\phi(t_\mathrm{f})\rangle$ cannot satisfy the requirement, and we need more complicated calculations with the prior knowledge of postselected wave function at time t to determine the enlarged state $|\Psi(t_\mathrm{i})\rangle$.

5.3.3 Example

In this example, we illustrate a simple case where a single spin-$\frac{1}{2}$ particle evolves under an external magnetic field applied along the z-axis. The Hamiltonian and the evolution operator are given by

$$\hat{\boldsymbol{H}} = \frac{\mu B}{2}\hat{\boldsymbol{\sigma}}_z, \text{ and } \hat{\boldsymbol{U}}(t) = e^{-\frac{i\omega t}{2}\hat{\boldsymbol{\sigma}}_z}, \tag{5.18}$$

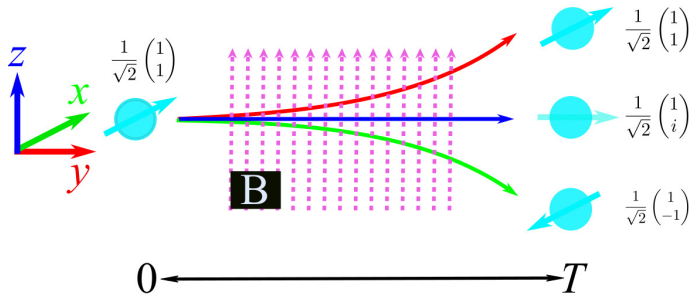

Figure 5.1: A schematic setup of a single spin-$\frac{1}{2}$ particle under a magnetic field applied along the z-axis. The particle is initially prepared in spin up along the x-axis, and then postselected onto the three cases of spin up along the x-axis, spin up along the y-axis, and spin down along the x-axis. We calculate the weak value of Pauli matrix $\hat{\boldsymbol{\sigma}}_x(t)$ at time t between 0 and T.

where μ and B are the amplitudes of the magnetic moment and the magnetic field, respectively, and $\omega = \frac{\mu B}{\hbar}$.

Suppose that we prepare an initial state, $|\uparrow_x\rangle$, which is a normalized eigenstate of Pauli matrix $\hat{\boldsymbol{\sigma}}_x$

$$|\psi(t_{\rm i})\rangle = \frac{1}{\sqrt{2}}\begin{pmatrix}1\\1\end{pmatrix}, \tag{5.19}$$

with the bases $|\uparrow_z\rangle = \binom{1}{0}$ and $|\downarrow_z\rangle = \binom{0}{1}$. For the postselection at time $t_{\rm f}$, we consider three examples as the postselected states

$$|\phi(t_{\rm f})\rangle = \frac{1}{\sqrt{2}}\begin{pmatrix}1\\1\end{pmatrix}; \frac{1}{\sqrt{2}}\begin{pmatrix}1\\-1\end{pmatrix}; \text{ and } \frac{1}{\sqrt{2}}\begin{pmatrix}1\\i\end{pmatrix}, \tag{5.20}$$

which correspond to $|\uparrow_x\rangle$, $|\downarrow_x\rangle$, and $|\uparrow_y\rangle$, respectively. Let us choose $t_{\rm i} = 0$ and $t_{\rm f} = T$ for simplicity. We schematic show the setup in Fig. 5.1.

Then the time-dependent weak values of $\hat{\boldsymbol{\sigma}}_x$ calculated in the normal Hilbert space from Eq. (5.11) are

$${}_{\uparrow_x}\langle\hat{\boldsymbol{\sigma}}_x\rangle^{\rm w}_{\uparrow_x} = \cos(\omega t) + \sin(\omega t)\tan(\frac{\omega T}{2}), \tag{5.21a}$$

$${}_{\downarrow_x}\langle\hat{\boldsymbol{\sigma}}_x\rangle^{\rm w}_{\uparrow_x} = \cos(\omega t) - \sin(\omega t)\cot(\frac{\omega T}{2}), \tag{5.21b}$$

$${}_{\uparrow_y}\langle\hat{\boldsymbol{\sigma}}_x\rangle^{\rm w}_{\uparrow_x} = \frac{\cos(\omega t - \frac{\omega T}{2} + \frac{\pi}{4})}{\cos(\frac{\omega T}{2} - \frac{\pi}{4})}. \tag{5.21c}$$

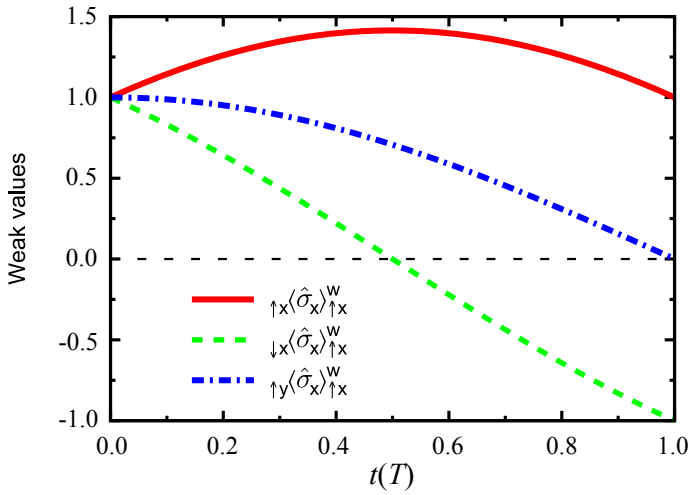

Figure 5.2: Weak values of $\hat{\boldsymbol{\sigma}}_x$ for preselection state in (5.19) and various postselection states as in (5.20), which are the same in both cases of normal Hilbert space and enlarged Hilbert space.

We next go through with the same calculations in the enlarged Hilbert space. For simplicity, let us choose $\hat{\boldsymbol{B}} = 0$ and $\hat{\boldsymbol{C}} = \hat{\boldsymbol{H}}$ in the decomposition $\hat{\boldsymbol{H}} = \hat{\boldsymbol{B}} + \hat{\boldsymbol{C}}$. The corresponding Hamiltonian and the evolution operator in the enlarged space are

$$\widetilde{\hat{\boldsymbol{H}}} = \frac{\mu B}{2} \hat{\boldsymbol{I}}^e \otimes \hat{\boldsymbol{\sigma}}_z^s \quad \text{and} \quad \widetilde{\hat{\boldsymbol{U}}}(t) = e^{-\frac{i\omega t}{2} \hat{\boldsymbol{I}}^e \otimes \hat{\boldsymbol{\sigma}}_z^s}, \tag{5.22}$$

where we have added superscripts 'e' and 's' for the extra spin (ancilla qubit) and the system spin.

We also need to calculate the state $|\phi(t_\mathrm{i})\rangle$ from the given $|\phi(t_\mathrm{f})\rangle$, which can be done using Eq. (5.17) for each postselected state of Eq. (5.20). The initial enlarged state is then given as

$$|\Psi(t_\mathrm{i})\rangle = \frac{1}{2} \begin{pmatrix} |\psi(t_\mathrm{i})\rangle + |\phi(t_\mathrm{i})\rangle \\ |\psi(t_\mathrm{i})\rangle - |\phi(t_\mathrm{i})\rangle \end{pmatrix}. \tag{5.23}$$

Under the enlarged evolution $\widetilde{\hat{\boldsymbol{U}}}(t, t_\mathrm{i})$, this enlarged state evolves to $|\Psi(t)\rangle = \widetilde{\hat{\boldsymbol{U}}}(t, t_\mathrm{i})|\Psi(t_\mathrm{i})\rangle$. Then the weak values obtained from Eq. (5.14) are the same as Eqs. (5.21). The detail calculation is shown in Appendix C.1.

As an example case when we choose $\omega T = \pi/2$, then the results of weak values are shown in Fig. 5.2. In general, the weak values depend on the measurement time.

At $t = 0$ for all postselection cases, the results of weak values always equal to 1, that means $\hat{\boldsymbol{\sigma}}_x$ will be measured up regardless of postselection since the initial preparation state is $|\uparrow_x\rangle$, which is an eigenstate of $\hat{\boldsymbol{\sigma}}_x$. As time t increases, the results will be depended on both pre- and postselection states at that time. For example, at $t = T/2$, the postselected onto $|\uparrow_x\rangle$ will give the maximum result of weak value (the red solid curve), which lie outside the range of $\hat{\boldsymbol{\sigma}}_x$ eigenvalues [-1,+1], while the postselected onto $|\downarrow_x\rangle$ will give the zero result (the green dashed curve), that means $\hat{\boldsymbol{\sigma}}_x$ will be measured up or down with equal probability. Finally, for $t = T$, similar $t = 0$ case, the weak values depend on postselection states, for those are eigenstates of $\hat{\boldsymbol{\sigma}}_x$ as we can see from the red and green curves for up and down orientations, respectively.

5.3.4 Time-dependent modular values in an enlarged Hilbert space

We now consider the time-dependent modular values. By using the spectral decomposition, a modular value can be expressed regarding weak values as can be seen from Eqs. (6.6,6.4) by

$$(\hat{\boldsymbol{A}}(t))_{\mathrm{m}} = \sum_i e^{-ig\lambda_i} \langle \hat{\boldsymbol{\Pi}}_{a_i}(t) \rangle_{\mathrm{w}} \, . \tag{5.24}$$

where we have used $\hat{\boldsymbol{\Pi}}_{a_i} = |a_i\rangle\langle a_i|$, and λ_i is one of the eigenvalues of the observable $\hat{\boldsymbol{A}}$, i.e., $\hat{\boldsymbol{A}} = \sum_i \lambda_i \hat{\boldsymbol{\Pi}}_{a_i}$. This means that the modular value at time t is obtained by scanning and collecting all the weak values of the projection operators at this time. Fortunately, these weak values can be simultaneously measured at a given time by using such "scan-free method" that was introduced by Shi *et al.*, [67]. As a result, time-dependent modular values in the enlarged Hilbert space can be determined via the time-dependent weak values.

5.4 Implementation of enlarged Hilbert spaces

In this section, we discuss how to implement the evolution associated with the enlarged Hamiltonian by a real quantum simulator. To do this, let us first consider the Trotter technique as follows

5.4.1 Trotter technique

In many cases of the quantum simulation, a Hamiltonian to be simulated is expressed by a many-body-system Hamiltonian, which is the summation of the subsystems Hamiltonians. So, we can assume that the Hamiltonian is expressed as

$$\hat{\boldsymbol{H}} = \sum_j \hat{\boldsymbol{H}}_j \ , \tag{5.25}$$

where $\hat{\boldsymbol{H}}_j$ are in general nonlocal and non-commuting operators. The Trotter technique for an evolution operator states that [68,69],

$$\hat{\boldsymbol{U}} = e^{-\frac{i}{\hbar}\sum_j \hat{\boldsymbol{H}}_j t} \simeq \left(\prod_j e^{-\frac{i}{\hbar}\hat{\boldsymbol{H}}_j t/k}\right)^k \ , \tag{5.26}$$

where k is the number of Trotter steps. If $\hat{\boldsymbol{H}}_j$ are local Hamiltonians, the evolution process can be implemented by using a "genetic algorithm" for digital quantum simulations [70]. Here, however, we assume that $\hat{\boldsymbol{H}}_j$ are nonlocal, so, the genetic algorithm is not applicable. Fortunately, however, each $\hat{\boldsymbol{H}}_j$ is decomposed into tensor products of Pauli matrices [57,71]. In this case, $e^{-\frac{i}{\hbar}\hat{\boldsymbol{H}}_j t/k}$ can be implemented by using nonlocal entangling Mølmer-Sørensen gates $\hat{\boldsymbol{U}}_{\rm MS}(\theta,\phi) = \exp[-i\frac{\theta}{4}(\cos\phi\hat{\boldsymbol{S}}_x + \sin\phi\hat{\boldsymbol{S}}_y)^2]$, and local single-qubit rotations (see Refs. [57,71]), where the operators $\hat{\boldsymbol{S}}_{x,y} = \sum_{i=1}^N \hat{\boldsymbol{\sigma}}^i_{x,y}$, θ and ϕ are two angle-parameters, and N is the number of local qubits [72,73].

Particularly, the Mølmer-Sørensen gate has been proposed to solve such kind of spin interaction [71–74]. These studies discuss on the Kitaev's toric code Hamiltonian, where the Hamiltonian describes four-body interactions of spins [75,76] or in general, the Hamiltonian can be expressed regarding the tensor products of Pauli matrices. Specifically, even for fermion interaction, Casanova et al., have been introduced and implemented explicitly that kind of interaction in the trapped ions within three-step [71]. Recently, Subaşı and Jarzynski have discussed on the simulating the highly nonlocal Hamiltonians with less nonlocal Hamiltonians [77].

5.4.2 Trotter technique for the enlarged spaces

We now apply the above method to our enlarged Hamiltonian Eq.(5.8). Here we use a nonlocal N-qubit system to realize an n-dimensional Hamiltonian $\hat{\boldsymbol{H}}$, where $n = 2^N$. In

most cases, as was discussed in Sec. 5.2 and will be discussed in this section, an N-body system in the original Hilbert space can be expressed by an $(N+1)$-body interaction in the enlarged Hilbert space. This means that the quantum simulation in the enlarged space is realized by adding one extra qubit to the original system [56,60]. Then we have

$$\widetilde{\hat{\boldsymbol{H}}} = \hat{\boldsymbol{I}}_2^e \otimes \hat{\boldsymbol{C}}^s + \hat{\boldsymbol{\sigma}}_x^e \otimes \hat{\boldsymbol{B}}^s = \sum_{j=1}^{2} \widetilde{\hat{\boldsymbol{H}}}_j \,, \tag{5.27}$$

where $\widetilde{\hat{\boldsymbol{H}}}_1 \equiv \hat{\boldsymbol{I}}_2^e \otimes \hat{\boldsymbol{C}}^s$ and $\widetilde{\hat{\boldsymbol{H}}}_2 \equiv \hat{\boldsymbol{\sigma}}_x^e \otimes \hat{\boldsymbol{B}}^s$. We assume that both $\hat{\boldsymbol{B}}^s$ and $\hat{\boldsymbol{C}}^s$ can be decomposed into tensor products of N Pauli matrices. We then use the Trotter technique to decompose the total evolution operator as

$$\widetilde{\hat{\boldsymbol{U}}} = e^{-igt\sum_j \widetilde{\hat{\boldsymbol{H}}}_j} = \Big(\prod_{j=1}^{2} e^{-igt\widetilde{\hat{\boldsymbol{H}}}_j/k}\Big)^k \,, \tag{5.28}$$

where g is the coupling constant of the simulated system. The evolution corresponding to $j=1$ can be implemented easily by using single qubit rotations. For $j=2$, the evolution can be implemented (see Fig. 5.3) as follows:

(**i**) Operate a Mølmer-Sørensen entangling gate, $\hat{\boldsymbol{U}}_{\rm MS}(\theta,\phi)$, to all $(N+1)$ qubits.
(**ii**) Apply a local single-qubit gate, $\exp(-i\frac{\varphi}{2}\hat{\boldsymbol{\sigma}}_\gamma^e \otimes \hat{\boldsymbol{I}}_{2^N}^s)$, to the extra qubit. Here, the phase φ is designed by controlling $2gt$ and γ is chosen from x, y or z, depending on the parity (odd or even) of N [71].
(**iii**) The total system is reversed by the inverse entangling gate $\hat{\boldsymbol{U}}_{\rm MS}^\dagger(\theta,\phi)$.

This sequence (**i**)-(**iii**) can be summarized as

$$\hat{\boldsymbol{U}}_{\rm MS}(\theta,\phi) e^{-igt\hat{\boldsymbol{\sigma}}_\gamma^e \otimes \hat{\boldsymbol{I}}_{2^N}^s} \hat{\boldsymbol{U}}_{\rm MS}^\dagger(\theta,\phi), \tag{5.29}$$

and can implement the desired enlarged evolution $\widetilde{\hat{\boldsymbol{U}}}$ in Eq. (5.28).

5.4.3 Example

As an example, let us apply this method to the case of the example in Sec.5.3.3, where we focus on the case $\widetilde{\hat{\boldsymbol{H}}} = \frac{\mu B}{2}\hat{\boldsymbol{\sigma}}_x^e \otimes \hat{\boldsymbol{\sigma}}_z$, i.e., $j=2$ in Eq. (5.27). The evolution

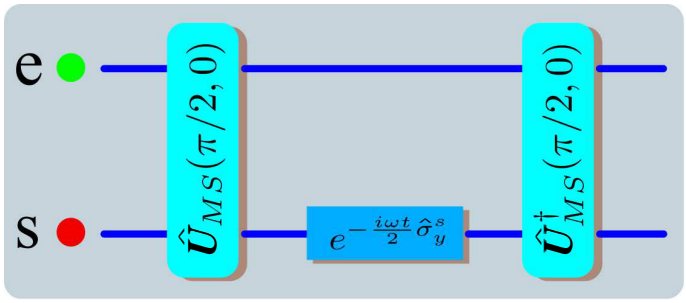

Figure 5.3: A scheme of quantum gates acting on both the extra spin (e) and the system single-particle spin (s).

$\widetilde{\hat{\boldsymbol{U}}} = \exp(-\frac{i\omega t}{2}\hat{\boldsymbol{\sigma}}_x^e \otimes \hat{\boldsymbol{\sigma}}_z^s)$ can be calculated (see Appendix C.2) as

$$\widetilde{\boldsymbol{U}} = \hat{\boldsymbol{U}}_{\mathrm{MS}}(\frac{\pi}{2},0)e^{-\frac{i\omega t}{2}\hat{\boldsymbol{I}}_2^e\otimes\sigma_y^s}\hat{\boldsymbol{U}}_{\mathrm{MS}}^{\dagger}(\frac{\pi}{2},0), \tag{5.30}$$

where the Mølmer-Sørensen gates $\hat{\boldsymbol{U}}_{\mathrm{MS}}(\pi/2,0)$ and $\hat{\boldsymbol{U}}_{\mathrm{MS}}^{\dagger}(\pi/2,0)$ act on both the extra spin and the system single-particle spin. Here, however, there is a slight difference from Eq. (5.29), that we apply the single-spin rotation onto the system spin, where it is simpler for this particular example. The process can be seen from Fig. 5.3. We also emphasize that such gates can be simulated by a physical system, such as ion-traps [52, 78–80], quantum photonics, superconducting circuits, and among others (See [81]).

Chapter 6

Probabilistic representation of complex modular values

In this chapter, we theoretically analyze the complex behavior of quantum modular values. We first use the spectral decomposition and show that a modular value is expressed by the average of the dynamical phase factors with the complex conditional probabilities. Concerning this expression, the chain rule of the conditional probabilities is also derived, which relates the initial-final-state modular value with the initial-transitional-state modular values and the transitional-final-state weak values.

6.1 Complex conditional probability

In this section, we extend the previous studies of Hofmann about weak values in Refs. [82, 83] to probabilistic interpretation for modular values. We show that, analogous to weak values, modular values can be understood in the context of complex conditional probabilities.

Let us first give a summary of the previous studies. The ordinary expectation value, that is, the expectation value without the postselection condition, can be interpreted as the average of weak values over all possible postselection states as postselect

$$\langle \hat{\boldsymbol{A}} \rangle_\psi \equiv \langle \psi | \hat{\boldsymbol{A}} | \psi \rangle = \sum_\phi \langle \hat{\boldsymbol{A}} \rangle_{\mathrm{w}} P(\phi|\psi) \, , \tag{6.1}$$

where $\langle \hat{\boldsymbol{A}} \rangle_\psi$ is the expectation value of the operator $\hat{\boldsymbol{A}}$. $P(\phi|\psi)$ is the conditional probability of observing state $|\phi\rangle$ on condition that the prepared state is $|\psi\rangle$, and is, of course, equal to $|\langle\phi|\psi\rangle|^2$ [2,84–87].

In the standard statistics of a discrete distribution, we denote by $\bar{x}$, the mean value of a random variable X, which is given by

$$\bar{x} = \sum_x x \; P(x) \; , \tag{6.2}$$

where x spans all possible values of the random variable X with the corresponding probability $P(x)$. Comparing the formula Eq. (6.1) to Eq. (6.2), the weak value can be treated as a $|\phi\rangle$ dependence variable, which can take complex values, but its expectation value is real with the real probability $P(\phi|\psi)$ [2].

Interestingly, a weak value itself can be regarded as the average of conditional probabilities. In this case, however, conditional probabilities themselves can take complex values [82,83,86,88]. In fact, using the spectral decomposition $\hat{\boldsymbol{A}} = \sum_a a \; \hat{\boldsymbol{\Pi}}_a$, where $\hat{\boldsymbol{\Pi}}_a \equiv |a\rangle\langle a|$, it is straightforward to obtain [82,83]

$$\langle \hat{\boldsymbol{A}} \rangle_{\rm w} = \sum_a a \; P(a|\psi,\phi) \; . \tag{6.3}$$

Here,

$$P(a|\psi,\phi) = \frac{\langle\phi|\hat{\boldsymbol{\Pi}}_a|\psi\rangle}{\langle\phi|\psi\rangle} = \langle \hat{\boldsymbol{\Pi}}_a \rangle_{\rm w} \; , \tag{6.4}$$

is known as the *complex conditional probability* [82,83], for the process: from the initially prepared state $|\psi\rangle$ to the finally postselected state $|\phi\rangle$ via the intermediate state $|a\rangle$. Typically, the weak value of the projection operator $\hat{\boldsymbol{A}} = |a\rangle\langle a|$ is the transition amplitude from the initial state to the final state via the intermediate state. The squared of its value which is known as the probability [2]. However, here we interpreted it as a complex conditional probability in the scene that the state $|a\rangle$ is might not observed by projective measurements, for example, "counter-factual probabilities" [89–91].

Using Eq. (6.3), the ordinary expectation value is expressed by the chain rule as

$$\langle \hat{\boldsymbol{A}} \rangle_\psi = \sum_a a \sum_\phi P(a|\psi,\phi) P(\phi|\psi) \; . \tag{6.5}$$

Here, $P(\phi|\psi)$ is real but $P(a|\psi,\phi)$, so to say a jointly conditioned probability, can be negative or even complex, and the finally obtained expectation value is real. Nevertheless, Hofmann also constructed quantum mechanics based on this generalized probability formalism, where he called the properties of these generalized probabilities as *physical properties* [92, 93], which provide the full framework of quantum mechanics, including quantum ergodicity [92], and quantum paradoxes [93].

6.2 Complex modular values

Our main result in this section is to show that the modular value is the average of the dynamic phase factor e^{-iga} over all eigenvalues with the complex conditional probability, which is expressed as

$$(\hat{\boldsymbol{A}})_{\mathrm{m}} = \sum_a e^{-iga} P(a|\psi,\phi) \ . \tag{6.6}$$

To prove this expression, we use the spectral decomposition of an arbitrary function of operator $\hat{\boldsymbol{A}} = \sum_a a|a\rangle\langle a|$, where all eigenvalues $\{|a\rangle\}$ form orthonormal bases. The spectral decomposition of $F(\hat{\boldsymbol{A}})$, where F is any analytic function, is written as

$$F(\hat{\boldsymbol{A}}) = \sum_a F(a)|a\rangle\langle a| \ , \tag{6.7}$$

which is derived from the Taylor (Maclaurin) expansion of function $F(\hat{\boldsymbol{A}})$. Choosing $e^{-ig\hat{\boldsymbol{A}}}$ as the function $F(\hat{\boldsymbol{A}})$, Eq. (6.7) immediately leads to

$$e^{-ig\hat{\boldsymbol{A}}} = \sum_a e^{-iga}|a\rangle\langle a| \ . \tag{6.8}$$

Putting this into the modular value, i.e., $\hat{\boldsymbol{A}} = \frac{\langle\phi|e^{-ig\hat{\boldsymbol{A}}}|\phi\rangle}{\langle\phi|\psi\rangle}$, and using Eq. (6.4), we obtain Eq. (6.6).

6.3 Chain rules

Next, we discuss the chain rules. We fix the initial state $|\psi\rangle$ and the final state $|\phi\rangle$, and consider the case that the intermediate state is found to be $|a\rangle$, assuming that there is another intermediate measurement that randomly projects the state onto one

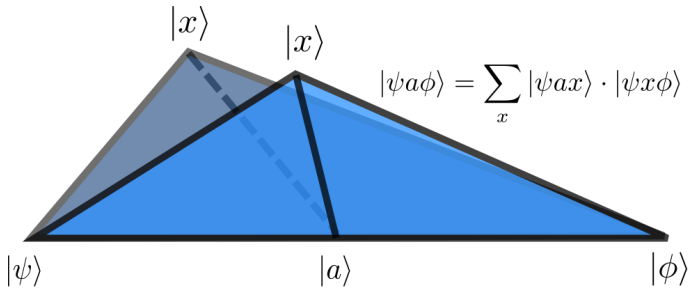

Figure 6.1: A vector graphic illustrates the chain rule. The chain rule describing the process of taking route $|\psi\rangle \to |a\rangle \to |\phi\rangle$ is the summation over all possible $|x\rangle$'s of the product of taking $|\psi\rangle \to |a\rangle \to |x\rangle$ and taking $|\psi\rangle \to |x\rangle \to |\phi\rangle$.

of the orthonormal states $|x\rangle$'s. In this case, the chain rule describing the process of taking route $|\psi\rangle \to |a\rangle \to |\phi\rangle$ is the summation over all possible $|x\rangle$'s with proper conditional probabilities. Therein, the process of taking route $|\psi\rangle \to |a\rangle \to |x\rangle \to |\phi\rangle$ for each $|x\rangle$ is the product of $P(x|\psi,\phi)$, which is the process of taking $|\psi\rangle \to |x\rangle \to |\phi\rangle$ conditioned by the initial $|\psi\rangle$ and the final $|\phi\rangle$, and $P(a|\psi,x)$, which is the process of taking $|\psi\rangle \to |a\rangle \to |x\rangle$ conditioned by $|\psi\rangle$ and $|x\rangle$ (See Fig. 6.1). Thus the chain rule becomes [92]

$$P(a|\psi,\phi) = \sum_x P(a|\psi,x)P(x|\psi,\phi) \ . \tag{6.9}$$

Substituting Eq. (6.9) into Eq. (6.3), and using $P(x|\psi,\phi) = \langle \hat{\mathbf{\Pi}}_x \rangle_{\rm w}$ with $\hat{\mathbf{\Pi}}_x \equiv |x\rangle\langle x|$, we obtain

$${}_\phi\langle \hat{\boldsymbol{A}} \rangle^{\rm w}_\psi = \sum_x {}_x\langle \hat{\boldsymbol{A}} \rangle^{\rm w}_\psi \cdot {}_\phi\langle \hat{\mathbf{\Pi}}_x \rangle^{\rm w}_\psi \ , \tag{6.10}$$

where ${}_f\langle \cdot \rangle^{\rm w}_i$ denotes the weak value between pre- and post- selection states $|i\rangle$ and $\langle f|$.

We obtain a chain rule for the modular value in a similar way. In fact, substituting Eq. (6.9) into Eq. (6.6), we obtain

$${}_\phi(\hat{\boldsymbol{A}})^{\rm m}_\psi = \sum_x {}_x(\hat{\boldsymbol{A}})^{\rm m}_\psi \cdot {}_\phi\langle \hat{\mathbf{\Pi}}_x \rangle^{\rm w}_\psi \ , \tag{6.11}$$

where ${}_f(\cdot)^{\rm m}_i$ denotes the modular value between pre- and post- selection states $|i\rangle$ and $\langle f|$. We can also generalize the expression if we define

$$(\hat{\boldsymbol{A}})_{\rm F} \equiv \frac{\langle \phi | F(\hat{\boldsymbol{A}}) | \psi \rangle}{\langle \phi | \psi \rangle} = \sum_a F(a) P(a|\psi,\phi) \ , \tag{6.12}$$

where function F can be any analytic function. Substituting Eq. (6.9) into Eq. (6.12), we also obtain the chain rule

$$ {}_{\phi}(\hat{\boldsymbol{A}})^{\mathrm{F}}_{\psi} = \sum_{x} x (\hat{\boldsymbol{A}})^{\mathrm{F}}_{\psi} \cdot {}_{\phi}\langle \hat{\boldsymbol{\Pi}}_x \rangle^{\mathrm{w}}_{\psi} \, . \tag{6.13} $$

When $F(a) = a$, it leads to the weak value, and when $F(a) = e^{-iga}$, it leads to the modular value.

Chapter 7

Polar representation of complex modular values

In this chapter, we investigate the modular value in the polar decomposition under various pointer state approaches. We also discuss a relationship between the modulus and phase, therein, the derivative of the phase is related to the derivative of the logarithm of the modulus via a Berry-Simon-like connection, which is in the form of a weak value. As a consequence, the modulus-phase relation allows us to obtain these polar components whenever the connection is specified. One of the possible applications of this results is to evaluate the weak value (the Berry-Simon- like connection) when the polar modular value is experimentally obtained.

7.1 Polar representation

In this section, we theoretically demonstrate a meaning of the modular value in the polar representation for both cases of the finite-dimensional discrete pointer and continuous pointer. We show that the modulus of the modular value is related to the pointer preselection conditional probabilities, and the phase of the modular value is connected to the summation of a geometric phase and an intrinsic phase regardless of the finite-dimensional discrete pointer state or continuous pointer state.

7.1.1 The modulus of modular values

To examine the meaning of the modulus of modular values, we analyze the adjoint-form modular values as discussed in Chap. 4. We derive the adjoint-form modular values as the modulus of the modular values in the polar representation. As a transitive result, these relations allow us to examine the modulus of the modular values regarding the pointer conditional probabilities.

For the discrete pointer case with pure system states, i.e., $\hat{\boldsymbol{\rho}}_i = |\psi\rangle\langle\psi|$ and $\hat{\boldsymbol{\rho}}_f = |\phi\rangle\langle\phi|$, the expression for the adjoint-form modular value (4.18) explicitly reads

$$\left(\mathrm{ad}\hat{\boldsymbol{A}}\right)_{\mathrm{m}} = \frac{\mathrm{Tr}_{\mathrm{s}}\left[\hat{\boldsymbol{\rho}}_f e^{-ig\hat{A}}\hat{\boldsymbol{\rho}}_i e^{ig\hat{A}}\right]}{\mathrm{Tr}_{\mathrm{s}}\left[\hat{\boldsymbol{\rho}}_f\hat{\boldsymbol{\rho}}_i\right]} = \frac{\left|\langle\phi|e^{-ig\hat{\boldsymbol{A}}}|\psi\rangle\right|^2}{\left|\langle\phi|\psi\rangle\right|^2} = \left|(\hat{\boldsymbol{A}})_{\mathrm{m}}\right|^2 , \tag{7.1}$$

where $\left|(\hat{\boldsymbol{A}})_{\mathrm{m}}\right|^2$ is the square of the modulus of the modular value. Then the modulus of the modular value can be derived easily regarding the conditional probabilities (4.17, 4.19) as

$$\left|(\hat{\boldsymbol{A}})_{\mathrm{m}}\right| = \left(1 - \frac{1}{|c_\lambda|^2} + \frac{|c_\mu|^2}{P(\mu \neq \lambda|f)}\right)^{1/2} , \tag{7.2}$$

for $\mu \neq \lambda$, and

$$\left|(\hat{\boldsymbol{A}})_{\mathrm{m}}\right| = \left[\frac{P(\mu = \lambda|f)\left(1 - |c_\lambda|^2\right)}{|c_\lambda|^2\left(1 + P(\mu = \lambda|f)\right)}\right]^{1/2} , \tag{7.3}$$

for $\mu = \lambda$. Here, we remind that μ is a possible outcome of the pointer and λ is the projection state, i.e., $\hat{\boldsymbol{P}} = |\lambda\rangle\langle\lambda|$.

We now turn to the case of the continuous pointer state. A similar adjoint-form modular value reads

$$\left(\mathrm{ad}\hat{\boldsymbol{A}}\right)^p_{\mathrm{m}} = \frac{\left|\langle\phi|e^{-igp\hat{\boldsymbol{A}}}|\psi\rangle\right|^2}{\left|\langle\phi|\psi\rangle\right|^2} = \left|(\hat{\boldsymbol{A}})^p_{\mathrm{m}}\right|^2 , \tag{7.4}$$

where we have also used explicitly $\hat{\boldsymbol{\rho}}_i = |\psi\rangle\langle\psi|$ and $\hat{\boldsymbol{\rho}}_f = |\phi\rangle\langle\phi|$. Then Eq.(4.47) yields,

$$P(p|f) = \frac{\exp(-2p^2\sigma^2)\left|(\hat{\boldsymbol{A}})^p_{\mathrm{m}}\right|^2}{\int \exp(-2p^2\sigma^2)\left|(\hat{\boldsymbol{A}})^p_{\mathrm{m}}\right|^2 dp} . \tag{7.5}$$

Furthermore, for the operator $\hat{\boldsymbol{A}}$ satisfies the property $\hat{\boldsymbol{A}}^2 = \hat{\boldsymbol{I}}^2$, e.g., Pauli mastics, the modular value is given as

$$\left(\hat{\boldsymbol{A}}\right)^p_{\rm m} = \cos(gp)\hat{\boldsymbol{I}} - i\sin(gp)\langle\hat{\boldsymbol{A}}\rangle_{\rm w} \ , \tag{7.6}$$

where $\langle\hat{\boldsymbol{A}}\rangle_{\rm w} \equiv \frac{\langle\phi|\hat{\boldsymbol{A}}|\psi\rangle}{\langle\phi|\psi\rangle}$ is the original weak value, and the modulus of the modular value yields,

$$\left|(\hat{\boldsymbol{A}})^p_{\rm m}\right|^2 = 1 + \left(|\langle\hat{\boldsymbol{A}}\rangle_{\rm w}|^2 - 1\right)\sin^2(gp) + {\rm Im}|\langle\hat{\boldsymbol{A}}\rangle_{\rm w}|\sin(2gp) \ . \tag{7.7}$$

Then, the integral of the denominator in (7.5) reads

$$C^2 = \sqrt{\frac{\pi}{2\sigma^2}} + \sqrt{\frac{\pi}{8\sigma^2}}\left(|\langle\hat{\boldsymbol{A}}\rangle_{\rm w}|^2 - 1\right)\left[1 - e^{-g^2/2\sigma^2}\right] \ , \tag{7.8}$$

where we have defined by C^2 for convenience. It is a constant for a fixed of pre- and postselection states for a given measured observable $\hat{\boldsymbol{A}}$, and can be evaluated experimentally from the completeness relation of the conditional probabilities. Then the modulus of the modular value reads from (7.5) as

$$\left|(\hat{\boldsymbol{A}})^p_{\rm m}\right| = C\exp(p^2\sigma^2)\sqrt{P(p)} \ , \tag{7.9}$$

which is also given in term of the conditional postselection probability.

Furthermore, to understand the meaning of the modulus of the modular value, we can look back to the definition of the modular value in Eq. (2.10) where the quantity of the modular value is the ratio of the transition amplitudes for going, over g, from the preselection state to the postselection state via Hamiltonians $\hat{\boldsymbol{H}} = \hat{\boldsymbol{A}}$, and $\hat{\boldsymbol{H}} = 0$, respectively. With this definition in mind, we can imply from Eq. (7.1) for the discrete case and also Eq. (7.4) for the continuous case that the square of the modulus of the modular value is the ratio of the corresponding probabilities for obtaining the postselection state from the preselection state via Hamiltonians $\hat{\boldsymbol{H}} = \hat{\boldsymbol{A}}$, and $\hat{\boldsymbol{H}} = 0$, respectively.

7.1.2 The phase of modular values

As was discussed by Cormann *et al.*, [94] the phase of a modular value can be measured by the phase in a quantum eraser interference experiment. Here, we analyze the phase of

the modular value more in detail, and we show that it is expressed by the Pancharatnam phases, particularly, by the summation of an intrinsic phase and a geometric phase, as is shown in the following.

We can imply from Eqs. (4.14) and (4.46) for the discrete and continuous cases that the system evolution state after the interaction is recast as

$$|\psi\rangle \xrightarrow{\hat{\boldsymbol{U}}} |\psi'\rangle \propto e^{-ig\hat{\boldsymbol{A}}}|\psi\rangle \ . \tag{7.10}$$

For the continuous case, g is replaced by $g' = gp$. Therefore, here after, we consider only case g. Since (7.10), we can conclude that the phase in the modular value includes an intrinsic property of the quantum system in the sense that the evolution operator $e^{-ig\hat{\boldsymbol{A}}}$ in the modular value solely depends on the system evolution but not on the measurement apparatus or environments.

For this reason, let us consider the following *system-state-evolution process*: Starting from an initial state, i.e., preselected $|\psi\rangle$, the state evolves to $|\psi'\rangle$, then the resultant state $|\psi'\rangle$ is projected onto the postselection state $|\phi\rangle$. The final state (after postselection) is given by $|\psi''\rangle = |\phi\rangle\langle\phi|e^{-ig|\hat{\boldsymbol{A}}}|\psi\rangle$ (not normalized). The phase difference between this final state and the initial state is calculated to be

$$\arg\big[\langle\psi|\psi''\rangle\big] = \arg\big[\langle\psi|\phi\rangle\langle\phi|e^{-ig\hat{\boldsymbol{A}}}|\psi\rangle\big] = \arg\Big[\frac{\langle\phi|e^{-ig\hat{\boldsymbol{A}}}|\psi\rangle}{\langle\phi|\psi\rangle}\Big] \ , \tag{7.11}$$

where the last term is the phase of the modular value. This phase-different is also the phase shift in a closed-loop projection $|\psi\rangle \rightsquigarrow |\psi'\rangle \to |\phi\rangle \to |\psi\rangle$, as we illustrate on the left-hand side of Fig. 7.1, where the wave arrow indicates the evolution process. This equation gives one meaning of the phase of the modular value, that it corresponds to the phase shift in the system-state-evolution process as above. To be more precise, a straightforward calculation of this phase yields

$$\arg\Big[\frac{\langle\phi|e^{-ig\hat{\boldsymbol{A}}}|\psi\rangle}{\langle\phi|\psi\rangle}\Big] = \arg\Big[\frac{\langle\psi|\phi\rangle\langle\phi|\psi'\rangle\langle\psi'|\psi\rangle}{|\langle\psi|\phi\rangle|^2\langle\psi'|\psi\rangle}\Big] = \Delta(\psi,\psi',\phi) + \delta(\psi,\psi') \ , \tag{7.12}$$

where we have used

$$\delta(\psi,\psi') = \arg\big[\langle\psi|\psi'\rangle\big] \ , \tag{7.13}$$

and

$$\Delta(\psi,\psi',\phi) = \arg\Big[\langle\psi|\phi\rangle\langle\phi|\psi(g)\rangle\langle\psi(g)|\psi\rangle\Big] \ . \tag{7.14}$$

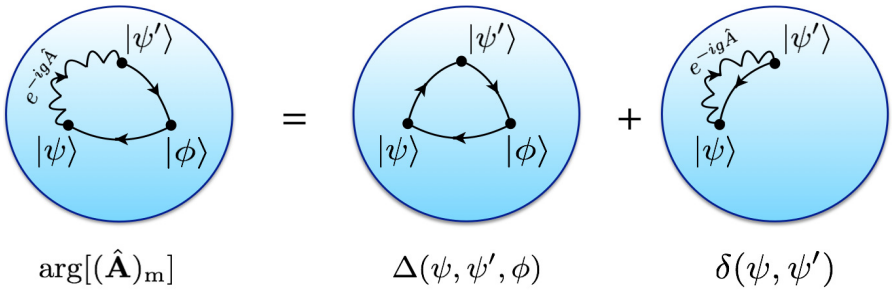

Figure 7.1: The phase of a modular value is the total phase shift of a system-state-evolution process that starting from an initial state, evolve onto an intermediate state, then project onto a final state and finally project back to the initial state. This total phase shift corresponds to the summation of the geometric phase and the intrinsic phase.

Here, δ and Δ are interpreted as the intrinsic phase and the geometric phase, respectively, as follows. The meaning of Δ is that this phase shift is induced by the closed-loop projection, $|\psi\rangle \to |\psi'\rangle \to |\phi\rangle \to |\psi\rangle$ [95–97]. This phase is gauge invariant because the local phase factor, which might be independently chosen for each quantum state, always appears with its complex conjugate due to a couple of bra and ket vectors, and thus all the local phases are canceled. Therefore, although $|\psi'\rangle$ is the result of the evolution induced by $e^{-ig\hat{\boldsymbol{A}}}$, Δ does not carry any phase shift by this evolution since the bra and ket vectors cancel out this phase shift. So, only the pre- and post-projections yield the geometric phase Δ, but the evolution does not. The evolution phase shift is solely carried by δ as can be seen from Eq. (7.13). In both of Δ and δ cases, one needs to project the final state onto the initial state to obtain the phase shift directly. We illustrate this situation in Fig. 7.1. Interestingly, as we show here, the phase of the modular value now becomes the summation of the geometric phase Δ of a geodesic triangle having three vertices $|\psi\rangle$, $|\psi'\rangle$, and $|\phi\rangle$, and the intrinsic phase δ between the initial state and the evolution state $|\psi'\rangle$.

Particularly, when the coupling g is sufficiently small, we can take the first order of

the Taylor series expansion of the exponential term and obtain

$$\begin{aligned}\arg\Big[\frac{\langle\phi|e^{-ig\hat{\boldsymbol{A}}}|\psi\rangle}{\langle\phi|\psi\rangle}\Big]\Big|_{g\to 0} &\approx \arg\Big[\frac{\langle\phi|(\hat{I}-ig\hat{\boldsymbol{A}})|\psi\rangle}{\langle\phi|\psi\rangle}\Big] \\ &= \arg\Big[1-ig\langle\hat{\boldsymbol{A}}\rangle_{\rm w}\Big] \\ &\approx \arg\Big[e^{-ig\langle\hat{\boldsymbol{A}}\rangle_{\rm w}}\Big] \\ &= -g{\rm Re}\langle\hat{\boldsymbol{A}}\rangle_{\rm w}\,. \end{aligned} \tag{7.15}$$

We thus emphasize that, for small g, the phase of the modular value does not reduce to the phase of the weak value, but instead, it is proportional to the real part of the weak value (see Ref. [98] also).

7.2 The modulus-phase relation

In this section, we indicate a relation of the modulus and phase of the modular value and show how this relationship may be used to evaluate the real and imaginary part of the corresponding weak value. Notable that in this section we discuss the polar modular values regardless of the pointer states.

7.2.1 The modulus-phase relation

Let us express the modular value in both the polar representation and the complex phase representation as

$$(\hat{\boldsymbol{A}})_{\rm m} = \Xi(g)e^{i\Phi(g)} = e^{i\Theta(g)}, \tag{7.16}$$

where $\Xi(g)\equiv|(\hat{\boldsymbol{A}})_{\rm m}|$ and $\Phi(g)\equiv\arg[(\hat{\boldsymbol{A}})_{\rm m}]$ are the modulus and phase of the modular value $(\hat{\boldsymbol{A}})_{\rm m}$, which are in general, deepened on g, and $\Theta(g)\equiv -i\ln(\hat{\boldsymbol{A}})_{\rm m}$ is the complex phase. Differentiating Eq. (7.16) with respect to g, we obtain the modulus-phase relation

$$\partial_g\Phi(g) - i\partial_g\ln\Xi(g) = \partial_g\Theta(g), \tag{7.17}$$

where $\partial_g\equiv\partial/\partial g$. We also introduce a connection $\mathcal{A}_g$ as

$$\mathcal{A}_g \equiv \partial_g\Theta(g) = -i\frac{\langle\phi|\partial_g|\psi'\rangle}{\langle\phi|\psi'\rangle}, \tag{7.18}$$

where, in this section, we use $|\psi'\rangle \equiv e^{-ig\hat{\boldsymbol{A}}}|\psi\rangle$ for simplicity. In this form, $\mathcal{A}_g$ plays a role as a *Berry-Simon connection* [99,100]. A straightforward calculation relates $\mathcal{A}_g$ to the weak value of the observable $\hat{\boldsymbol{A}}$ in between the evolution state $|\psi'\rangle$ and postselection state $|\phi\rangle$ [84,101] as

$$\mathcal{A}_g = -\frac{\langle\phi|\hat{\boldsymbol{A}}|\psi'\rangle}{\langle\phi|\psi'\rangle}. \tag{7.19}$$

Then the relation (7.17) is recast as

$$\partial_g \Phi(g) - i\partial_g \ln \Xi(g) = \mathcal{A}_g. \tag{7.20}$$

We note that in Eq. (7.20), the derivative $\partial_g\Phi(g)$ corresponds to the real part of the connection $\mathcal{A}_g$, while the derivative $\partial_g \ln \Xi(g)$ can be expressed by the imaginary part of the connection. This relation, therefore, allowing the reconstruction of the modulus and phase of the modular value when the value of g changes from 0 to g as

$$\frac{\Xi(g)}{\Xi(0)} = \exp\Big[\int_0^g -\mathrm{Im}[\mathcal{A}_g]dg\Big], \tag{7.21}$$

and

$$\Phi(g) - \Phi(0) = \int_0^g \mathrm{Re}[\mathcal{A}_g]dg, \tag{7.22}$$

whenever the connection is specified. These equations imply that the modulus and phase of the modular value play the same role as the imaginary and real parts of the weak value (the connection), respectively, even for a large g. From the experimental point of view, we can evaluate the corresponding weak value by experimentally measuring the modulus and phase of the modular values.

7.2.2 An illustration for the modulus-phase relation on the Bloch sphere

On the Bloch sphere, the quantum pre- and postselection states are represented by their directions in polar coordinates as

$$|\psi\rangle = \begin{pmatrix} \cos\frac{\theta}{2} \\ \sin\frac{\theta}{2}\, e^{i\varphi} \end{pmatrix}, \text{ and } |\phi\rangle = \begin{pmatrix} \cos\frac{\theta'}{2} \\ \sin\frac{\theta'}{2}\, e^{i\varphi'} \end{pmatrix}, \tag{7.23}$$

where $\theta(\theta')$ and $\phi(\phi')$ are polar angles on the Bloch sphere. For simplicity, we also consider the evolution operator as $\hat{\boldsymbol{U}} = e^{-i\frac{\alpha}{2}\hat{\boldsymbol{\sigma}}_z}$, where α is the rotating angle around the z-axis. The evolution state is given as

$$|\psi'\rangle = \begin{pmatrix} \cos\frac{\theta}{2}\, e^{-i\frac{\alpha}{2}} \\ \sin\frac{\theta}{2}\, e^{i\varphi} e^{i\frac{\alpha}{2}} \end{pmatrix}. \tag{7.24}$$

Then the modular value of $\hat{\boldsymbol{\sigma}}_z$ is calculated to be

$$(\hat{\boldsymbol{\sigma}}_z)_{\rm m} = \frac{\cos\frac{\theta}{2}\cos\frac{\theta'}{2}\, e^{-i\frac{\alpha}{2}} + \sin\frac{\theta}{2}\sin\frac{\theta'}{2}\, e^{i\varphi''} e^{i\frac{\alpha}{2}}}{\cos\frac{\theta}{2}\cos\frac{\theta'}{2} + \sin\frac{\theta}{2}\sin\frac{\theta'}{2}\, e^{i\varphi''}}\ , \tag{7.25}$$

where $\varphi'' = \varphi - \varphi'$. For convenience, we transform θ from the polar coordinates on the sphere to the stereographic coordinates r on the plane where the radial coordinate is

$$r = \tan\frac{\theta}{2}\ , \text{and}\ r' = \tan\frac{\theta'}{2}\ . \tag{7.26}$$

Then Eq. (7.25) is recast as

$$(\hat{\boldsymbol{\sigma}}_z)_{\rm m} = \frac{e^{-i\frac{\alpha}{2}} + Re^{i\varphi''} e^{i\frac{\alpha}{2}}}{1 + Re^{i\varphi''}} = X + iY\ , \tag{7.27}$$

where $R = rr'$ and

$$X = \frac{(1+R^2)\cos\frac{\alpha}{2} + 2R\cos(\frac{\alpha}{2} + \varphi'')}{1 + R^2 + 2R\cos\varphi''}\ , \tag{7.28}$$

$$Y = \frac{(R^2-1)\sin\frac{\alpha}{2}}{1 + R^2 + 2R\cos\varphi''}\ . \tag{7.29}$$

Following this modular value, its polar components can be evaluated to be

$$|(\hat{\boldsymbol{\sigma}}_z)_{\rm m}| = \sqrt{\frac{1 + R^2 + 2R\cos(\alpha + \varphi'')}{1 + R^2 + 2R\cos\varphi''}}, \text{and} \tag{7.30}$$

$$\arg[(\hat{\boldsymbol{\sigma}}_z)_{\rm m}] = \arctan\Big[\frac{(R^2-1)\sin\frac{\alpha}{2}}{(R^2+1)\cos\frac{\alpha}{2} + 2R\cos(\frac{\alpha}{2} + \varphi'')}\Big]\ . \tag{7.31}$$

Furthermore, from Eq. (7.20), we calculate

$$-\partial_{\alpha/2} \ln|(\hat{\boldsymbol{\sigma}}_z)_{\rm m}| = \frac{2R\sin(\alpha + \varphi'')}{1 + R^2 + 2R\cos(\alpha + \varphi'')}, \text{and} \tag{7.32}$$

$$\partial_{\alpha/2} \arg[(\hat{\boldsymbol{\sigma}}_z)_{\rm m}] = \frac{R^2 - 1}{1 + R^2 + 2R\cos(\alpha + \varphi'')}\ . \tag{7.33}$$

We then compare with the Berry-Simon connection that

$$\mathcal{A}_g = -\frac{\langle\phi|\hat{\boldsymbol{A}}|\psi'\rangle}{\langle\phi|\psi'\rangle} = \frac{R^2 - 1 + i\,2R\sin(\alpha+\varphi'')}{1+R^2+2R\cos(\alpha+\varphi'')}\,, \tag{7.34}$$

where, obviously, its real and imaginary parts are equal to Eq. (7.33) and Eq. (7.32), respectively, then the relation (7.20) is verified.

One of the advantages of modular values in comparison to weak values is that we can easy to carry out modular measurements as we discussed in Chap. 3. Therefore, it is useful to connect the modular values to the weak values as we did (in Chap. 3), and then evaluate the weak values from the modular values. For example, we can calculate the weak value in between the evolution state $|\psi'\rangle$ and the postselection state $|\phi\rangle$ by experimentally measuring the modulus and phase of the modular value. Assuming that the pre- and postselection states are chosen as

$$|\psi\rangle = \begin{pmatrix} 1/\sqrt{2} \\ 1/\sqrt{2} \end{pmatrix}\,, \text{ and } |\phi\rangle = \begin{pmatrix} \sqrt{2+\sqrt{2}}/2 \\ -\sqrt{2-\sqrt{2}}/2 \end{pmatrix}\,, \tag{7.35}$$

such that $\theta = \pi/2, \theta' = \pi/4$ and $\varphi = 0, \varphi' = \pi$. We first perform a strong measurement of the $\hat{\boldsymbol{\sigma}}_z$ operator. Right after the measurement, the initial state will evolve to $|\psi'\rangle = \exp(-ig\hat{\boldsymbol{\sigma}}_z)|\psi\rangle$, i.e., $g = \alpha/2$. At this moment, a weak measurement of $\hat{\boldsymbol{\sigma}}_z$ is performed, which reveals the corresponding weak value in between $|\psi'\rangle$ and $|\phi\rangle$ after postselected the system state.

The polar components of the modular value in the first strong measurement are given by

$$|(\hat{\boldsymbol{\sigma}}_z)_{\rm m}| = \sqrt{\cos^2 g + (1+\sqrt{2})^2 \sin^2 g}, \text{and} \tag{7.36}$$

$$\arg[(\hat{\boldsymbol{\sigma}}_z)_{\rm m}] = -\arctan[(1+\sqrt{2})\tan g]. \tag{7.37}$$

Practically, these polar components can be measured experimentally. Here, we perform a numerical simulation instead. The results for $\ln|(\hat{\boldsymbol{\sigma}}_z)_{\rm m}|$ and -arg$[(\hat{\boldsymbol{\sigma}}_z)_{\rm m}]$ are shown in Fig. 7.2 (a) and (b), respectively, where the simulation results (cross curves) are well agreement with the analytical results (solid curves).

To evaluate the weak value of the second measurement, we use the relation (7.20), where the derivative of the logarithm of the modulus is the imaginary part of the weak value, and the minus of the derivative of the phase is the real part of the modular value.

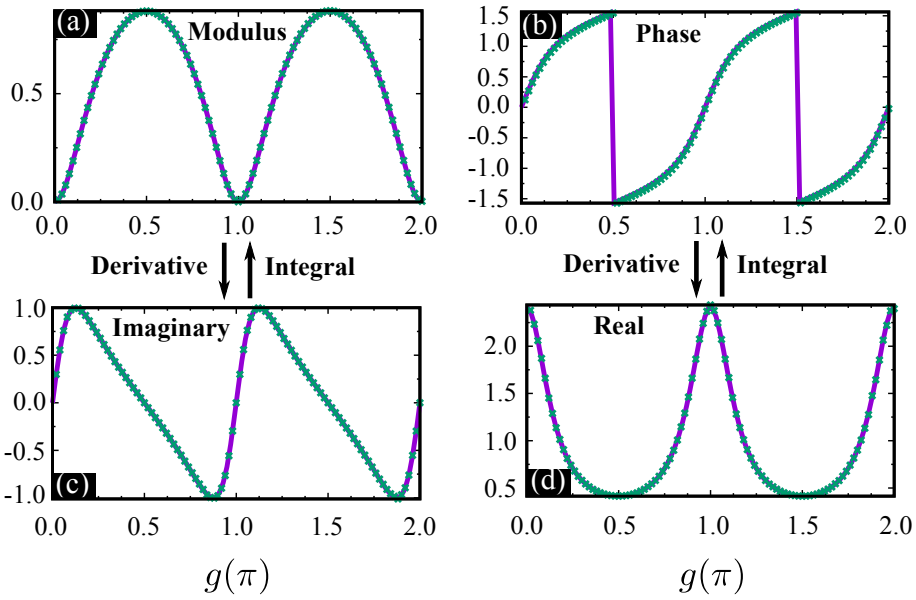

Figure 7.2: (a, b) The logarithm of the modulus and the minus of the phase of the complex modular value $(\hat{\boldsymbol{\sigma}}_z)_{\mathrm{m}}$, where their derivatives respect to g will give the corresponding imaginary and the real parts of the weak value in (c, d). The discrete values are obtained from an identical ensemble of 10^5 pre- and postselection states, while the curves are analytical results.

The results are shown in Fig. 7.2 (c) and (d). In Fig. 7.2, the simulation results are performed in between an identical ensemble of 10^5 pre- and postselection states. The simulation scheme following the method was introduced in Ref [102].

Chapter 8

Conclusions and Outlook

8.1 Conclusions

In this dissertation, we have theoretically studied the concept of quantum modular values of measured observables in quantum mechanics and its relations to quantum weak values. Our study provides detailed generalizations of the quantum modular value as well as its complex behaviors in various aspects of quantum mechanics. We first carried out full relations of modular values to weak values for finite-dimensional systems. Subsequently, on the one hand, we have presented and investigated the generalized modular values under various pointer states, extended from the original proposal with the qubit pointer to the finite-dimensional discrete pointer and the continuous pointer. We have also described the concept of time-dependent quantum weak and modular values in an enlarged Hilbert space, which can be viewed as a quantum simulator that simulates weak/modular measurement scheme. On the other, we have carried out some statistical/physical properties of modular values under the viewpoint of complex modular values. Our study, therefore, provides a more powerful and efficient tool than weak values to look inside the quantum world via quantum measurements. Furthermore, this work gives significant contributions to quantum physics in the sense that the quantum modular value is a topic that requires a close examination of the use in quantum physics in the coming years.

8.2 Outlook

In future, we intuitively believe that quantum modular values and quantum strong measurements which are based on modular values can be potential concepts to motivate and guide further various exciting studies in the field.

8.2.1 Quantum state estimation

One possible application is the quantum state estimation. In this concept, a practical technique for quantum state identification is known as quantum state tomography (QST). This indirect method requires measurements on multiple copies of the system in a complete set of noncommuting observables and then reconstructs the quantum state that reveals from the measurement results by using a reliable numerical algorithm. However, this method still has a limitation of usage because of the requirement of the advanced experimental equipment and the reliable algorithm especially in high-dimensional. There is another approach, which is known as the direct state measurement (DSM). In this method, the wave function amplitudes of the quantum states are proportional to the weak values of the weak measurements. However, the precision of the DSM based on weak measurement is not so high in comparison with QST because of the bias error caused by the finiteness of the weak interaction. A strong measurement, therefore, would give a better result for the estimations. Moreover, strong measurement schemes combining with enlarged quantum states can possibly improve the accuracy result in the direct state reconstruction or estimate the unknown quantum states and also provides a reliable tool for universal quantum computing, testing of quantum circuits.

8.2.2 Continuous monitoring enlarged systems

Another possible application is *continuous monitoring enlarged systems*. Particularly, we can consider an enlarged quantum density matrix in an enlarged Hilbert space that incorporate both the preselection and postselection density matrices. Using this enlarged density matrix, we can evaluate quantum weak and modular values of some physical properties for any quantum systems, such as superconducting qubit system. This proposal might provide a convenient tool for continuous monitoring a quantum system and could motivate and guide further various exciting experiments.

References

[1] Y. Aharonov, D. Z. Albert, and L. Vaidman, Phys. Rev. Lett. **60**, 1351 (1988).

[2] A. Hosoya and Y. Shikano, J. Phys. A: Math. Theor. **43**, 385307 (2010).

[3] M. F. Pusey, Phys. Rev. Lett. **113**, 200401 (2014).

[4] Y. Aharonov, D. Rohrlich, *Quantum Paradoxes: Quantum Theory for the Perplexed*, Wiley-VCH, Weinheim, Ch. 17 (2005).

[5] Y. Aharonov, S. Nussinov, S. Popescu, and L. Vaidman, Phys. Rev. A **87**, 014105 (2012).

[6] L. Hardy, Phys. Rew. Lett. **68**, 2981 (1992).

[7] Y. Aharonov, A. Botero, S. Popescu, B. Rezink, and J. Tollaksen, Phys. Lett. A **301**, 130-138 (2002).

[8] J. S. Lundeen, and A. M. Steinberg, Phys. Rev. Lett. **102**, 020404 (2009).

[9] K. Yokota, T. Yamamoto, M. Koashi, and N. Imoto, New J. Phys. **11**, 033011 (2009).

[10] Y. Aharonov, S. Popescu, D. Rohrlich, and P. Skrzypczky, New J. Phys. **15**, 113015 (2013).

[11] T. Denkmayr, H. Geppert, S. Sponar, H. Lemmel, A. Matzkin, J. Tollaksen, and Y. Hasegawa, Nature Commun. **5**, 4492 (2014).

[12] S. Pang, J. Dressel, and T. A. Brun, Phys. Rev. Lett. **113**, 030401 (2014).; S. Huang, and G.S. Agarwal, New. J. Phys. **17**, 093032 (2015).; A. Nishizawa, Phys.

Rev. A **92**, 032123 (2015).; Y. Susa, and S. Tanaka, Phys. Rev. A **92**, 012112 (2015).; S. Pang, and T.A. Brun, Phys. Rev. Lett. **115**, 120401 (2015).; S. Pang, and T.A. Brun, Phys. Rev. A **92**, 012120 (2015).

[13] O. Hosten and P. Kwiat, Science **319**, 787 (2008); P. B. Dixon, D. J. Starling, A. N. Jordan, and J. C. Howell, Phys. Rev. Lett. **102**, 173601 (2009).; M. D. Turner, C. A. Hagedorn, S. Schlamminger, and J. H. Gundlach, Opt. Lett. **36**, 1479 (2011).; M. Pfeifer and P. Fischer, Opt. Express **19**, 16508 (2011).; X. Zhou, Z. Xiao, H. Luo, and S. Wen, Phys. Rev. A **85**, 043809 (2012).; L. Zhou, Y. Turek, C. P. Sun, and F. Nori, Phys. Rev. A **88**, 053815 (2013).;G. Jayaswal, G. Mistura, and M. Merano, Opt. Lett. **39**, 2266-2269 (2014).

[14] D. J. Starling, P. B. Dixon, A. N. Jordan, and J. C. Howell, Phys. Rev. A **82**, 063822 (2010).; X.-Y. Xu, Y. Kedem, K. Sun, L. Vaidman, C.-F. Li, and G.-C. Guo, Phys. Rev. Lett. **111**, 033604 (2013).; G. Strubi and C. Bruder, Phys. Rev. Lett. **110**, 083605 (2013).; G. I. Viza, J. Martnez-Rincn, G. A. Howland, H. Frostig, I. Shomroni, B. Dayan, and J. C. Howell, Opt. Lett. **38**, 2949 (2013).; O. S. Magana-Loaiza, M. Mirhosseini, B. Rodenburg, and R. W. Boyd, Phys. Rev. Lett. **112**, 200401 (2014).

[15] L. Zhang, A. Datta, and I. A. Walmsley, Phys. Rev. Lett. **114**, 210801 (2015).

[16] G. I. Viza, J. Martinez-Rincon, G. B. Alves, A. N. Jordan, and J. C. Howell, Phys. Rev. A **92**, 032127 (2015).

[17] M. Altorio, M. G. Genoni, F. Somma, and M. Barbieri, Phys. Rev. Lett. **116**, 100802 (2016).

[18] G. B. Alves, A. Pimentel, M. Hor-Meyll, S. P. Walborn, L. Davidovich, and R. L. de M. Filho, Phys. Rev. A **95**, 012104 (2017).

[19] A. P. Lund and H. M. Wiseman, New. J. Phys. **12**, 093011 (2010).; L. A. Rozema, A. Darabi, D. H. Mahler, A. Hayat, Y. Soudagar, and A. M. Steinberg, Phys. Rev. Lett. **109**, 100404 (2012), Erratum Phys. Rev. Lett. **109**, 189902 (2012).; S.Y. Baek, F. Kaneda, M. Ozawa, and K. Edamatsu, Sci. Rep. **3**, 2221 (2013).

[20] J. S. Lundeen, B. Sutherland, A. Patel, C. Stewart, and C. Bamber, Nature **474**, 188-191 (2011).; J. S. Lundeen, and C. Bamber, Phys. Rev. Lett. **108**, 070402 (2012).; J. Z. Salvail, M. Agnew, A. S. Johnson, E. Bolduc, J. Leach, and R. W. Boyd, Nat. Photon. **7**, 316 (2013).; A.D. Lorenzo, Phys. Rev. A **88**, 042114 (2013).; A. D. Lorenzo, Phys. Rev. Lett. **110**, 010404 (2013).; S. Wu, Sci. Rep. **3** (2013), 10.1038/srep01193.; M. Mirhosseini, O.S. Magana Loaiza, S.M.H. Rafsanjani, and R. W. Boyd, Phys. Rev. Lett. **113**, 090402 (2014).; C. Bamber, and J. S. Lundeen, Phys. Rev. Lett. **112**, 070405 (2014).; M. Malik, M. Mirhosseini, M.P.J. Lavery, J. Leach, M. J. Padgett, and R. W. Boyd, Nat. Comm. **5** (2014),10.1038/ncomms4115.; L. Maccone, and C.C. Rusconi, Phys. Rev. A **89**, 022122 (2014).; J. A. Gross, N. Dangniam, C. Ferrie, and C. M. Caves, Phys. Rev. A **92**, 062133 (2015).; Z. Shi, M. Mirhosseini, J. Margiewicz, M. Malik, F. Rivera, Z. Zhu, and R. W. Boyd, Optica **2**, 388 (2015).; S. Pang, J. R. G. Alonso, T. A. Brun, and A. N. Jordan, Phys. Rev. A **94**, 012329 (2016).;G. Vallone, and D. Dequal, Phys. Rev. Lett. **116**, 040502 (2016).; E. Bolduc, G. Gariepy, and J. Leach, Nat. Commun. **7** (2016), 10.1038/ncomms10439.

[21] W. Qiao, J. Phys. A: Math. Gen. **29**, 2257 (1996).; A. Kempf, J. Math. Phys. **41**, 2360-2374 (2000).; P. J. S. G. Ferreira and A. Kempf, IEEE Trans. on Sig. Proc. **54**, 3732-3740 (2006),; Y. Aharonov, F. Colombo, I. Sabadini, D. C. Struppa, and J. Tollaksen, J. Phys. A: Math. Theor. **44**, 365304 (2011).; M. V. Berry, N. Brunner, S. Popescu, P. Shukla, J. Phys. A: Math.Theor. **44**, 492001 (2011).; I. Chremmos and G. Fikioris, J. Phys. A: Math. Theor., **48**, 265204 (2015).; L. Chojnacki and A. Kempf, J. Phys. A: Math. Theor. **49** 505203 (2016).; Y. Aharonov, F. Colombo, I. Sabadini, D. C. Struppa, J. Tollaksen, *The Mathematics of Superoscillations* (Memoirs of the American Mathematical Society, 2017).

[22] J. Dressel and A. N. Jordan, Phys. Rev. Lett. **109**, 230402 (2012).

[23] T. A. Brun, L. Diosi, and W. T. Strunz, Phys. Rev. A **77**, 032101 (2008).

[24] S. Wu and Molmer, Phys. Lett. A **374**, 34 (2009).

[25] Y. Kedem and L. Vaidman, Phys. Rev. Lett. **105**, 230401 (2010).

[26] http://www.theory.caltech.edu/people/preskill/ph219/chap3_15.pdf

[27] M. A. Nielsen, and I. L. Chuang, *Quantum Computation and Quantum Information*, Cambridge, (2000).

[28] Y. Kedem, *Applications of the Two-state Formalism for Improvement of Measurement Efficiency*, doctoral dissertation.

[29] J. Dressel, M. Malik, F.M. Miatto, A.N. Jordan, and R.W. Boyd, Rev. Mod. Phys. **86**, 307 (2014).

[30] J. Dressel, Phys. Rev. A **91**, 032116 (2015).

[31] R. Jozsa, Phys. Rev. A, **76**, 044103 (2007).

[32] J. Dressel and A. N. Jordan, **85**, 012107 (2012).

[33] J. von Neumann, *Mathematische Grundlage der Quanten mechanik* (Springer, Berlin, 1932; English translation Princeton University Press, Princeton, NJ, 1955).

[34] C. Moler and C. V. Loan, SIAM Rev. **20**, 801-836 (1978).

[35] A.D. Lorenzo, Phys. Lett. A **379**, 1681-1688 (2015).

[36] K.J. Resch, and A.M. Steinberg, Phys. Rev. Lett. **92**, 130402 (2004).

[37] K.J. Resch, J. Opt. B: Quant. Semi. Opt. **6**, 482 (2004).

[38] J.S. Lundeen, and K.J. Resch, Phys. Lett. A **334**, 337 (2005).

[39] L. Vaidman, Phys. Rev. Lett. **70**, 3369 (1993).

[40] L. Carroll, *Alice's Adventures In Wonderland* (reprinted in The Annotated Alice) (ed. Gardner, M.) 90?91 (Penguin Books, 1965).

[41] A. DiLorenzo, Phys. Rev. A **85**, 032106 (2012).

[42] S. Wu, and Y. Li, Phys. Rev. A **83**, 052106 (2011).

[43] D.J. Griffiths, *Introduction to Quantum Mechanics* Ch. 4, 2nd Edition, Pearson Education (2005).

[44] A.G. Kofman, S.Ashhab, and F. Nori, Phys. Rep. **420**, 43 (2012).

[45] K. Nakamura, A. Nishizawa, and M.K. Fujimoto, Phys. Rev. A **85**, 012113 (2012).

[46] M. Combescure, and D. Robert, *Coherent States and Applications in Mathematical Physics*, Ch. 10, (Springer, 2012).

[47] We note that the choice of n is not relevant here, which can be seen from the fact that the right-hand site of Eq.(4.24) does not contain $\lambda(= n$ in the present subsection case). It depends, however, on the system states $\hat{\boldsymbol{\rho}}_i$ and $\hat{\boldsymbol{\rho}}_f$.

[48] Y. Aharonov, and L. Vaidman, J. Phys. A: Math. Gen. **24**, 2315-2328 (1991).

[49] R. S. Cohen, M. Horne, and J. J. Stachel (eds.), *Potentiality, Entanglement and Passion-at-a-Distance*, Quantum Mechanical Studies for A. M. Shimony (Kluwer Academic, 1997).

[50] J. G. Muga, R. S. Mayato, and I. Egusquiza (eds.), *Time in Quantum Mechanic*, 2nd ed. (Springer, 2007).

[51] I. M. Duck, P. M. Stevenson, and E. C. G. Sudarshan, Phys. Rev. D **40**, 2112 (1989).

[52] J. Casanova, C. Sabin, J. Leon, I. L. Egusquiza, R. Gerritsma, C. F. Roos, J. J. Garcia-Ripoll, and E. Solano, Phys. Rev. X **1**, 021018 (2011).

[53] C. Noh, B. M. Rodriguez-Lara, and D. G. Angelakis, Phys. Rev. A **87**, 040102(R) (2013).

[54] B. M. Rodriguez-Lara, and H. M. Moya-Cessa, Phys. Rev. A **89**, 015803 (2014).

[55] X. Zhang, Y. Shen, J. Zhang, J. Casanova, L. Lamata, E. Solano, M. H. Yung, J. N Zhang, and K. Kim, Nat. Commu **6**, doi:10. 1038/ncomms8917 (2015).

[56] R. DiCandia, B. Mejia, H. Castillo, J. S. Pedernales, J. Casanova, and E. Solano, Phys. Rev. Lett. **111**, 240502 (2013).

[57] J. S. Pedernales, R. DiCandia, P. Schindler, T. Monz, M. Hennrich, J. Casanova, and E. Solano, Phys. Rev. A **90**, 012327 (2014).

[58] J. C. Loredo, M. P. Almeida, R. Di Candia, J. S. Pedernales, J. Casanova, E. Solano, and A. G. White, Phys. Rev. Lett. **116**, 070503 (2016).

[59] M. C Chen, D. Wu, Z. E Su, X. D Cai, X. L Wang, T. Yang, L. Li, N. L. Liu, C. Y Lu, and J. W. Pan, Phys. Rev. Lett. **116**, 070502 (2016).

[60] U. Alvarez-Rodriguez, J. Casanova, L. Lamata, and E. Solano, Phys. Rev. Lett. **111**, 090503 (2013).

[61] X. H. Cheng, U. Alvarez-Rodriguez, L. Lamata, X. Chen, and E. Solano, Phys. Rev. A **92**, 022344 (2015).

[62] A. D. Parks, J. Phys. A **41**, 335305 (2008).

[63] P. C. W. Davies, Phys. Rev. A **79**, 032103 (2009).

[64] M. Ban, J. Mod. Phys. **4**, 1-8 (2013).

[65] Y. Aharonov, E. Cohen, and A. C. Elitzur, Ann. of Phys. **355**, 258-268 (2015).

[66] B. Reznik, and Y. Aharonov, Phys. Rev. A **52**, 2538 (1995).

[67] Z. Shi, M. Mirhosseine, J. Margiewicz, M. Malik, F. Rivera, Z. Zhu, and R. W. Boyd, Optical **2**, 388-392 (2015).

[68] H. F. Trotter, Proc. Am. Math. Soc. **10**, 545 (1959).

[69] S. Lloyd, Science **273**, 1073 (1996).

[70] U. LasHeras, U. Alvarez-Rodriguez, E. Solano, and M. Sanz, Phys. Rev. Lett. **116**, 230504 (2016).

[71] J. Casanova, A. Mezzacapo, L. Lamata, and E. Solano, Phys. Rev. Lett. **108**, 190502 (2012).

[72] K. Mølmer, and A. Sørensen, Phys. Rev. Lett **82**, 1835-1838 (1999).

[73] M. Müller, K. Hammerer, Y. L. Zhou, C. F. Roos, and P. Zoller, New J. Phys. **13**, 085007 (2011).

[74] J. T. Barreior, M. Müller, P. Schindler, D. Nigg, T. Monz, M. Chwalla, M. Hennrich, C. F. Roos, P. Zoller, and R. Blatt, Nature **470**, 486 (2011).

[75] A. Y. Kitaev, A. Shen, and M. N. Vyalyi, *Classical and quantum computation*, **47** (American Mathematical Society Providence, 2002).

[76] A. Y. Kitaev, Ann. Phys. **303**, 2-30 (2003).

[77] Y. Y. Subaşı, and C. Jarzynski, Phys. Rev. A **94**, 012342 (2016).

[78] D. Leibfried, R. Blatt, C. Monroe, and D. Wineland, Rev. Mod. Phys. **75**, 281 (2003).

[79] R. Batt, and C. F. Roos, Nat. Phys. doi: 10. 1038/NPHS2252 (2012).

[80] L. Lamata, A. Mezzacapo, J. Casanova, and E. Solano, EPJ Quant. Techn. 1:9 (2014).

[81] I. M. Georgescu, S. Ashhab, and F. Nori, Rev. Mod. Phys. **86**, 153 (2014).

[82] H. Hofmann, New J. Phys. **13**, 103009 (2011).

[83] H. Hofmann, New J. Phys. **14**, 043031 (2012).

[84] Y. Aharonov and A. Botero, Phys. Rev. A **72**, 052111 (2005). .

[85] J. Tollaksen, J. Phys. A: Math. Theor. **40**, 9033 (2007)

[86] Y. Shikano and A. Hosoya, J. Phys. A: Math. Theor. **43**, 025304 (2010).

[87] A. Hosoya and M. Koga, J. Phys. A: Math. Theor. **44**, 415303 (2011).

[88] G. Mitchison, R. Jozsa and S. Popescu, Phys. Rev. A **76**, 062105 (2007).

[89] P.A.M. Dirac, Proc. R. Soc. A 1801 (1942).

[90] R.P. Feynman, *Negative probability Quantum Implications: essays in Honour of David Bohm* ed B J Hiley and F D Peat (London: Routledge & Kegan Paul) p 235 (1987).

[91] H.F. Hofmann, Phys. Rev. A **81**, 012103 (2010).

[92] H.F. Hofmann, Phys. Rev. A **89**, 042115 (2014).

[93] H.F. Hofmann, Phys. Rev. A **91**, 062123 (2015).

[94] M. Cormann, M. Remy, B. Kolaric, and Y. Caudano, Phys. Rev. A **93**, 042124 (2016).

[95] E. Sjöqvist, Phys. Lett. A **359**, 187 (2006).

[96] M. V. Berry, J. Mod. Opt. **34**, 1401 (1987).

[97] N. Mukunda and R. Simon, Ann. Phys. **228**, 205 (1993).

[98] S. Tamate, H. Kobayashi, T. Nakanishi, K. Sugiyama, and M. Kitano, New J. Phys. **11**, 093025 (2009).

[99] M. V. Berry, Proc. Roy. Soc. London, Ser A **392**, 45 (1984).

[100] B. Simon, Phys. Rev. Lett. **51**, 2167 (1983).

[101] D. R. Solli, C. F. McCormick, and R. Y. Chiao, Phys. Rev. Lett. **92**, 043601 (2004).

[102] V. Monachello, R. Flack, B. J. Hiley, and R. E. Callaghan, arXiv:1701.04808v1 (2017).

[103] A. Cayley, Phil. Trans. **148**, (1858).

[104] W. R. Hamilton, *Lectures on Quaternions*, (Dublin, 1853).

[105] G. Frobenius, J. reine angew. Math. **84**, 1-63 (1878).

[106] J.J. Sakurai, *Modern Quantum Mechanics* (Addision-Wesley, 1985).

[107] W. Dür, M. J. Bremner, and H. J. Briegel, Phys. Rev. A **78**, 052325 (2008).

Appendix A

The Lagrange interpolation

In this appendix, we will revise and prove the Lagrange interpolation that we have used in Chap. 3. Before doing this, let us introduce the Cayley-Hamilton theorem, which will be used later for proving the interpolation, as below.

A.1 The Cayley-Hamilton theorem

The idea that every square matrix satisfies its own characteristic equation was first explicitly proposed by Arthur Cayley in 1858 [103]. The author did not prove the theorem in general but generalized from the proof of 3-by-3 matrices. Before this claim was introduced, William Rowan Hamilton also had stated that a three-dimensional rotation transformation satisfies its own characteristic equation [104]. Even though they did not prove the theorem generally, to give the reference on their works in the literature, we usually name it as the Cayley-Hamilton theorem. The theorem then was first generally proved by Georg Frobenius in 1878 [105].

Let us now describe the theorem in the language of mathematics. Suppose that $\boldsymbol{A}(n,n)$ is a square n-by-n matrix with the characteristic polynomial is denoted and given as

$$\chi(\lambda) = \det(\boldsymbol{A} - \lambda \boldsymbol{I}). \tag{A.1.1}$$

Then expanding the full determinant and collecting terms the same power of λ, we have

$$\begin{aligned}
&\det(\boldsymbol{A}-\lambda\boldsymbol{I}) \\
&=\det\big(\boldsymbol{a}_1-\lambda\boldsymbol{e}_1,\boldsymbol{a}_2-\lambda\boldsymbol{e}_2,...,\boldsymbol{a}_n-\lambda\boldsymbol{e}_n\big) \\
&\overset{(0)}{=}\det(\boldsymbol{a}_1,\boldsymbol{a}_2,...,\boldsymbol{a}_n) \\
&\overset{(1)}{+}\Big[\det(\boldsymbol{a}_1,....,\boldsymbol{a}_{n-1},\boldsymbol{e}_n)+\det(\boldsymbol{a}_1,....,\boldsymbol{e}_{n-1},\boldsymbol{a}_n)+...+\det(\boldsymbol{e}_1,\boldsymbol{a}_2,....,\boldsymbol{a}_n)\Big](-\lambda) \\
&... \\
&\overset{(n-1)}{+}\Big[\det(\boldsymbol{a}_1,\boldsymbol{e}_2,...,\boldsymbol{e}_n)+\det(\boldsymbol{e}_1,\boldsymbol{a}_2,...,\boldsymbol{e}_n)+...+\det(\boldsymbol{e}_1,...,\boldsymbol{e}_{n-1},\boldsymbol{a}_n)\Big](-\lambda)^{n-1} \\
&\overset{(n)}{=}\det(\boldsymbol{e}_1,\boldsymbol{e}_2,...,\boldsymbol{e}_n)(-\lambda)^n\ , \qquad \text{(A.1.2)}
\end{aligned}$$

where we have assumed $\boldsymbol{A}=[\boldsymbol{a}_1,\boldsymbol{a}_2,....,\boldsymbol{a}_n]$. From (0) we have

$$\det(\boldsymbol{a}_1,\boldsymbol{a}_2,...,\boldsymbol{a}_n)=\det(\boldsymbol{A})\ . \qquad \text{(A.1.3)}$$

From (n) we have

$$\det(\boldsymbol{e}_1,\boldsymbol{e}_2,...,\boldsymbol{e}_n)(-\lambda)^n=(-1)^n\lambda^n\ . \qquad \text{(A.1.4)}$$

And let us consider, for example, (n-1), we derive

$$\det(\boldsymbol{a}_1,\boldsymbol{e}_2,...,\boldsymbol{e}_n)=\det(a_{11}\boldsymbol{e}_1+...+a_{1n}\boldsymbol{e}_n,\boldsymbol{e}_2,...,\boldsymbol{e}_n)=a_{11} \qquad \text{(A.1.5)}$$

Perform similarly and take the summation, we obtain

$$(n-1)=a_{11}+a_{22}+...+a_{nn}=\mathrm{trace}(\boldsymbol{A})\ . \qquad \text{(A.1.6)}$$

Then Eq. (A.1.2) can recast as

$$\begin{aligned}
\chi(\lambda)&=\det(\boldsymbol{A})+...+(-1)^{n-1}\mathrm{trace}(\boldsymbol{A})\lambda^{n-1}+(-1)^n\lambda^n \\
&=\sum_{i=0}^{n}\chi_i\lambda^i\ . \qquad \text{(A.1.7)}
\end{aligned}$$

The Cayley-Hamilton theorem states that $\chi(\boldsymbol{A})=\boldsymbol{0}$, where $\boldsymbol{0}$ is the zero matrix, and therefore

$$\begin{aligned}
\chi(\boldsymbol{A})&=\sum_{i=0}^{n}\chi_i\boldsymbol{A}^i \\
&=\det(\boldsymbol{A})\boldsymbol{I}+...+(-1)^{n-1}\mathrm{trace}(\boldsymbol{A})\boldsymbol{A}^{n-1}+(-1)^n\boldsymbol{A}^n. \qquad \text{(A.1.8)}
\end{aligned}$$

As an example, let us choose

$$\boldsymbol{A} = \begin{pmatrix} 1 & 2 & 2 \\ 2 & 4 & 5 \\ 5 & 6 & 8 \end{pmatrix} \tag{A.1.9}$$

Then we have

$$\boldsymbol{A} - \lambda \boldsymbol{I} = \begin{pmatrix} 1-\lambda & 2 & 2 \\ 2 & 4-\lambda & 5 \\ 5 & 6 & 8-\lambda \end{pmatrix}, \tag{A.1.10}$$

and the characteristic polynomial is calculated to be

$$\chi(\lambda) = \det(\boldsymbol{A} - \lambda \boldsymbol{I}) = 4 + 13\lambda^2 - \lambda^3. \tag{A.1.11}$$

We can also easy to verify that

$$\chi(\boldsymbol{A}) = 4 + 13\boldsymbol{A}^2 - \boldsymbol{A}^3 = \boldsymbol{0}. \tag{A.1.12}$$

Since the Cayley-Hamilton theorem is not our main subject to study, so we will not prove this theorem, but use as a result instead.

A.2 Proof of the Lagrange interpolation

To prove the Lagrange interpolation, let us define a matrix function F by the following equation

$$F(g) \equiv e^{-ig\boldsymbol{A}} = \sum_{k=1}^{n} e^{-ig\lambda_k} L_k(\boldsymbol{A}), \tag{A.2.1}$$

where $L_k(\boldsymbol{A})$ is a Lagrange interpolation coefficient as mentioned in Eq. (3.2) in the main text. All we need to do is that verify the differential equation and the initial condition, such that

$$\begin{cases} \partial_g F(g) & = -i\boldsymbol{A}F(g) \\ F(0) & = \boldsymbol{I} \end{cases} \tag{A.2.2}$$

From Eq. (A.2.1) we can see that

$$i\boldsymbol{A}F(g) + \partial_g F(g) = i\sum_{k=1}^{n} e^{-ig\lambda_k}(\boldsymbol{A} - \lambda_k \boldsymbol{I})L_k(\boldsymbol{A}). \tag{A.2.3}$$

Using the Cayley-Hamilton theorem above, we have $(\boldsymbol{A} - \lambda_k \boldsymbol{I})L_k(\boldsymbol{A}) = 0$ for each k, then F satisfies the differential equation $\partial_g F(g) = -i\boldsymbol{A}F(g)$.

Next, to show the initial condition, we express it as

$$\sum_{k=1}^{n} L_k(\boldsymbol{A}) = \boldsymbol{I}. \tag{A.2.4}$$

Let us define by $L_k(\lambda)$ the polynomial in λ of degree $n-1$ as

$$L_k(\lambda) = \prod_{j=1,\ j\neq k}^{n} \frac{\lambda - \lambda_j}{\lambda_k - \lambda_j}, \tag{A.2.5}$$

where $\lambda_1, ..., \lambda_n$ are n distinct scalars. For $\lambda_i \neq \lambda_k$, we have,

$$L_k(\lambda_i) = \frac{\lambda_i - \lambda_1}{\lambda_k - \lambda_1} \cdot \frac{\lambda_i - \lambda_2}{\lambda_k - \lambda_2} ..... \frac{\lambda_i - \lambda_i}{\lambda_k - \lambda_i} ..... \frac{\lambda_i - \lambda_n}{\lambda_k - \lambda_n} = 0, \tag{A.2.6}$$

and for $\lambda_i = \lambda_k$, then we have,

$$L_k(\lambda_i) = \prod_{j=1,\ j\neq k}^{n} \frac{\lambda_k - \lambda_j}{\lambda_k - \lambda_j} = 1. \tag{A.2.7}$$

Then, for each λ, it gives

$$\sum_{k=1}^{n} L_k(\lambda) = 1. \tag{A.2.8}$$

As a consequence, we have

$$\sum_{k=1}^{n} L_k(\boldsymbol{A}) = \boldsymbol{I}. \tag{A.2.9}$$

that we prove the initial condition Eq. (A.2.4), and also, the Lagrange interpolation was proved.

Appendix B

The generalized modular-value based scheme

In this appendix, we perform the detail calculations for the joint probability in the generalized modular-value-based scheme as we discussed in Chap. 4. We later also calculate the expectation value of a pointer observable and the final state of the pointer.

B.1 Joint probability and the expectation value

Let us first derive explicitly the joint state of the system and the pointer after the interaction which is given as

$$\begin{aligned}\hat{\boldsymbol{\rho}}' &= \hat{\boldsymbol{U}}\hat{\boldsymbol{\rho}}\hat{\boldsymbol{U}}^{\dagger} \\ &= \hat{\boldsymbol{U}}\big(\hat{\boldsymbol{\rho}}_i \otimes |\xi\rangle\langle\xi|\big)\hat{\boldsymbol{U}}^{\dagger}\,. \end{aligned} \tag{B.1.1}$$

Substituting this expression into the joint probability, Eq.(4.4) yields

$$\begin{aligned} P(\mu, f) &= \mathrm{Tr}\big[(\hat{\boldsymbol{\rho}}_f \otimes |\mu\rangle\langle\mu|)\hat{\boldsymbol{\rho}}'\big] \\ &= \mathrm{Tr}\big[(\hat{\boldsymbol{\rho}}_f \otimes |\mu\rangle\langle\mu|)\hat{\boldsymbol{U}}(\hat{\boldsymbol{\rho}}_i \otimes |\xi\rangle\langle\xi|)\hat{\boldsymbol{U}}^{\dagger}\big] \\ &= \mathrm{Tr}_{\mathrm{s}}\big[\hat{\boldsymbol{\rho}}_f \cdot \mathrm{Tr}_{\mathrm{p}}\big[(\hat{\boldsymbol{I}} \otimes |\mu\rangle\langle\mu|)\hat{\boldsymbol{U}}(\hat{\boldsymbol{\rho}}_i \otimes |\xi\rangle\langle\xi|)\hat{\boldsymbol{U}}^{\dagger}\big]\big] \\ &= \mathrm{Tr}_{\mathrm{s}}\big[\hat{\boldsymbol{\rho}}_f \cdot \langle\mu|\hat{\boldsymbol{U}}|\xi\rangle\hat{\boldsymbol{\rho}}_i\langle\xi|\hat{\boldsymbol{U}}^{\dagger}|\mu\rangle\big] \\ &= \mathrm{Tr}_{\mathrm{s}}\big[\hat{\boldsymbol{\rho}}_f\hat{\boldsymbol{\Omega}}_{\mu}\hat{\boldsymbol{\rho}}_i\hat{\boldsymbol{\Omega}}_{\mu}^{\dagger}\big]\,, \end{aligned} \tag{B.1.2}$$

where the operator $\hat{\boldsymbol{\Omega}}_\mu = \langle\mu|\hat{\boldsymbol{U}}|\xi\rangle$ represents the Kraus operator.

The probability $P(f)$ can be straightforwardly calculated by taking the sum of all μ's for Eq.(B.1.2), resulting in

$$P(f) = \mathrm{Tr_s}[\hat{\boldsymbol{\rho}}_f \hat{\boldsymbol{\rho}}'_i] \,, \tag{B.1.3}$$

where $\hat{\boldsymbol{\rho}}'_i$ is calculated, by tracing out the pointer Hilbert space of Eq. (B.1.1), to be

$$\begin{aligned} \hat{\boldsymbol{\rho}}'_i &= \mathrm{Tr_p}\big[\hat{\boldsymbol{U}}\big(\hat{\boldsymbol{\rho}}_i \otimes |\xi\rangle\langle\xi|\big)\hat{\boldsymbol{U}}^\dagger\big] \\ &= \sum_\mu \hat{\boldsymbol{\Omega}}_\mu \hat{\boldsymbol{\rho}}_i \hat{\boldsymbol{\Omega}}_\mu^\dagger \,. \end{aligned} \tag{B.1.4}$$

We next calculate the expectation value of an arbitrary observable in the pointer, which is given as

$$\langle \hat{\boldsymbol{O}}_\mathrm{p} \rangle_\eta = \frac{\mathrm{Tr}[(\hat{\boldsymbol{\rho}}_f \otimes \hat{\boldsymbol{O}}_\mathrm{p})\hat{\boldsymbol{\rho}}']}{\mathrm{Tr}[(\hat{\boldsymbol{\rho}}_f \otimes \hat{\boldsymbol{I}}_\mathrm{p})\hat{\boldsymbol{\rho}}']} \,, \tag{B.1.5}$$

We now insert $\hat{\boldsymbol{O}}_\mathrm{p} = \sum_k o_k |k\rangle\langle k|$ into the numerator and $\hat{\boldsymbol{I}}_\mathrm{p} = \sum_{k'} |k'\rangle\langle k'|$ into the denominator, and then perform calculations as in (B.1.2). The result is Eq.(4.10) in the main text.

B.2 Kraus operator

Consider the basis $\{|k\rangle, k = 0, 1, 2, ..., n-1\}$, where n denotes the dimension of the discrete pointer Hilbert space $\mathcal{H}_\mathrm{p}$. The initial pointer state can be expressed in the form

$$|\xi\rangle = \sum_k c_k |k\rangle, \;\; c_k = \langle k|\xi\rangle \,, \tag{B.2.1}$$

and the projection operator $\hat{\boldsymbol{P}} = |\lambda\rangle\langle\lambda|$ can be explicitly expressed as

$$\begin{aligned} \hat{\boldsymbol{P}} &= \sum_k k|k\rangle\langle k| \quad \text{with} \begin{cases} k = 1 & \text{if } k = \lambda \\ k = 0 & \text{if } k \neq \lambda \end{cases} \\ &= \sum_k \delta_{kl} |k\rangle\langle k| \,. \end{aligned} \tag{B.2.2}$$

Now, the action of the unitary operator $\hat{\boldsymbol{U}}$ on the initial pointer $|\xi\rangle$ can be characterized as follows [106]

$$\begin{aligned}\hat{\boldsymbol{U}}|\xi\rangle &= \sum_k \exp(-ig\hat{\boldsymbol{A}}\delta_{k\lambda})\ \langle k|\xi\rangle|k\rangle \\ &= \sum_k \exp(-ig\hat{\boldsymbol{A}}\delta_{k\lambda})\ c_k|k\rangle\ . \end{aligned} \tag{B.2.3}$$

Then, the Kraus operator yields

$$\begin{aligned}\hat{\boldsymbol{\Omega}}_\mu &= \langle\mu|\hat{\boldsymbol{U}}|\xi\rangle \\ &= \sum_k \exp(-ig\hat{\boldsymbol{A}}\delta_{k\lambda})\ c_k\langle\mu|k\rangle \\ &= \sum_k \exp(-ig\hat{\boldsymbol{A}}\delta_{k\lambda})\ c_k\delta_{\mu k} \\ &= c_\mu e^{-ig\hat{\boldsymbol{A}}\delta_{\mu\lambda}}, \end{aligned} \tag{B.2.4}$$

where $c_\mu = \langle\mu|\xi\rangle$.

B.3 The final state of the pointer

The final state of the pointer is given as

$$\hat{\boldsymbol{\rho}}_{\rm p}^{\rm out} = \frac{{\rm Tr_s}[(\hat{\boldsymbol{\rho}}_f \otimes \hat{\boldsymbol{I}})\hat{\boldsymbol{\rho}}']}{{\rm Tr}[(\hat{\boldsymbol{\rho}}_f \otimes \hat{\boldsymbol{I}})\hat{\boldsymbol{\rho}}']}. \tag{B.3.1}$$

In the numerator, let us insert $\sum_\mu |\mu\rangle\langle\mu| (= \hat{\boldsymbol{I}})$ and $\sum_\nu |\nu\rangle\langle\nu| (= \hat{\boldsymbol{I}})$, then we have

$$\begin{aligned}&{\rm Tr_s}\Big[\Big(\hat{\boldsymbol{\rho}}_f \otimes \sum_\mu |\mu\rangle\langle\mu|\Big)\hat{\boldsymbol{U}}\Big(\hat{\boldsymbol{\rho}}_i \otimes |\xi\rangle\langle\xi|\Big)\hat{\boldsymbol{U}}^\dagger \sum_\nu |\nu\rangle\langle\nu|\Big] \\ &= \sum_{\mu,\nu} c_\mu c_\nu^* {\rm Tr_s}\big[\hat{\boldsymbol{\rho}}_f\hat{\boldsymbol{\Omega}}_\mu\hat{\boldsymbol{\rho}}_i\hat{\boldsymbol{\Omega}}_\nu^\dagger\big]|\mu\rangle\langle\nu|. \end{aligned} \tag{B.3.2}$$

Similarly, in the denominator, we insert $\sum_\mu |\mu\rangle\langle\mu|$, and then trace out the pointer Hilbert space, which leads to

$$\begin{aligned}&{\rm Tr}\Big[\Big(\hat{\boldsymbol{\rho}}_f \otimes \sum_\mu |\mu\rangle\langle\mu|\Big)\hat{\boldsymbol{U}}\Big(\hat{\boldsymbol{\rho}}_i \otimes |\xi\rangle\langle\xi|\Big)\hat{\boldsymbol{U}}^\dagger\Big] \\ &= \sum_\mu |c_\mu|^2 {\rm Tr_s}\big[\hat{\boldsymbol{\rho}}_f\hat{\boldsymbol{\Omega}}_\mu\hat{\boldsymbol{\rho}}_i\hat{\boldsymbol{\Omega}}_\nu^\dagger\big]. \end{aligned} \tag{B.3.3}$$

After that, we divide both the numerator and denominator by the nonzero factor $\mathrm{Tr}_{\mathrm{s}}[\hat{\boldsymbol{\rho}}_f \hat{\boldsymbol{\rho}}_i]$, and use the definition of modular value Eq. (4.21). Then we finally obtain

$$\hat{\boldsymbol{\rho}}_{\mathrm{p}}^{\mathrm{out}} = \frac{\sum_{\mu,\nu} c_\mu c_\nu^* (\hat{\boldsymbol{A}})_{\mathrm{m}}^{\mu,\nu|\lambda} |\mu\rangle\langle\nu|}{\sum_\mu |c_\mu|^2 (\hat{\boldsymbol{A}})_{\mathrm{m}}^{\mu,\mu|\lambda}} \,, \tag{B.3.4}$$

which is Eq.(4.26).

Appendix C

Enlarged weak values

This appendix shows the detail calculation the weak value in the enlarged Hilbert space as given in the example in Chap. 6 and the implementation of the enlarged evolution operator.

C.1 Weak values in the enlarged Hilbert space

In this section, we will show how to calculate the weak value of $\hat{\boldsymbol{\sigma}}_x$ in the enlarged Hilbert space. Let us assume that the pre- and postselection states are both $|\uparrow_x\rangle$, and other cases can be treated similarly. We first calculate the postselection state at time $t_\mathrm{i} = 0$ by performing the backward evolution as

$$\begin{aligned} |\phi(0)\rangle &= \hat{\boldsymbol{U}}(0,T)|\phi(T)\rangle \\ &= e^{\frac{i\omega T}{2}\hat{\boldsymbol{\sigma}}_z}\frac{1}{\sqrt{2}}\begin{pmatrix}1\\1\end{pmatrix} \\ &= \frac{1}{\sqrt{2}}\begin{pmatrix}e^{\frac{i\omega T}{2}}\\e^{-\frac{i\omega T}{2}}\end{pmatrix}\ , \end{aligned} \tag{C.1.1}$$

where we also choose $t_\mathrm{f} = T$. Then the enlarged state at time $t_\mathrm{i} = 0$ is given by

$$|\Psi(0)\rangle = \frac{1}{2\sqrt{2}}\begin{pmatrix}1+e^{\frac{i\omega T}{2}}\\1+e^{-\frac{i\omega T}{2}}\\1-e^{\frac{i\omega T}{2}}\\1-e^{-\frac{i\omega T}{2}}\end{pmatrix}\ . \tag{C.1.2}$$

Under the evolution Eq. (5.22), the enlarged state propagates forward in time according to

$$\begin{aligned}|\Psi(t)\rangle &= \widetilde{\hat{\boldsymbol{U}}}(t,0)|\Psi(0)\rangle \\ &= \frac{1}{2\sqrt{2}}\begin{pmatrix} e^{-\frac{i\omega t}{2}}(1+e^{\frac{i\omega T}{2}}) \\ e^{\frac{i\omega t}{2}}(1+e^{-\frac{i\omega T}{2}}) \\ e^{-\frac{i\omega t}{2}}(1-e^{\frac{i\omega T}{2}}) \\ e^{\frac{i\omega t}{2}}(1-e^{-\frac{i\omega T}{2}}) \end{pmatrix} .\end{aligned} \tag{C.1.3}$$

Then the weak value of $\hat{\boldsymbol{\sigma}}_x$, which is given by Eq. (5.14), yiels

$$\begin{aligned}{}_{\uparrow_x}\langle\hat{\boldsymbol{\sigma}}_x\rangle^{\mathrm{w}}_{\uparrow_x} &= \frac{\langle\Psi(t)|(\hat{\boldsymbol{\sigma}}_z + i\hat{\boldsymbol{\sigma}}_y)\otimes\hat{\boldsymbol{\sigma}}_x|\Psi(t)\rangle}{\langle\Psi(t)|(\hat{\boldsymbol{\sigma}}_z + i\hat{\boldsymbol{\sigma}}_y)\otimes\hat{\boldsymbol{I}}_2|\Psi(t)\rangle} \\ &= \cos(\omega t) + \sin(\omega t)\tan(\frac{\omega T}{2}),\end{aligned} \tag{C.1.4}$$

which is the same result as Eq.(5.21a) of the normal case in the main text.

C.2 An implementation the enlarged evolution

In this section, we will show how to implement the evolution

$$\widetilde{\hat{\boldsymbol{U}}}(t) = e^{-\frac{i\omega t}{2}\hat{\boldsymbol{\sigma}}^c_x\otimes\hat{\boldsymbol{\sigma}}^s_z} , \tag{C.2.1}$$

by using two Mølmer-Sørensen gates and a local rotation gate. We start from two Mølmer-Sørensen gates applied onto both the extra spin and the system spin and one local rotation gate applied on the system spin only (see Fig. 5.3 in the main text):

$$\hat{\boldsymbol{U}}_{\mathrm{MS}}(\theta,\phi)e^{-\frac{i\omega t}{2}\hat{\boldsymbol{\sigma}}^s_y}\hat{\boldsymbol{U}}^\dagger_{\mathrm{MS}}(\theta,\phi) = e^{-\frac{i\omega t}{2}\cdot\hat{\boldsymbol{U}}_{\mathrm{MS}}(\theta,\phi)\hat{\boldsymbol{\sigma}}^s_y\hat{\boldsymbol{U}}^\dagger_{\mathrm{MS}}(\theta,\phi)} . \tag{C.2.2}$$

Here, we have used the useful formula [107]

$$\hat{\boldsymbol{U}}e^{\hat{\boldsymbol{H}}}\hat{\boldsymbol{U}}^\dagger = e^{\hat{\boldsymbol{U}}\hat{\boldsymbol{H}}\hat{\boldsymbol{U}}^\dagger} . \tag{C.2.3}$$

We write the Mølmer-Sørensen gate explicitly as

$$\hat{\boldsymbol{U}}_{\mathrm{MS}}(\theta,\phi) = e^{-\frac{i\theta}{4}(\cos\phi\hat{\boldsymbol{S}}_x+\sin\phi\hat{\boldsymbol{S}}_y)^2} , \tag{C.2.4}$$

where $\hat{\boldsymbol{S}}_{x,y} = \sum_{k=1}^{K} \hat{\boldsymbol{\sigma}}_{x,y}^{k}$, and K is the number of qubits that the Mølmer-Sørensen gate acting on. In our case, $K = 2$, and $\phi = 0$, which leads to

$$\hat{\boldsymbol{U}}_{\mathrm{MS}}(\theta, 0) = e^{-\frac{i\theta}{4}(\hat{\boldsymbol{\sigma}}_x^e + \hat{\boldsymbol{\sigma}}_z^s)^2}. \tag{C.2.5}$$

Then the term $\hat{\boldsymbol{U}}_{\mathrm{MS}}(\theta,\phi)\hat{\boldsymbol{\sigma}}_y^s\hat{\boldsymbol{U}}_{\mathrm{SM}}^{\dagger}(\theta,\phi)$ in Eq. (C.2.2) is calculated to be

$$\begin{aligned}\hat{\boldsymbol{U}}_{\mathrm{MS}}(\theta,\phi)\hat{\boldsymbol{\sigma}}_y^s\hat{\boldsymbol{U}}_{\mathrm{MS}}^{\dagger}(\theta,\phi) &= e^{-\frac{i\theta}{4}(\hat{\boldsymbol{\sigma}}_x^e + \hat{\boldsymbol{\sigma}}_z^s)^2}\hat{\boldsymbol{\sigma}}_y^s e^{\frac{i\theta}{4}(\hat{\boldsymbol{\sigma}}_x^e + \hat{\boldsymbol{\sigma}}_z^s)^2} \\ &= \cos\theta\hat{\boldsymbol{\sigma}}_y^s + \sin\theta\hat{\boldsymbol{\sigma}}_x^e\hat{\boldsymbol{\sigma}}_z^s\,,\end{aligned} \tag{C.2.6}$$

where we have used the Baker-Campbell-Hausdorff relation

$$e^{\hat{\boldsymbol{A}}}\hat{\boldsymbol{B}}e^{-\hat{\boldsymbol{A}}} = \hat{\boldsymbol{B}} + [\hat{\boldsymbol{A}}, \hat{\boldsymbol{B}}] + \frac{1}{2!}\big[\hat{\boldsymbol{A}}, [\boldsymbol{A}, \hat{\boldsymbol{B}}]\big] + ... \tag{C.2.7}$$

Then with the choice of $\theta = \pi/2$, Eq. (C.2.2) reduces to Eq. (C.2.1), which is the result in Eq. (5.30).

Acknowledgements

Despite my efforts over the past three years, this work would never be done unless the firm support of many pivotal people. I would love to give special thanks to my supervisor, Professor Nobuyuki Imoto, who has provided me a golden chance to pursue the doctoral course at Osaka University. He has provided me not only the profound knowledge but also the strong belief in my going road. It seems a light catches me up whenever I talk to him and of course, more ideas come to me at that moment. And also, with his enthusiastic guidance, I indeed pass the hardest periods of my life and gradually get more confidence. I am sincerely grateful to Professor Takashi Yamamoto for his computer software supports and many of others. I also warmly thank Matsuki Kenichiro for many hours of helpful discussion in the beginning stages joined the Laboratory and further supports of him and Yuichi Nagamatsu for my daily life in the early days in Japan. I also want to give many of my thanks to Akihiro Mizutani and Yuki Takeuchi for a lot of their devoted assistance. Last, but not least, I must thank my family, especially, my wife and my little daughter, who always stand by me.

Dedication

This work is dedicated to my wife and my little daughter.

List of Publications

The following papers were published during the completion of this Ph.D. Chapters 2-7 are based on some of these works.

Papers

1. Le Bin Ho and Nobuyuki Imoto, *"Quantum weak and modular values in enlarged Hilbert spaces"*, Phys. Rev. A **97**, 012112 (2018).

2. Le Bin Ho and Nobuyuki Imoto, *"Generalized modular-value-based scheme and its generalized modular value"*, Phys. Rev. A **95**, 032135 (2017).

3. Le Bin Ho and Nobuyuki Imoto, *"Full characterization of modular values for finite-dimensional systems"*, Phys. Lett. A **380**, 2129-2135 (2016).

4. Le Bin Ho and Tran Nguyen Lan, *"Photoenhanced spin/valley polarization and tunneling magnetoresistance in a ferromagnetic-normal-ferromagnetic silicene junction"*, J. Phys. D: Appl. Phys. **49**, 375106 (2016).

5. Vu Thi Ngoc Huyen, Le Bin Ho, Vu Cong Lap, and Nguyen Van Lien, *"Self-Optimized Biological Channels in Facilitating the Transmembrane Movement of Charged Molecules"*, J. of Biophysics **2016**, 1657679 (2016).

6. Tran Nguyen Lan, Le Bin Ho, and Tran Hoang Hai, *"Electronic, magnetic, and spin-polarized transport properties of hybrid graphene/boron-nitride nanoribbons having 5-8-5 line defects at the heterojunction"*, Phys. Status Solidi B **252**, 573-581 (2015).

Oral Presentations

1. Le Bin Ho and Nobuyuki Imoto, *"Continuous pointer state approach to modular-value amplification"*, 3rd International Conference on Quantum Foundations, National Institute of Technology, Patna, India (Dec. 2017).

2. Le Bin Ho and Nobuyuki Imoto, *"Quantum weak values and modular values with an embedding quantum simulator"*, 10th Vietnam-Japan Scientific Exchange Meeting, Shibaura Institute of Technology, Tokyo, Japan (Sep. 2017).

3. Le Bin Ho and Nobuyuki Imoto, *"Modular value and its generalized form"*, 36th Technical Committee on Quantum Information Technology, Kyoto University, Kyoto, Japan (May. 2017).

4. Le Bin Ho and Nobuyuki Imoto, *"An understanding and usage of modular values"*, 72nd JPS meeting, Osaka University, Osaka, Japan (Mar. 2017).

Poster Presentations

1. Le Bin Ho and Nobuyuki Imoto, *"Introduction to quantum weak values and modular values"*, Okinawa School in Physics: Coherent Quantum Dynamics, Okinawa, Japan (Oct. 2017).

2. Le Bin Ho and Nobuyuki Imoto, *"A general relation between modular values and weak values"*, International conference for young quantum information scientists, Barcelona, Spain (Oct. 2016).